Dioxygen Activation by Enzymes Containing Binuclear Non-Heme Iron Clusters

ARTICLE *in* CHEMICAL REVIEWS · DECEMBER 1996

Impact Factor: 46.57 · DOI: 10.1021/cr9500489 · Source: PubMed

Dioxygen Activation by Enzymes Containing Binuclear Non-Heme Iron Clusters

Bradley J. Wallar and John D. Lipscomb*

Department of Biochemistry, Medical School, 4-225 Millard Hall, University of Minnesota, Minneapolis, Minnesota 55455

Received May 16, 1996 (Revised Manuscript Received August 12, 1996)

Contents

* Corresponding author: John D. Lipscomb, Department of Chemistry, 4-225 Millard Hall, 435 Delaware St. SE, University of Minnesota, Minneapolis, MN 55455. E-mail: lipsc001@maroon.tc.umn.edu. Phone: 612-625-6454. Fax: 612-625-2163.

I. Introduction

Dioxygen activation by metalloenzymes generally proceeds through one of two fundamentally different routes. Some enzymes, such as the ferric ion containing intradiol aromatic ring-cleaving dioxygenases,[1,2] activate oxygen by facilitating the localization of electron density on the substrate so that direct electrophilic attack by O_2 can occur. Other metalloenzymes, such as extradiol ring-cleaving dioxygenases[2,3] and cytochrome P450 monooxygenase (P450),[4,5] activate O_2 by a reductive process in which the oxygen first binds to the ferrous form of the enzyme resulting in delocalization of electron density onto the bound O_2. Subsequently, the electronegative dioxygen either attacks an electropositive substrate directly (extradiol dioxygenases) or it is further reduced by a second reducing equivalent (P450). In the widely accepted mechanism proposed for P450,[4−6] the reduction by the second electron results in heterolytic O−O bond cleavage to yield water and a highly electron-deficient iron-bound oxenoid species that can attack unactivated hydrocarbons by an electrophilic mechanism.

Although the mechanism for P450 has been studied by a large number of approaches, it has not yet proven possible to identify a specific intermediate in the reaction cycle which would allow the iron−oxenoid theory to be directly examined. Moreover, there are some alternative mechanisms for O−O bond cleavage and oxygen insertion (see for example, ref 7) that could pertain to the doubly reduced iron−O_2 complex and which might be utilized in nature by other metalloenzymes or, indeed, by P450 itself. Until recently, P450 was the only well-characterized iron-containing metalloenzyme in which the mechanism of oxygen activation by a two-electron reduction process could be examined. However, during the past few years, the O_2-activating properties of a new type of iron-containing metalloenzyme utilizing an oxygen-bridged binuclear non-heme iron cluster has been recognized, and some members of this class have been extensively characterized.

The first member of the oxygen-activating binuclear iron class to be recognized, iron-containing

S0009-2665(95)00048-3 CCC: $25.00

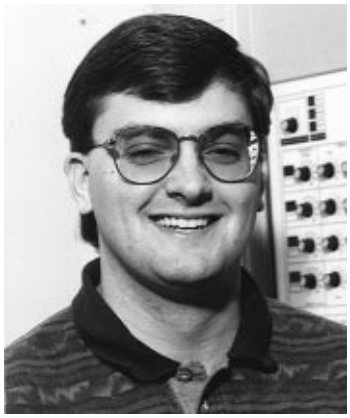

Brad Wallar (b. 1971) got his first exposure to research while an undergraduate at the University of Michigan—Flint, where he studied cytochrome P450 from water hyacinths under the guidance of Dr. David O'Keeffe. He received a B.S. in biology in 1993. After a year of graduate work in biochemistry at Colorado State University, he joined the laboratory of John D. Lipscomb at the University of Minnesota, where he is currently working on a Ph.D. in biochemistry. In the Lipscomb laboratory, his research focuses on the protein component interactions and their regulatory and mechanistic implications in the methane monooxygenase enzyme system. In his time off, he loves to watch University of Michigan sports (Go Blue!), spend time with his wife, and participate in outdoor sports, such as basketball, golf, and hiking.

John D. Lipscomb (b. 1947) received his undergraduate degree in chemistry from Amherst College in 1969 and his Ph.D. in biochemistry from the University of Illinois, Urbana in 1974. There he developed his long-term interest in metal-containing oxygenase enzymes through his work with I. C. Gunsalus on cytochrome $P450_{cam}$. During postdoctoral studies with J. M. Wood at the Gray Freshwater Biological Institute of the University of Minnesota, his interests focused on mechanistic and structural studies of non-heme iron oxygenases, an interest which remains strong today. Later, after joining the Department of Biochemistry of the University of Minnesota Medical School, Dr. Lipscomb broadened his studies to include oxygenases containing binuclear iron clusters, which is the topic of the current review. He is currently Professor and Interim Head of the department. Dr. Lipscomb also enjoys traveling with his wife and daughter and bicycling on the shores of Lake Minnetonka.

ribonucleotide reductase (class I),[8−11] is not an oxygenase during its primary catalyzed reaction, which is the reduction of ribonucleotides at the active site on its large subunit (R1). However, it does activate oxygen at a secondary active site on its small subunit (R2) in conjunction with the generation of a stable tyrosyl radical that is essential to the overall mechanism. The first true oxygenase of this class to be described was methane monooxygenase (MMO).[7,12−14] This has been an important enzyme in the sense that it can be obtained in high yield and purity and has proven amenable to a wide range of spectroscopic, kinetic, and crystallographic studies. The studies of MMO have made it possible for the first time to compare the proposed oxygen-activating mechanism of P450 with that of a structurally dissimilar metallooxygenase. Recently, several other enzymes which are apparently similar to MMO, such as toluene 2-monooxygenase (T2MO),[15] toluene 4-monooxygenase (T4MO),[16] stearoyl-acyl carrier protein Δ^9 desaturase (Δ9D),[17] phenol hydroxylase,[18] xylene monooxygenase, and alkane hydroxylase,[19] have been described in the literature.

In this review, we will focus on the current state of the knowledge of the mechanisms of O_2 activation by MMO and R2. Brief reviews of the literature for related enzymes will also be included. Many relevant reviews of aspects of this field have appeared recently. These include reviews of R2,[10,11,20−23] MMO,[7,14,24] and model complexes for these enzymes.[25,26]

II. Methane Monooxygenase

Methane is produced in enormous quantities in the environment as the primary end product of anaerobic metabolism by methanogenic bacteria. The atmospheric egress of a large fraction of this methane that is generated in lakes, oceans, and wet soils is blocked by the action of methanotrophic bacteria which oxidize methane as their sole source of carbon and energy.[12,13] Part of the carbon from methane is assimilated as biomass by the methanotrophs themselves. The remainder is released as CO_2 which can readily be taken up by other organisms, such as those that are capable of photosynthesis.

The key initializing step of the methane oxidation pathway, in which the stable C−H bond of methane is broken, is catalyzed by MMO. MMO catalyzes a classic monooxygenase reaction in which two reducing equivalents from NAD(P)H are utilized to split the O−O bond of O_2. One atom of oxygen is reduced to water while the second is incorporated into the substrate to yield methanol:[13]

$$CH_4 + O_2 + NAD(P)H + H^+ \rightarrow CH_3OH + NAD(P)^+ + H_2O$$

Although P450 catalyzes similar reactions with the same overall stoichiometry, only MMO is capable of catalyzing the efficient oxidation of methane. MMO also catalyzes the adventitious oxidation of a remarkably large number of other hydrocarbons, including saturated, unsaturated, linear, branched, and cyclic hydrocarbons up to approximately C_8 in size.[13,27−32] Moreover, halogenated alkenes and alkanes, one and two ring aromatics, heterocycles, and several other specialized classes of hydrocarbons are turned over by MMO. It is clear that a very powerful, but relatively nonspecific, oxidizing species is created during the catalytic cycle of MMO. The broad substrate range has facilitated structural and mechanistic studies of MMO because characteristic ligand complexes can be formed and diagnostic reactions are catalyzed.

MMO exists in mutually exclusive soluble and particulate forms in some methanotrophs.[12,33] Three

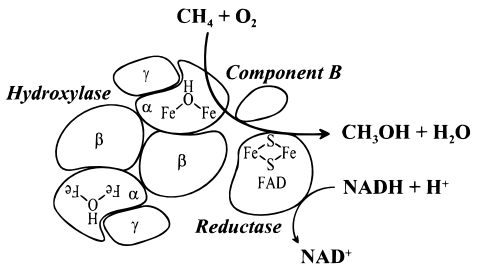

Figure 1. A representation of the quaternary structure and cofactor content of the soluble methane monooxygenase.

subclasses of these organisms (I, II, and X) have been described which differ in their cellular morphology, metabolic pathways, and the type of MMO expressed.[14] Types II and X can elaborate both soluble and particulate forms of MMO depending upon growth conditions, whereas the type I microorganisms elaborate only the particulate form. Interestingly, one of the key factors in determining whether the soluble or particulate form of MMO is produced appears to be the copper concentration of the growth medium.[33] The particulate MMO (pMMO) has not been completely stabilized or purified, although significant advances have been made recently.[34−39] In one study, the hydroxylase component of pMMO has been reported to contain a trinuclear copper center.[38] In another study, the catalytic site of pMMO was suggested to contain either a binuclear iron, a mononuclear iron, or a binuclear iron−copper site.[34] A more definitive understanding of the active site will require further study. In contrast, soluble MMO has been purified to homogeneity[40−45] and shown to harbor the oxygen-bridged binuclear iron cluster. Most of the discussion for this review will be directed toward the better-characterized soluble form.

A. MMO Protein Components

The best-characterized forms of soluble MMO contain three protein components (Figure 1), each of which is required for efficient substrate hydroxylation coupled to NADH oxidation: a 245 kDa hydroxylase (MMOH), a 15 kDa protein called component B (MMOB), and a 40 kDa reductase (MMOR). The hydroxylase is a dimer, each half of which contains three types of subunits (α,β,γ) and a hydroxo-bridged binuclear iron cluster.[40,46−50] The resting MMOH ($MMOH_{ox}$) diiron cluster is in the diferric state [Fe^{III}-Fe^{III}]. It can accept one or two electrons to generate the mixed-valence [Fe^{III}-Fe^{II}] or diferrous state [Fe^{II}-Fe^{II}], respectively. However, the diferrous state ($MMOH_{red}$) is the only one capable of reacting with dioxygen which is the reaction that initiates the catalytic cycle.[40,51,52] When diferrous MMOH is exposed to oxygen and substrate, in the absence of MMOB and MMOR, it can catalyze a single turnover of the substrate hydroxylation reaction showing that both oxygen activation and substrate hydroxylation occur in the diiron cluster site of the MMOH.[40,51−53] The MMOR and MMOB components do have substantial and diverse effects on the reaction rate and specificity of the enzyme, which will be described in more detail below.

1. Hydroxylase

a. Spectroscopic Studies. Many of the spectroscopic parameters that have been reported for MMOH are summarized in Table 1. The binuclear iron cluster of MMOH as isolated has two $S = {}^5/_2$ irons antiferromagnetically spin coupled to yield a diamagnetic center. Mössbauer spectra of this state[46,49,54] are consistent with this assignment, although in high magnetic fields the cluster exhibits a residual paramagetism that has not been fully explained.[49] As expected, the as-isolated (diferric) form of MMOH exhibits no ground-state EPR signals, but a signal from an integer spin excited state has been observed.[49] EXAFS studies of the oxidized state for MMOH isolated from two different organisms showed Fe−Fe distances of 3.05[55] and 3.43 Å,[54,56] respectively. However, these measurements were complicated by the fact that the diferric MMOH was observed to be easily reduced in the X-ray beam, leading to uncertainty in the redox state being observed. Studies of the *Methylococcus capsulatus* MMOH did not reveal a short Fe−O bond suggesting that the bridging oxygen(s) is protonated or otherwise substituted.[54] The same conclusion was reached from Mössbauer and integer spin EPR studies,[46,49] which showed a much weaker coupling constant than is typically observed for this type of cluster when the bridging oxygen is not substituted. Moreover, in contrast to other proteins containing μ-oxo-bridged clusters such as hemerythrin,[26,57−59] the optical spectrum of resting MMOH is weak and essentially devoid of features. This suggests that the usual Fe−O charge transfer band is absent,[40] which is again consistent with a substituted bridging oxygen. The lack of a chromophore prevented resonance Raman studies of the diferric enzyme, but addition of phenol resulted in a purple color which gave a resonance Raman spectrum.[60] Evaluation of the spectrum showed that it resulted from a ligand to metal charge transfer, which indicated that the phenol bound directly to the iron. This result demonstrated that relatively large molecules have direct access to the iron. Interestingly, at high concentrations of phenol, two different sets of resonance Raman signals with the same electronic origin were observed, suggesting either that phenol interacts differently with the two clusters present in the dimeric MMOH or that each iron has a binding site for phenol. The latter explanation is more reasonable based on the crystallographic studies (see below).

The $S = {}^5/_2$ and $S = 2$ irons of the mixed-valence state also antiferromagnetically couple to give an $S = {}^1/_2$ species that exhibits the characteristic EPR spectrum for the oxygen-bridged binuclear iron cluster, where g_{av} is well below $g = 2$ and all of the resonances are also usually found below $g = 2$.[46,54,61] The g values observed for the resonances are very sensitive to factors such as the presence of solvents, substrates, and MMOB (see below).[62,63] ENDOR studies showed that one or more nitrogens from histidine are present in the ligation sphere of each iron.[62] Moreover, at least nine protons are either associated with the cluster through bonds or within a few angstroms of the cluster.[62] Surprisingly, these protons exchanged only very slowly with deuterium

Table 1. Spectroscopic and Kinetic Properties of the Various Forms of the Hydroxylase Component of MMO

	Methylosinus trichosporium OB3b						*Methylococcus capsulatus* (Bath)					
	H_{ox}	H_{mv}	H_{red}	ref	P	Q	ref	H_{ox}	H_{mv}	H_{red}	ref	P	Q	ref
optical														
λ_{max} (nm)	282			40	unobserved	330,430	51	280			54	625−650	350,420	94
k_{form} (s^{-1})[a]					22	1	51					22	0.5	94
k_{decay} (s^{-1})[a]					1	0.05	51					0.5	0.07	94
exchange coupling														
J (cm^{-1})[e]	-7 ± 3	−30	0.35	49,63,65		>60	97		−32		54			
EPR														
g_{av}	8.0	1.85	16	46,49					1.83		245,54			
g_{max}		1.94							1.92					
g_{mid}		1.86							1.86					
g_{min}		1.75							1.71					
Mössbauer														
ΔE_Q (mm s^{-1}), Fe1	1.16[b]	−1.3[c]	3.1[b]	49	1.51[b]	0.53[b]	97,246	1.05[d]		3.01[d]	54	1.51[b]	0.68[b]	94,95
δ (mm s^{-1}), Fe1	0.51[b]	0.48[c]	1.3[b]		0.66[b]	0.17[b]		0.5[d]		1.3[d]		0.66[b]	0.21[b]	
ΔE_Q (mm s^{-1}), Fe2	0.87[b]	2.4[c]	2.4−3.0[b]	49									0.55[b]	94,95
δ (mm s^{-1}), Fe2	0.5[b]	1.19[c]	1.3[b]										0.14[b]	
k_{form} (s^{-1})												28	0.4	94,95
k_{decay} (s^{-1})												0.4	0.03	94,95
ENDOR														
A (MHz)		13−23		50					14−30		48			
Raman														
ν_{O-O} (cm^{-1})												905		94,96

[a] The data were collected at 4 °C with MMOB/MMOH = 2, pH 7.7 (OB3b), pH 7.0 (Bath). [b] The data were collected at 4.2 K. [c] The data were collected at 150 K. [d] The data were collected at 80 K. [e] These values are reported using the convention $H = -2JS_1S_2$.

in the solvent. In particular, two proton resonances that exhibited unusually large coupling constants of 8 and 13 MHz were not observed to exchange over an eight hour period, suggesting that they were either not exchangeable or were in positions sequestered from solvent. Subsequent pulsed EPR[50] and pulsed ENDOR[48] studies showed that the proton resonance at 8 MHz was associated with a terminal solvent ligand of one of the iron atoms while the resonance at 13 MHz was attributable to the proton on the oxygen bridge. The latter resonance also showed a characteristic dependence on the magnetic field direction. In the pulsed studies, exchange of these protons was observed, but a 24 h incubation was required. ENDOR signals from deuterium associated with the solvent DMSO were observed, suggesting that access of substratelike molecules to the cluster was possible;[62,64] however, the crystal structure of MMOH that had been soaked in DMSO failed to reveal this molecule in the active site,[65] suggesting that it is disordered when it binds. Mössbauer studies[49] of the mixed-valence state showed that the irons do not exhibit a delocalized spin system, but rather a trapped valence state, suggesting that the protein provides an asymmetric environment for the cluster.

Diferrous MMOH exhibits ferromagnetic coupling of two $S = 2$ ferrous ions to give an $S = 4$ ground state. This species exhibits an intense EPR signal at about $g = 16$[40,46,66] which intensifies when the microwave field is aligned parallel with the fixed magnetic field in the EPR spectrometer cavity. This is characteristic of a signal from an integer spin state[67,68] of the cluster, although the precise electronic description of the origin of the signal remains controversial. High-field Mössbauer studies[49] confirmed the $S = 2$ nature of each of the irons and showed that the two metals reside in similar but distinguishable environments. MCD/CD studies indicated that each of the irons is in five-coordinate ligand environments with distorted square-pyramidal ligation geometries.[69] It should also be noted that EXAFS studies on the diferrous form of MMOH did not detect any significant Fe−Fe contribution, indicating that the two irons are further apart than in the other oxidation states, and thus may be less strongly coupled.[54] This result agrees with the crystal structure of diferrous MMOH[70] which shows the loss of a hydroxo bridge, among other ligand structural rearrangements.

b. Crystallographic Studies. The crystal structure of the oxidized form of MMOH has been determined for both the *M. capsulatus* (2.2 Å)[71] and the *Methylosinus trichosporium* (2.0 Å) enzymes[72] (see Figures 2 and 3a). Further crystallographic studies have led to the 1.7 Å structures of both the oxidized and reduced forms of MMOH from *M. capsulatus* flash frozen at −160 °C.[70] The overall structures of the enzymes from the two widely divergent methanotrophs are remarkably similar. For the purposes of this review, only the binuclear iron site structure will be addressed. The structure of this site in *M. trichosporium* MMOH at 18 °C is very similar to that of the flash-frozen structure from *M. capsulatus* MMOH in that they both have a binuclear [Fe^{III}-Fe^{III}]

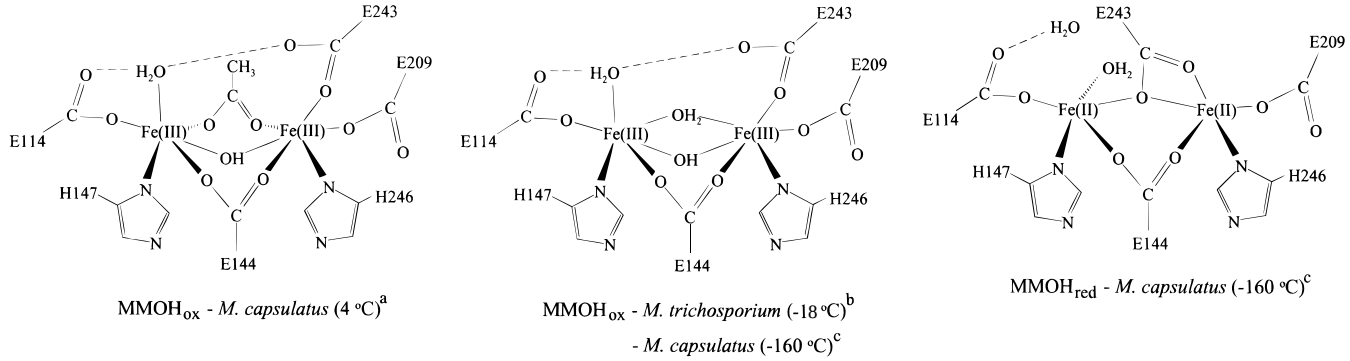

Figure 2. Structural representation of the binuclear iron center of diferric MMOH and diferrous MMOH: (a) from Rosenzweig, A. et al., ref 71; (b) from Elango, N. et al., ref 72; and (c) from Rosenzweig, A., et al., ref 70.

center in which the two irons are linked by two single oxygen bridges in the α subunit (see Figure 2). This so-called "diamond core" center is a feature that has been found in model compounds of activated intermediates of MMOH and R2 and may play an important role in the O_2 activation chemistry of this class of enzymes. Each iron in the MMOH cluster is six coordinate, having one nitrogen ligand (His) and five oxygen ligands comprised of glutamic acid residues, bridging hydroxides, and a terminal water. The binuclear iron cluster resides in the center of a four-helix bundle, or more specifically, two Glu-X-X-His segments that serve as ligands to the irons. The four-helix bundle is a structural motif that has been observed in many other metalloenzymes.[73,74] One specific ligand, Glu-243, (in *M. capsulatus*) undergoes a so called "carboxylate shift"[75] upon reduction of the binuclear iron cluster to the diferrous [Fe^{II}-Fe^{II}] form.[70] This carboxylate shifts from a terminal, monodentate ligand to Fe2 to a monodentate, bridging ligand between the two irons. The second oxygen of the Glu-243 carboxylate also appears to coordinate to Fe2. A similar carboxylate shift had previously been reported for R2.[76,77] In addition, one of the hydroxo bridges is lost, and the other hydroxo/water bridge shifts from serving as a bridge to being terminally bound to Fe1. Also, the terminal water bound to Fe1 in the oxidized form of MMOH seems to move out of bonding distance (2.63 Å) upon reduction of the cluster. With the advent of these perturbations in the ligand environment, the irons become effectively five coordinate in the reduced form of MMOH, which is a reasonable result since this is the form of the cluster that reacts with O_2.

The crystal structures of both enzymes show the existence of a hydrophobic pocket adjacent to the binuclear iron cluster toward the interior of the protein, which may mark the direction of approach for substrates. However, there is no obvious entry channel into the interior of the protein. This may mean that substrate entry is dependent upon flexibility of the protein structure. Alternatively, the structure may be altered by binding of the MMOB or MMOR components to create an entry channel (see section E "Regulation"). It is interesting that the crystal structures show the presence of unassigned electron density in the hydrophobic pocket which may not be solvent. In the case of the *M. capsulatus* enzyme at −160 °C, the density was tentatively assigned as acetate, because acetate was present in the crystallization buffer. However, in the case of the *M. trichosporium* enzyme at 18 °C, nothing from the crystallization buffer other than solvent could be confidently placed into this electron density. This density was also observed in the initial structure of the *M. capsulatus* MMOH determined from the data accumulated at 4 °C. However, in this structure, the density was found as a bridging ligand, replacing one of the bridging hydroxide or water ligands in accord with its assignment as acetate.

The fact that crystallographic studies support both diamond core structures with short Fe−Fe distances, as well as a structure with a longer Fe−Fe distance dictated by the loss of one on the μ-hydroxo bridges, suggests that the core structure is relatively flexible. This is supported by recent EXAFS studies of the diferric MMOH from *M. trichosporium*[78] which showed that the Fe−Fe distance appears to be different in two populations within a single sample. Approximately 60% of the population had Fe−Fe distances consistent with a diamond core structure (∼3.0 Å) while the rest had distances indicative of a single bridge structure (∼3.4 Å).

2. Reductase

MMOR contains both FAD and [Fe_2S_2] cofactors in a single polypeptide chain.[40,79,80] The iron−sulfur cluster has been characterized by EPR and Mössbauer spectroscopies.[49] MMOR is believed to transduce the chemical bond energy of NADH to yield relatively low potential electrons required to initiate O−O bond-breaking chemistry in the active site of MMOH. The two electrons from NADH are stored transiently in the flavin and metal cofactors of MMOR before transport to the diiron site of MMOH.[79,80] This is a reasonable role for the MMOR given that its complement of cofactors are those commonly found in the reductase components of other oxygenase systems.[81,82] Despite the fact that the reaction only requires two reducing equivalents, MMOR can be reduced by three electrons in discrete one-electron steps. In the case of the *M. capsulatus* MMO system, it has been proposed that the MMOR oscillates between the one-electron- and three-electron-reduced states during the catalytic cycle.[83,84] There are now several indications that MMOR binding to MMOH also causes mechanistically relevant changes in the structure and/or reactivity of MMOH through formation of a tight complex with the β-subunit.[63]

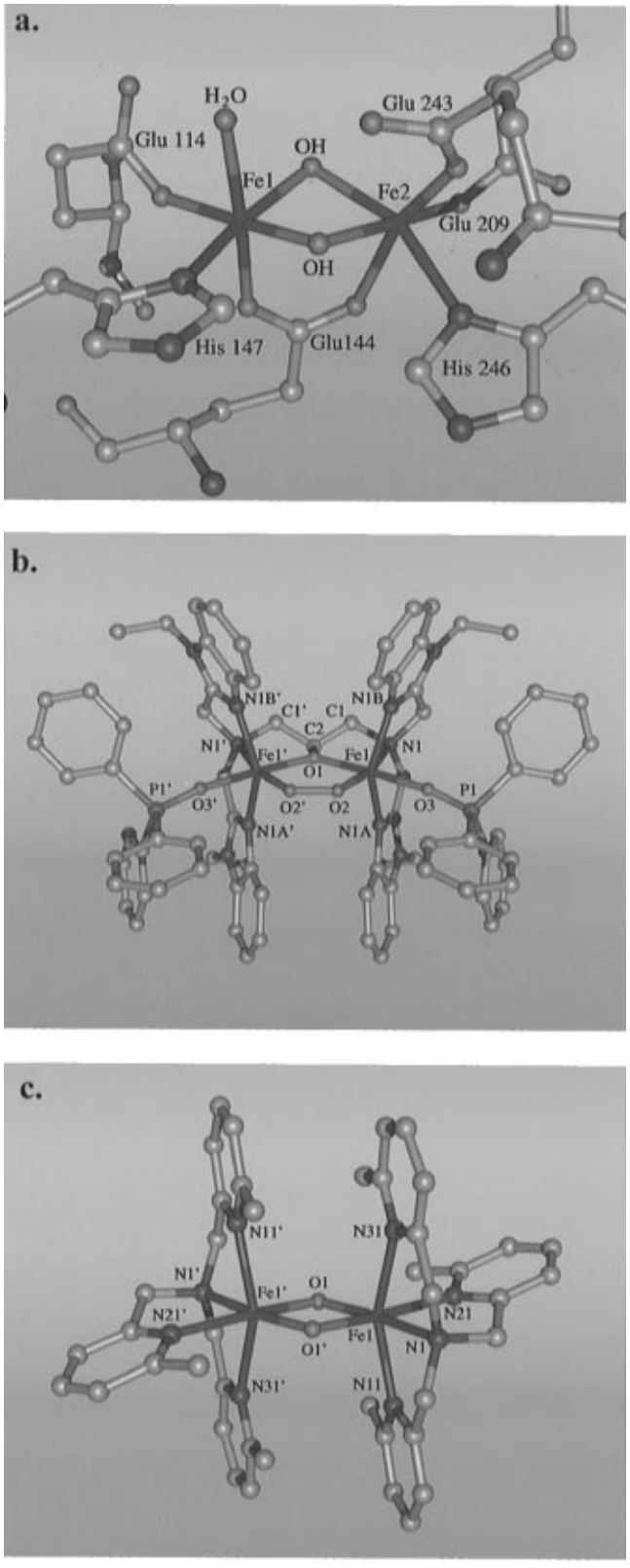

Figure 3. (a) Crystal structure of the binuclear iron site of MMOH from *Methylosinus trichosporium* OB3b (Elango, N.; Radhakrishman, R.; Froland, W. A.; Wallar, B. J.; Earhart, C. A.; Lipscomb, J. D.; Ohlendorf, D. H. Unpublished results). (b) Ball and stick representation of the crystal structure of diferric peroxy compound, $[Fe_2(\mu\text{-}1,2\text{-}O_2)(N\text{-Et-HPTB})(Ph_3PO)_2]^{3+}$ (adapted with permission from ref 102). (c) Ball and stick representation of the crystal structure of the diferric, "diamond core" compound, $[Fe_2(\mu\text{-}O)(\mu\text{-}OH)(6TLA)_2]^{3+}$ (adapted with permission from ref 110).

These will be discussed in the section describing the regulatory roles of MMOR and MMOB below.

3. Component B

MMOB contains no cofactors or metals,[40,85] thus it does not appear to serve the electron-transfer role usually assigned to the small component in multicomponent oxygenase systems. It has been shown to develop a tight complex with the α subunit of MMOH, as detected by chemical cross-linking, fluorescence quenching, and its effect on the redox potential of MMOH.[52,63,86,87] The formation of the complex has profound effects on the rate of various reactions in the catalytic cycle, the structure of MMOH, and the product distribution of the overall reaction.[53] These and other effects of MMOB will be discussed in the context of regulation below.

4. Molecular Genetic Studies

The gene cluster containing the genes for all subunits of the MMOH, MMOR, and MMOB has been cloned and sequenced from both *M. capsulatus* (Bath)[88,89] and *M. trichosporium* OB3b.[90,91] Expression of the MMOR and MMOB genes to yield active proteins has been reported.[92] Attempts to overexpress the MMOH genes to yield active enzyme have not been successful. However, the entire gene cluster of MMO has been successfully cloned into *Escherichia coli* and five different strains of *Pseudomonas*, with the best results coming from the *Pseudomonas putida* F1 strain.[93] The resulting recombinant bacterium exhibits low MMO activity but can effectively oxidize alternate MMO substrates, such as trichlorethylene, when grown on common carbon sources, suggesting that this technique may be useful in bioremediation applications.

B. Transient Intermediates in the Catalytic Cycle of MMO

The observation that diferrous MMOH, in the presence of 2-fold MMOB, can generate high yields of product during a single turnover suggests that meaningful mechanistic information can be extracted from transient kinetic studies. Recently, it has been shown that the catalytic cycle of MMOH proceeds through several discrete intermediates,[51] many of which form in significant yield before they decay. The intermediates in this cycle and their rates of interconversion are summarized in Figure 4. The natural cycle is initiated by reduction of the resting diferric MMOH to the diferrous state by NADH via MMOR. For transient kinetic studies, MMOH can be reduced by chemical, electrochemical, or photochemical techniques using nonbiological mediators. Reduction to the mixed-valence state is also possible, but no further kinetically relevant reaction with O_2 or substrate has been observed with this state of the enzyme.[40]

1. Compound O

Rapid mixing of $MMOH_{red}$ with O_2 in the presence of MMOB results in rapid loss of the $g = 16$ EPR signal characteristic of the diferrous state.[51] At 4 °C, this reaction, which corresponds to the formation of

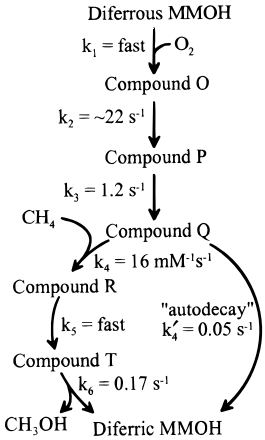

Figure 4. The sequence of reaction cycle intermediates in the single turnover of MMOH in the presence of MMOB. The step labeled k_4' represents the first-order autodecay of compound Q which occurs in the absence of substrates and may also occur in their presence. All rate constants are for a reaction at 4 °C.[99]

compound P, occurs approximately 100 times faster than turnover of the fastest substrate (methane). The reaction rate is not affected by the presence or absence of substrate, and it is unchanged by variation of the concentration of O_2 between 300 and 700 μM.[52] The latter observation suggests that an intermediate, which retains the $g = 16$ signal and has no other detectable differences from $MMOH_{red}$, is essentially irreversibly formed as O_2 enters the active site. A likely possibility is that oxygen binds in the active site prior to association with the diferrous cluster. This intermediate has been termed compound O (for oxygen adduct).[53]

2. Compound P

Compound O spontaneously converts to a species which has no EPR signal [52] but which can be trapped and examined by Mössbauer spectroscopy,[94,95] as illustrated in Figure 5b. These studies show that the both irons are ferric in the complex, but the isomer shift (0.66 mm s^{-1}) and quadrupole splitting (ΔE_Q = 1.55 mm s^{-1}) are unusual. The intermediate formed with MMOH from *M. trichosporium* was not observed to exhibit an optical chromophore,[51] but that from *M. capsulatus* was reported to have a weak chromophore at 625−650 nm (ϵ = 1500 M^{-1} cm^{-1}).[95] Investigation of the intermediate using resonance Raman spectroscopy[96] showed a band at 905 cm^{-1}, which is consistent with peroxide-stretching frequencies in other complexes. The band was shifted when $^{18}O_2$ was utilized, proving that the band represented a ν_{O-O} stretch; however, the observed shift was only one half that of the theoretical ^{18}O shift. When O_2 containing one atom of ^{16}O and one of ^{18}O was used, only a single band was observed, suggesting that both oxygens are bound symmetrically to the irons. Moreover, only a single quadrupole doublet was observed in the Mössbauer spectrum of the species, showing that the oxygen is bound symmetrically in the complex. The binding mode of the O_2 is not known as of yet, but a symmetric peroxy bridge is favored, such as the μ-η^2,η^2 (in plane or out of plane) or μ-1,2 binding modes. This species was first termed compound P (for peroxide adduct)[51] but has also been termed compound L[94] and the peroxy complex.[95,96]

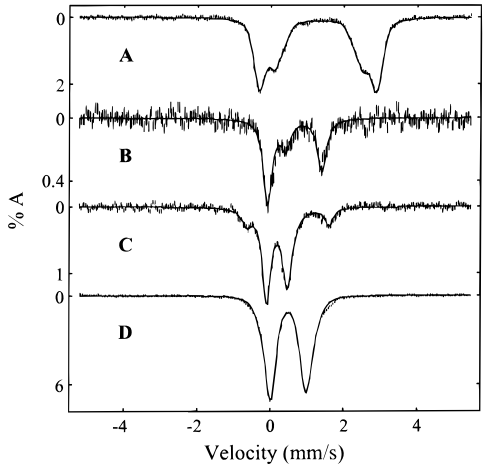

Figure 5. Mössbauer spectra of the observable states of MMOH during a single turnover reaction of diferrous MMOH with O_2. In the presence of MMOB, ^{57}Fe-enriched diferrous MMOH from *M. trichosporium* OB3b was rapidly mixed with O_2 and frozen at different time points for Mössbauer analysis at 4.2 K. The spectra display the various forms of MMOH that are observed during the course of the reaction: diferrous MMOH (A), compound P (B), compound Q (C), and the resting diferric state (D). Spectra B and D are shown after subtraction of the spectra of diferrous and/or diferric MMOH also present at the time the sample was frozen. (Data compiled from refs 46 and 49 and from unpublished observations by K. Kauffmann, E. Münck, J. Nesheim, Y. Liu, and J. D. Lipscomb.)

Note. Definitions of oxygen-bridging nomenclature: μ-1,2 = oxygens bridge the two irons such that each oxygen in bound only to one iron

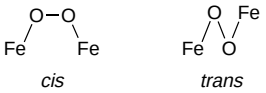

μ-η^2,η^2 = oxygens bridge the two irons such that each oxygen atom is bound to both irons

3. Compound Q

Compound P spontaneously converts to a yellow (λ_{max} = 330, 430 nm) species termed compound Q.[51,95] In the absence of substrates, compound Q forms much more rapidly than it decays, allowing it to be trapped in high yield for spectroscopic studies. The Mössbauer spectrum of compound Q (Figure 5c) consists of a single quadrupole doublet for the enzyme from *M. trichosporium*[97] with parameters (δ = 0.17 mm s^{-1}, ΔE_Q = 0.53 mm s^{-1}) that are consistent with high-spin Fe(IV) or low-spin Fe(III) (see Table 1 for *M. capsulatus* Mössbauer data). Because low-spin Fe(III) is unlikely in a non-heme system with an oxygen-rich ligand environment, compound Q was proposed to contain Fe(IV). The facts that a single quadrupole doublet was observed from two irons and that the high-field Mössbauer spectrum showed that the cluster was diamagnetic suggest that compound Q contains two antiferromagnetically coupled high-spin Fe(IV) atoms. If correct, this is the first non-heme biological system to stabilize Fe(IV) and the first Fe(IV) binuclear iron cluster to be recognized

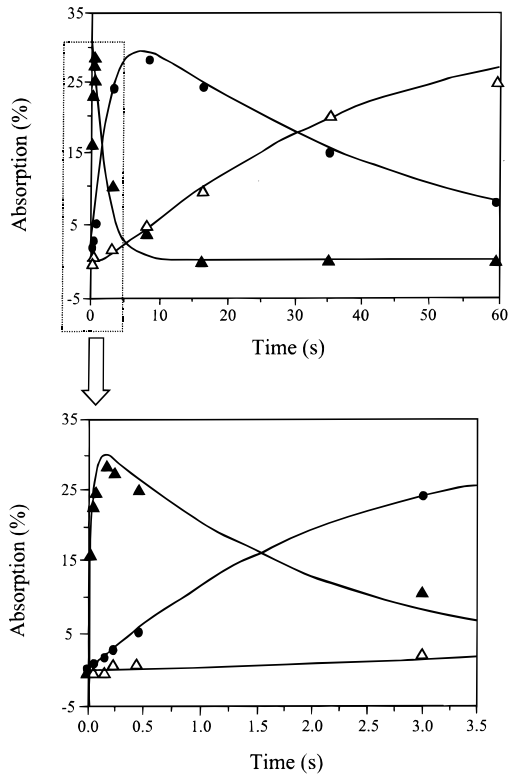

Figure 6. Time-dependent concentration of compound P (▲), compound Q (●), and diferric MMOH (△) in a single turnover reaction of diferrous MMOH with O_2 at 4 °C, as monitored by Mössbauer spectroscopy. Samples were rapidly frozen at the times shown and analyzed by Mössbauer spectroscopy at 4.2 K. The upper figure shows the full 60 s time course, whereas, the bottom is an expansion of the first 3.5 s of reaction time to demonstrate the buildup and decay of compound P. The MMOH is from *M. capsulatus* Bath. (Adapted with permission from ref 94.)

in any context. Compound Q has also been trapped from *M. capsulatus*[94,95] and is similar to that just described except that two quadrupole doublets are observed with parameters assignable as Fe(IV) or low-spin Fe(III). This demonstrates that the two irons of compound Q in this enzyme are in slightly different environments, but the overall conclusions about the nature of compound Q are unchanged.

With known Mössbauer parameters for diferric MMOH, diferrous MMOH, compound P, and compound Q, the use of the rapid freeze quench Mössbauer technique has allowed their relative populations to be monitored over time in single turnover reactions, as illustrated in Figure 6. In addition, the rate of decay of compound Q is readily measured due to the fact that it is the only strongly chromophoric intermediate in the MMOH catalytic cycle. The decay rate was found to increase linearly with the concentration of substrate present[51] as illustrated in Figure 7. This is unexpected for an enzyme-catalyzed reaction, which would normally display saturation kinetics (i.e. hyperbolic dependence of decay rate constant on substrate concentration). Furthermore, the rate was observed to be strongly dependent on the specific substrate utilized. Methane gives the highest rate of any substrate examined to date. Alternate substrates that have lower turnover numbers (e.g. nitrobenzene) also generally react more slowly with compound Q, although this correlation

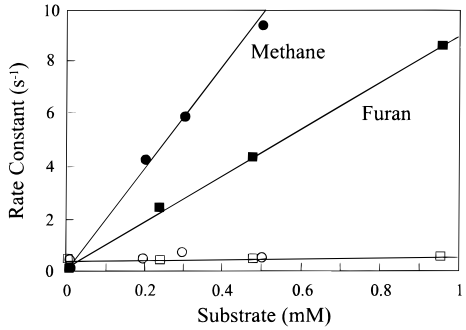

Figure 7. The formation and decay rates of compound Q as a function of substrate concentration for methane and furan. The compound Q formation (open symbols) and decay (closed symbols) rates are shown at different concentrations of methane (●, ○) and furan (■, □). The formation and decay rates were measured by following the absorbance at 430 nm in a single turnover reaction of diferrous MMOH with O_2 at 4 °C (MMOB/MMOH = 2).

is probably fortuitous because compound Q decay is not the rate-limiting step in the catalytic cycle (see below).

4. Compound R

The mechanism by which compound Q reacts with substrates is the key to the monooxygenase chemistry of this enzyme and the general topic of this review. We have proposed that this reaction proceeds via substrate hydrogen atom abstraction by compound Q to form a radical substrate intermediate.[14,27,40,53] This postulated intermediate has been termed compound R (for radical adduct). All experiments indicate that this intermediate does not live long enough to be trapped. Supportive evidence for this intermediate has come from the use of chiral[98] and isotopically enriched substrates,[32,99,100] which will be discussed below.

5. Compound T

The decay of compound Q in the presence of the alternate substrate nitrobenzene yields the chromophoric products *m*- and *p*-nitrophenol.[27] The formation of these products can be observed with the use of stopped flow spectroscopy and quantitated using chemical quench techniques.[51] The formation occurs through an intermediate with spectroscopic features similar to those of nitrophenol in nonpolar solvent. Moreover, the chemical quench experiment shows that the nitrophenol products are formed at the same rate as compound Q decays and the new intermediate forms. The new intermediate decays to give a species with the same optical spectrum as the nitrophenols in aqueous buffer at a rate equal to the turnover number for nitrobenzene. Thus, it appears that the new intermediate, termed compound T (for terminal adduct), is the final product complex of the enzyme, and that product release is the overall rate-limiting step in the cycle. The decay of compound T yields diferric MMOH to complete the cycle.

C. Structural Considerations of Compounds P and Q Based on Model Studies

Studies of binuclear iron chelate model complexes have contributed much to our understanding of the

spectroscopic and catalytic properties of these clusters in enzymes. This work is summarized briefly in section V in this review. However, it is useful at this stage to cite recent studies of model complexes that mimic some spectroscopic features of compounds P and Q, and may, therefore, give insight into the structure of the binuclear iron center in these critical complexes.

1. Models for Compound P

Recently, the first crystal structures of peroxy complexes of binuclear iron clusters in small molecule chelates were reported.[101−104] The structure of one of these is shown in Figure 3b. This complex belongs to a family differing in the identity of the nonchelate iron ligand. Two of the complexes contain a *cis* μ-1,2-bridging peroxide,[102,103] while the other one contains a *trans* μ-1,2-bridging peroxide,[104] and they all exhibit a blue or green color (benzoate adduct, $\lambda_{max} = 588$ nm, $\epsilon = 1500\ M^{-1}\ cm^{-1}$) (see Table 7, structures **16**−**20**). Both the λ_{max} and extinction coefficient are similar to those reported for compound P.[94] Mössbauer spectra show that both the models[101,103,104] and compound P[94] are diamagnetic and exhibit only one quadrupole doublet. Moreover, both compound P and the model complexes have resonance Raman ν_{O-O} stretches near 900 cm^{-1}, which indicates that both may share the same μ-1,2-peroxo-binding mode.[25] However, it was initially shown that compound P exhibited a significantly greater isomer shift in the Mössbauer spectrum (0.66 mm s^{-1}), which had only been seen in mononuclear iron complexes with η^2-peroxo ligation.[105−107] Thus, a μ-η^2,η^2-peroxo ligation in compound P is possible, although the resonance Raman spectra of the mononuclear peroxo complexes show ν_{O-O} stretching frequencies that are significantly lower (~800 cm^{-1}) than reported for compound P. An exciting observation of the *trans* μ-1,2-peroxo complex was that the Mössbauer spectrum showed that it had the same isomer shift as compound P (0.66 mm s^{-1}), lending insight into the possible O−O binding mode in the elusive intermediate. It is obvious that the available model complexes clearly support the proposal that compound P is a diferric peroxo complex; however, the binding mode of the peroxide is still not definitively established.

2. Models for Compound Q

The unique spectroscopic features and spin state of compound Q have presented a new challenge in the synthesis of appropriate model compounds. Recently, it has been shown that reaction of hydrogen peroxide with a series of binuclear iron complexes, based on the tripodal chelating ligand tris(2-pyridylmethyl)amine (TPA) and its analogs (see Table 7, structures **3** and **15**) can yield transient green intermediates.[108,109] Stabilization of these intermediate species at −40 °C has allowed spectroscopic characterization of their structure. The 5-Me TPA adduct (**3**) has been the most thoroughly studied. This species has a visible absorption maximum at ~616 nm, a rhombic $S = {}^3/_2$ EPR spectrum and Mössbauer features consistent with high-valent iron.[109] Resonance Raman and mass spectrometric studies of the green intermediate indicate that it contains two bridging oxygen atoms, but that they are not bound as a peroxide. EXAFS studies show that the Fe−Fe distance in the green intermediate is 2.89 Å, which is significantly shorter than in binuclear iron complexes that are bridged by μ-peroxo or single μ-oxo ligands in combination with carboxylate and/or similar ligands. It has been proposed that the structure of the green intermediate includes a diamond core formed by a binuclear iron with a bis-μ-oxo bridge.[109] Support for this structure has been derived from the synthesis, crystallization, and structure determination of the chelate complex shown in Figure 3c[110] (see Table 7, structure **1**). The chelating ligand for this complex is an analog of TPA, and the complex is formed by reaction of a precursor with an organic peroxide. However, the resulting complex is red (λ_{max} = 396 and 550 nm) and Mössbauer spectroscopy shows that both irons are ferric. The presence of the diamond core structure and the characteristic Fe−Fe distance of 2.91 Å are clearly demonstrated by the crystal structure. EXAFS spectroscopy shows asymmetry in the Fe−O distances for the μ-oxo bridges, suggesting that one of these oxygens is protonated. Recently, the properties of an unprotonated analog (**2**) have also been reported.[111]

EXAFS[78] and crystallographic[70,72] studies of the binuclear iron site of MMOH are in agreement with the diferric models described above in that they both show a diamond core structure with a short Fe−Fe distance (2.7−3.0 Å). Thus, it seems reasonable that a similar structure oxidized by two reducing equivalents might also pertain to compound Q. Plausible structures for compound Q are depicted in Figure 8. Under this model, the 5-Me-TPA (**3**)-based green intermediate[109] would also have the diamond core structure, but it would be one equivalent more oxidized than the diferric model shown in Figure 3c (**1**), and one equivalent more reduced than compound Q. The electronic structure of the green compound is very interesting. According to Mössbauer spectroscopy,[109] the $S = {}^3/_2$ complex is formally $Fe^{III}Fe^{IV}$ and is valence delocalized. It is currently thought[109] that the iron sites of this intermediate are low-spin ($S = 1$) Fe(IV) and low-spin ($S = {}^1/_2$) Fe(III) and that the delocalized system reflects the presence of strong double exchange (resonance delocalization) interactions between the two iron sites. Although the isomer shift (δ = 0.14 mm s^{-1}) and quadrupole splittings (ΔE_Q = 0.49 mm s^{-1}) of the green intermediate are very similar to those of compound Q, complex **3** is not a good electronic model for the MMO intermediate. This is so because the green intermediate is a valence-delocalized mixed-valence system with apparent low-spin sites while compound Q is a homovalent dimer containing most likely (see below) high-spin sites. Arguments for high-spin Fe(IV) sites in compound Q are supported by recent Mössbauer studies of another TPA-based complex in which the methyl substituent of the pyridyl groups is in the 6 position (Table 4, complex **11**). This complex is brown and has $S = {}^1/_2$ ground state which results from strong antiferromagnetic coupling between a high-spin ($S = {}^5/_2$) Fe(III) and a high-spin Fe(IV).[112] The Mössbauer spectra of **11** show trapped valence states with $\delta = 0.08$ mm s^{-1} for the Fe(IV) site and

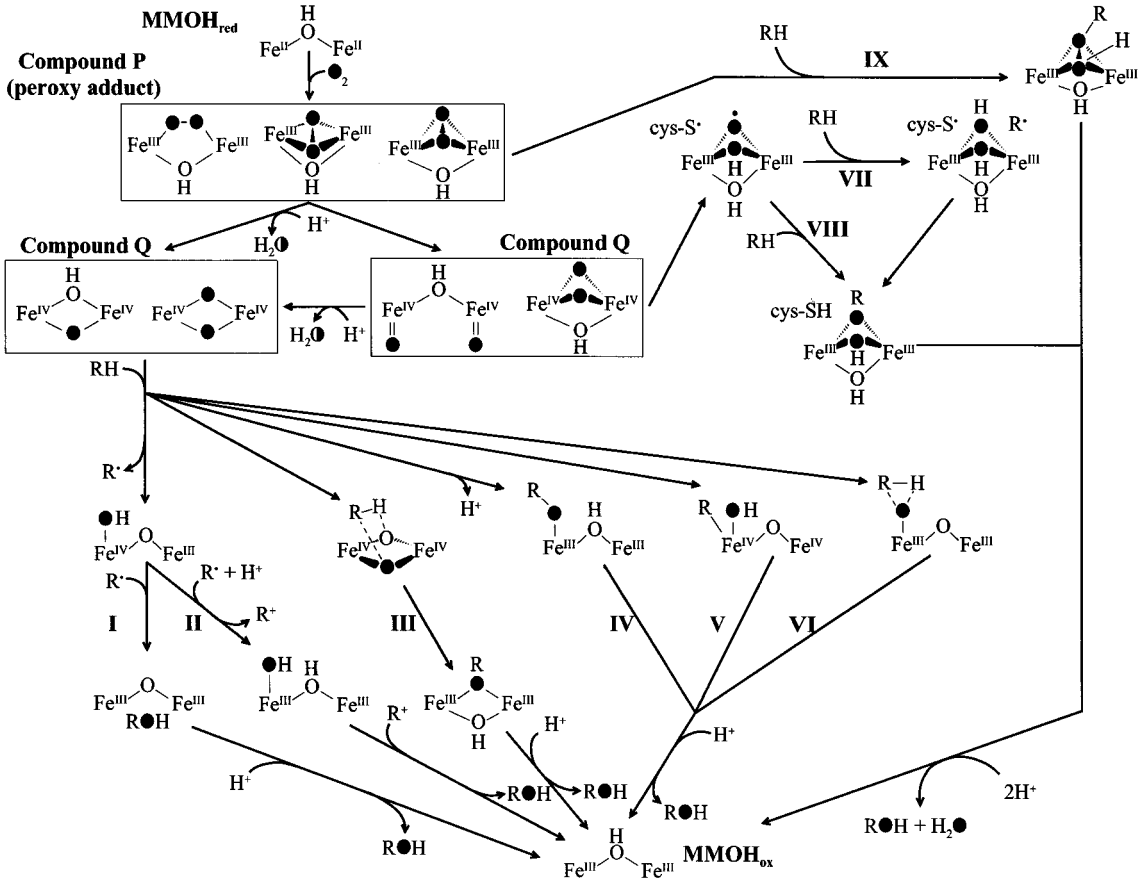

Figure 8. Summary of the possible mechanisms for the hydroxylation of substrate by MMO. For compounds P and Q, the oxygen atoms derived from O_2 are filled. It is known that the labeled oxygen from O_2 is incorporated into the product, thus this oxygen in all mechanisms is filled. The fate of the second oxygen from labeled O_2 has not been directly determined, consequently we have not attempted to designate this oxygen in the figure. References for the different proposed mechanisms are as follows: (**I**) 14, 27, 29, 51, 53, 97; (**II**) 122, 133; (**III**) 130, 131, 261; (**IV**) 7, 123; (**V**) 7, 123, 135, 262; (**VI**) 7, 123, 133; (**VII**) 7, 263; (**VIII**) 7; (**IX**) 7.

$\delta = 0.48$ mm s^{-1} for the Fe(III) site. As judged from the magnetic hyperfine interactions, the Fe(IV) site exhibits the same degree of covalency as the Fe(III) site. The latter has similar A values as typical Fe(III) complexes with octahedral N/O coordination. Since the 4-N,2-O coordination of the iron of the brown complex (suggested by mass spectroscopic data) provides a high-spin Fe(IV) environment, one would anticipate a high-spin configuration also for an Fe(IV) site in the more oxygen-rich compound Q binuclear cluster. Taking all information of the Fe(IV) site of the brown intermediate into account would suggest an isomer shift around 0.1 mm s^{-1} for an MMO Fe(IV) site. If compound Q is judged, in the absence of other benchmarks, against this value, and it is taken into account that the $Fe^{III}Fe^{III}$ of MMOH has $\delta = 0.5$ mm s^{-1}, it can tentatively be concluded that the value $\delta = 0.17$ mm s^{-1} of compound Q of the enzyme from *M. trichosporium* suggests a high-spin $Fe^{IV}Fe^{IV}$ configuration with perhaps 20% $Fe^{III}Fe^{III}$ character.

D. The Mechanism of Hydrocarbon Hydroxylation by MMO

Now that the crystal structures of two forms of MMOH are known and the existence of compound Q and other intermediates have been demonstrated in the MMOH reaction cycle, it is of great interest to elucidate the specific chemistry that is involved in the substrate hydroxylation mechanism. These investigations have been greatly enhanced by the fact that many molecules serve as adventitious substrates for MMO, and some of these are diagnostic for certain types of chemistry. Also, the availability of new data from studies of model systems and other oxygenases is of use in consideration of the MMO mechanism. Figure 8 summarizes some of the possible mechanisms for substrate hydroxylation following generation of the dioxygen-activated binuclear iron cluster. The distinctive features of the individual mechanisms labeled **I**−**IX** are: (**I**) homolytic breakage of R−H; (**II**) a two-step oxidation of substrate to yield a net heterolytic cleavage of RH; (**III**) simultaneous attack of two bridging oxyens of compound Q on the R−H bond; (**IV**) heterolytic breakage of R−H; (**V**) oxygen insertion into substrate proceeding from the formation of an iron−carbon bond in the reactive intermediate; (**VI**) direct oxygen insertion; (**VII**, **VIII**) diradical mechanisms, involving an amino residue radical in the active site; and (**IX**) electrophilic attack on the substrate with O−O bond cleavage occurring after the C−H bond-breaking step. Pathway **III** involves the transient formation of a pentavalent carbon intermediate, pathways **I**, **II**, and **VII** involve the transient formation of a substrate-derived alkyl radical, while pathway **II** and possibly **IV** also involve a carbocationic intermediate.

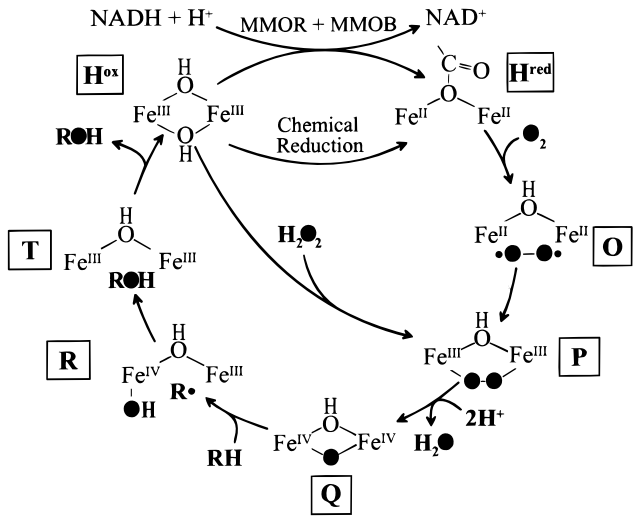

Figure 9. The proposed catalytic cycle of methane monooxygenase based on a radical recombination process for substrate hydroxylation. The oxygen atoms derived from O_2 are filled. (Compiled from refs 14, 27, 29, 40, 52, 53, and 70.)

1. A Mechanism Based on Hydrogen Atom Abstraction from Substrate

The mechanism of P450 has long been considered a likely model for that of MMO. Some of the most important observations in the development of the P450 mechanism demonstrated the formation of a discrete substrate intermediate that is likely to be a substrate radical. This intermediate would presumably arise from a hydrogen atom abstraction reaction by the activated form of P450; the heme Fe^{IV}=O π cation radical species equivalent to compound I of peroxidases has been postulated to be this activated species[4,6] (see Figure 8, mechanism **I**).

This P450 mechanism is readily adapted to MMO catalysis. Figure 9 shows a hypothesis for the chemical nature of the intermediates in this mechanism based on the properties and structural characteristics of the reaction cycle intermediates as they are now understood. In this scheme, compound Q is a symmetrical analog of an [Fe^{IV}-Fe^{IV}]=O species that is the electronic equivalent of the heme Fe^{IV}=O π cation radical species of P450. In essence, the second iron of the cluster fulfills the role of the porphyrin in supplying the second electron that is required to fill the octet of the oxygen atom resulting from heterolytic cleavage of the O−O bond during the conversion of compounds P to Q. Compound Q would then act to abstract a hydrogen atom from substrate to yield a substrate radical and a hydroxyl radical bound to the cluster. Recombination of the radicals would form compound T which would eventually break down to release product.

One test of this type of mechanism is that it should be possible to substitute the addition of hydrogen peroxide for the two "charging" steps of the cycle in which two electrons and O_2 are added to MMOH. This so called "peroxide shunt" has been shown to be functional in P450,[4] as well as in MMOH from *M. trichosporium*[27,53] and *M. capsulatus*;[113] however, the product yields in the latter enzyme are quite low.[7,113] Although the peroxide shunt is in accord with the mechanistic cycle shown in Figure 9, it is not unique to this mechanism as indicated in Figure 8. The most unique feature of the mechanism in Figure 9 is the formation of a substrate radical. The formation of this species has been examined using several approaches which are reviewed below.

a. Rearrangement, Epimerization, and Radical Clock and Radical Trap Reactions. These types of diagnostic reactions have all been utilized in the case of P450.[5,6,114−118] In some cases, the same diagnostic substrates have been used for MMO and P450 allowing a direct comparison.[30,32] For example, allylic rearrangement of 3,3,6,6-tetradeuteriocyclohexene and epimerization of *exo,exo,exo,exo*-2,3,5,6-tetradeuterionorbornane upon hydroxylation were observed for both enzymes, although, for both substrates, the rearrangement was greater in the case of the P450 reactions.[32] Likewise, radical clock reactions of P450[114,115,119−121] and MMO[122,123] have been reported. In the case of P450, these experiments have shown rearranged products, indicative of the existence of substrate radical intermediates. In contrast, results from MMO systems are less consistent. The enzyme from *M. trichosporium* catalyzed the oxidation of a range of radical clock reagents and gave varying extents of rearranged products,[122,123] whereas the MMOH from *M. capsulatus* gave little or no rearranged product.[123,124] In the case of the radical clock 1,1-dimethylcyclopropane, Frey and co-workers[122] also observed formation of 1-methylcyclobutanol (13%), which was attributed to the transient formation of a carbocation intermediate as in Figure 8, mechanism **II**. Spin traps have also been applied to the oxygenase systems to detect radical intermediates. Carbon-centered radical intermediates have been reported by spin trapping in reactions with MMO from *M. capsulatus* (Bath).[100]

b. Chiral Substrates. A different approach for the detection of a substrate intermediate is the use of chiral substrates. Substrate intermediates that are free to rotate in the active site may undergo partial or complete loss of chirality during the reaction. This approach has been used successfully in the case of P450, but it was limited by the fact that P450 substrates are generally comparatively large and asymmetric, introducing the possibility of steric restriction to motion in the active site.[125] In the case of MMO, it was possible to utilize carrier free (*R*)- and (*S*)-[1-^{2}H,1-^{3}H]ethane as a substrate. This substrate is small and not expected to be significantly constrained in the active site given the wide range of substrates that can be turned over by MMO. The only organic product of this reaction is ethanol which was converted to a diastereomeric analog and analyzed by ^{3}H-NMR.[98] It was observed that both (*R*)- and (*S*)-ethane underwent approximately 35% inversion of configuration, thus providing direct evidence for a substrate intermediate that can rotate in the active site before the completion of the reaction. Given the fact that ethyl cations have not been reported for aqueous solution at neutral pH, it was postulated that the substrate intermediate was an ethyl radical. In contrast to the radical clock experiments, nearly identical results have been observed in this chiral ethane experiment for the enzymes from *M. trichosporium* and *M. capsulatus*.[126]

c. Isotope Effects. If the mechanism of MMO involves the formation of a substrate intermediate in which the C−H bond of substrate is broken, then a substantial deuterium kinetic isotope effect (KIE) is expected. In steady-state experiments using the reconstituted MMO system from *M. trichosporium*, Donnelly and co-workers[32] observed a $^{D}(V/K)$ KIE of approximately 8.4 when comparing initial velocities of CH_4 and CD_4 turnover. There was little effect on V_{max} in these same experiments. Different results have recently been obtained for the reconstituted MMO system from *M. capsulatus*.[127] These results show that there was a small isotope effect on V_{max} (1.75), but the isotope effect on K_M was negligible (0.88). The MMO system presents a unique opportunity to determine the specific step in the reaction cycle that is isotope sensitive. This is because MMO is the only oxygenase that catalyzes the oxidation of unactivated hydrocarbons in which the kinetics of the reaction of hydrocarbons with an activated intermediate can be directly observed. Inter- and intramolecular KIEs for methane turnover have recently been determined for the single turnover reaction of *M. trichosporium* MMOH.[99,128] The only process in the catalytic cycle that showed a deuterium KIE during its reactions was the decay of compound Q, in accord with the previous observation that the presence of substrate had no effect on any of the other intermediates. No KIE was observed on the formation of compound Q, but a dramatic effect was observed on the decay reaction, which appears to encompass the oxygenation reaction. As described above, the addition of substrates causes the decay of compound Q to increase linearly with substrate concentration. The second-order rate constant obtained from this experiment was found to be 50−100 times larger for CH_4 than for CD_4. This is one of the largest KIEs ever observed in biology and strongly supports complete C−H bond breaking in the transition state. If assumed that the rate-limiting step in catalysis is C−H bond breakage, then this result provides support for all of the mechanisms in Figure 8 except for **III**, **VI**, and **VIII**. As illustrated in Figure 10, the use of the other isotopic homologs of methane showed a linear decrease in rate constant with increase in substrate deuterium content. This supports the observation of a large isotope effect and shows that the effect must be due in large part to a primary KIE, since a substantial secondary KIE would cause a nonlinear dependence on deuterium content.

It was also possible to determine the KIE on the basis of product analysis after a single turnover of MMOH in the presence of each of the deuterated homologs of methane. In this case, the maximum intermolecular KIE of 19.3 was observed for a 1:1 mixture of CH_4 and CD_4.[99,128] Smaller intramolecular isotope effects were observed for the other isotopic homologs to a minimum KIE of 3.9 for CH_3D. These values are large, supporting the general conclusion that C−H bond breaking occurs during the transition state, but they are uniformly less than the values obtained by direct observation of compound Q decay. This suggests that the formation of products is more complex than simple reaction with compound Q. One

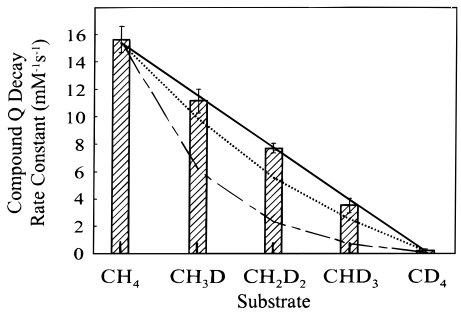

Figure 10. Compound Q second-order decay rate constants for differentially deuterated methane. Shown are the second-order rate constants for the reaction between compound Q and methane deuterated to various degrees. The second-order rate constant is obtained from the slope of the plot of compound Q decay rate constant vs methane concentration (see Figure 7). The solid line is drawn to highlight the linear trend with a primary KIE of 100, and a secondary KIE of 1. Error bars represent one standard deviation, data per point ≥30. The broken lines are the results of simulations as described in experimental procedures. The parameters chosen for each simulation give an apparent KIE of ∼100: (···) Primary KIE of 60 and a secondary KIE of 1.2; (- — -) Primary KIE of 12 and a secondary KIE of 2. Data from ref 99.

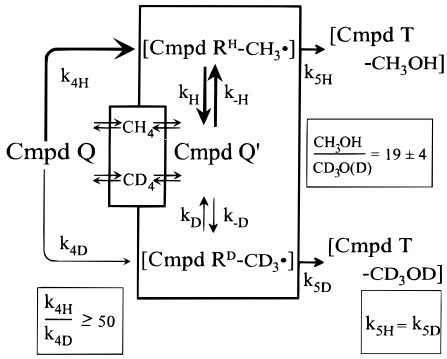

Figure 11. Hypothetical scheme to account for observed isotope effects in MMOH turnover.[99]

possibility, illustrated in Figure 11 is that the hydrogen abstraction reaction is quasi-reversible, generating an altered form of compound Q with a somewhat different optical spectrum. Because there would be an isotope effect on this reabstraction, a putative substrate radical intermediate initially formed by abstraction of deuterium would be more likely to abstract OD• and go on to product than the substrate radical intermediate formed by hydrogen atom abstraction. Consequently, the product distribution would be enriched in the products from deuterium abstraction, thereby decreasing the apparent isotope effect. The difference in observed intramolecular isotope effects in the product distribution from the isotopic homologs is unexpected; in the absence of other factors it should equal the primary KIE divided by the secondary KIE in each case. A similar change in observed KIE with deuterium content was observed for methane activation on a zirconium complex by Wolczanski and co-workers.[129] In this case, the unexpected shift was attributed to a variable secondary KIE. In any case, it seems likely that there is a contribution from a significant secondary KIE for the product-forming reaction. Since this does not appear to be true for the compound Q decay reaction, it seems likely that there

are at least two reactions in which the C−H bond can be broken. If this is the case, then it is possible that other MMO substrates will show very different isotope effects than methane. This is borne out in the reaction of ethane which was shown to exhibit no deuterium KIE for compound Q decay, but a KIE of 4.2 for product formation.[98] The large difference between these similar substrates for compound Q decay suggests that their interactions with compound Q are different. This may reveal a selectivity for methane which is not apparent from any other experimental approach. However, given that methane is the only physiologically relevant substrate for MMO, such selectivity should not be surprising.

2. Mechanisms Based on Concerted Oxygen Insertion and C–H Bond Cleavage

a. Activation Invoking an Active Site Residue. The absence of rearranged products in the turnover of radical clock substrates for MMO isolated from *M. capsulatus*[123] raises the possibility that there is more than one mechanism or that the enzymes derived from different bacterial sources may have different mechanisms. Alternative pathways involving concerted insertion reactions, such as those illustrated in Figure 8 (**III**−**VI**, **VIII**, and **IX**), have been proposed[7,123,130,131] One such proposal[7] invokes the participation of Cys-151, since it resides in the active site of MMOH in a position analogous to that of Tyr-122 of R2, which is the site of the essential stable protein radical for that enzyme.[71,132] Under this proposal, the reaction of MMOH might begin by an activated form of MMOH abstracting a hydrogen atom from Cys-151 to yield a cysteinyl radical and a radical form of the binuclear iron cluster [Fe^{III}-Fe^{III}−O•]. In a subsequent reaction, the cysteinyl radical would abstract a hydrogen atom from methane simultaneously with insertion of an oxygen radical from the cluster into the C−H bond (Figure 8, **VIII**). This would restore the singlet cysteine and leave methanol as a transient bridging moiety for the cluster. The postulated active site cysteinyl radical could also be invoked in a hydrogen abstraction/rebound mechanism if its role is to regenerate a cluster-based radical following hydrogen atom abstraction from methane by the [Fe^{III}-Fe^{III}]−O• state of the cluster (Figure 8, **VII**). This would allow radical recombination between CH_3• and the cluster radical to yield the bound methanol. Presently there is no evidence for or against these mechanisms. However, they both invoke a reaction between methane and a reactive state of the cluster which is one equivalent more reduced and consequently significantly less electrophilic than compound Q. Model systems at this oxidation state do not react with methane, but these systems also do not have an equivalent of the cysteinyl radical placed to facilitate the reaction. Site-directed mutagenesis and/or chemical modification of MMOH or related enzymes should provide a method to test this hypothesis in the future.

b. A Nonsynchronous Concerted Insertion Mechanism. In investigations of the P450 mechanism using radical clock probes, it has been reported that the lifetime of the substrate radical observed is dependent on the particular radical clock substrate. Recently, Newcomb and co-workers[133] have used the ultrafast, cyclopropyl-based radical clock, (*trans*,*trans*-2-*tert*-butoxy-3-phenylcyclopropyl)methane to study the mechanism of P450. This probe yields distinguishable products for radical-based and cation-based mechanisms. Oxidation by P450 gave products from reactions which suggest the involvement of both radical and cation intermediates. In the previous studies with other radical clocks, each of the analogous intermediates collapsed to the same product and all of the products were interpreted as deriving from radical intermediates. It is proposed that cation formation occurs to different extents in these reactions accounting for the inconsistency of the results. The new probe allowed for the accurate quantitation of radical formation, and a radical intermediate lifetime of 70 fs was calculated. This amount of time is too short for formation and rebound of a discrete intermediate, so a concerted mechanism was proposed. The radical revealed by the probe is proposed to derive from the difference in the bond vibration rates of C−H and Fe−O bonds. This difference causes the oxygen insertion reaction to proceed in a nonsynchronous manner giving the substrate a radical character for a short time during which rearrangements can occur. The short lifetime also suggests that there is minimal motion of atoms in the reaction, ruling out a linear transition state. Thus, a side-on approach of the substrate to the activated oxygen species was proposed.

Clearly, a similar mechanism could be proposed for MMO, and it would account for some discrepancies that have been noted. For example, the degree of inversion of configuration noted for chiral ethane oxidation by MMO indicates a radical intermediate lifetime of only about 10^{-12} s if inversion involves rotation around an unrestricted single bond, which appears likely. This short lifetime is difficult to rationalize for a linear transition state as proposed for the hydrogen atom abstraction/rebound mechanism, but it is easily accounted by the nonsynchronous concerted mechanism (Figure 8, mechanism **VI**). On the other hand, the exceptionally large deuterium KIE observed for methane turnover[99,128] is not compatible with either a concerted reaction or a side-on transition state complex. This new mechanism is potentially a very important development in the oxygenase field and further experimentation using the MMO systems is clearly warranted.

c. A Cluster-Based Concerted Mechanism. Another interesting new mechanistic proposal invokes direct reaction of methane with a resonance form of compound Q in which both of the bridging oxygens play roles in the chemistry[130,131] (Figure 8, **III**). In this mechanism, one oxygen acts as an electrophile to attack the C−H bond carbon while the second oxygen serves as a nucleophile to attack the H and weaken the bond. This process yields a pentavalent carbon intermediate. Subsequent insertion of the carbon-bound oxygen into the activated C−H bond would restore the tetravalent carbon in the form of product and the diferric cluster. The process as a whole can be considered as an electrophilic attack on the C−H bond with nucleophilic assistance via the multicentered cyclic transition

state. One interesting aspect of this proposed mechanism is that it would require a precise alignment in the active site, and thus could explain why MMO most efficiently turns over methane. It is possible that the large deuterium isotope effects observed for methane turnover could result from substantial secondary isotope effects inherent in formation of the pentavalent intermediate in this mechanism. However, analysis of the KIE data for the isotopic homologs of methane suggests that the KIE is related to primary rather than secondary isotope effects.

d. Activation Based on Formation of an Iron−Carbon Bond. A mechanism invoking an intermediate iron−methane carbon bond has been proposed for MMO on the basis of so called "Gif" chemistry (Figure 8, **V**). It has been shown that mixtures of Fe(II) and oxygen or Fe(III) and peroxides in various solvents will catalyze the oxidation of alkanes. In order to account for the product mixture, the formation of an intermediate Fe(III) organometallic species into which O can insert is postulated.[134−136] Although this type of mechanism has not been ruled out for MMO, it generally gives a different product distribution which favors ketone formation at secondary carbons rather than hydroxylation at primary carbons. It is also not apparent how this mechanism could account for the partial inversion of configuration and intermediate formation suggested by the oxidation of chiral ethane or the large deuterium KIE observed for methane turnover by MMO.

E. Regulation

1. Complex Formation between the Components

a. Effect on Steady-State Kinetics. Despite the fact that catalysis by MMOH alone is possible if the enzyme is reduced by nonenzymatic techniques or supplied with hydrogen peroxide, the MMOB and MMOR components do have profound effects on catalysis. These effects can be classified as regulatory in nature, and appear to be mediated through the formation of component complexes[63] (see Table 2). The first indication of these effects arose from the observation that the initial velocity of steady-state turnover does not increase in a linear fashion with increases in the concentration of MMOB or MMOR, nor does it rise to a constant level and saturate.[41,63] Instead, addition of either component causes the initial velocity to increase sharply to a maximum and then decrease. The effect is most dramatic in the case of MMOB where the maximum increase is 150-fold for some substrates. The amount of increase and the ratio of the concentrations of the components that gives the maximum rate depends upon the absolute concentrations of each component, which is consistent with the formation of an active MMOH−MMOB−MMOR complex. The steady-state kinetic behavior can be accounted for on the basis of the model shown in Figure 12, in which several types of complexes form between the components.[63] According to this model, the inhibition observed at high MMOB and MMOR concentrations derives from two factors. First, an inhibitory complex involving two MMOB per active site of MMOH is proposed to form. Second, ancillary complexes between MMOB and

Table 2. Significance of Component Complexes on MMOH Catalysis

process	MMOH alone	effect of added B	effect of added R	effect of added B + R	importance to catalysis
component binding[63,87]	NA	K_D (H_{red}·B) = 500 μM K_D (H_{ox}·B) = 70 nM	K_{D1} (H_{ox}·R) = 10 nM	no effect up to 1:1:1 complex. Excess B inhibits R binding.	component complexes are essential for efficient catalysis
electron-transfer kinetics from NADH[47]	none	none	MMOH reduction $k \approx 3$ s^{-1}	MMOH reduction $k \approx 3$ s^{-1}	MMOR necessary for reduction of MMOH by NADH
electron-transfer[86,87] thermodynamics	$E_m = +48$ mV $E_1 > E_2$	$E_m = -84$ mV overall decrease in E_m of 132 mV $E_1 > E_2$	$E_m = +97$ mV $E_2 > E_1$	$E_m = \sim+100$ mV $E_2 > E_1$	R stabilizes the reduced state, and 2e$^-$ transfer.
rate of reaction between diferrous MMOH and O_2[52,94]	$k = 0.02$ s^{-1}	$k = 22$ s^{-1}	$k = 0.02$ s^{-1}	Substrate has no effect $k = 1.5$ s^{-1}	B has little effect if R is present B complexes greatly enhance the rate of the first step in oxygen activation
rate of compound Q formation and decay[51]	Q is unobservable	$k_{form} \approx 1.2$ s^{-1} $k_{decay} \approx 0.05$ s^{-1}	Q is unobservable	$k_{form} \approx 1.2$ s^{-1} $k_{decay} \approx 0.05$ s^{-1}	B effects control rates of O_2 activation and compound Q formation
rate of product release[94]	NA	B inhibitory at B:H > 2	not investigated	B inhibitory at B:H > 2	decrease in turnover rate under nonphysiological conditions
yield of product from a single turnover of MMOH[52,86]	40%	80%	44%	89%	B increases the fidelity of catalysis; R may also play a minor role
rate-determining step in catalysis if MMOH artificially reduced[52]	reaction between diferrous MMOH and O_2 for most cases	reaction between compound Q and substrate or product release	reaction between diferrous MMOH and O_2 for most cases	reaction between compound Q and substrate or product release	B required for rapid O_2 activation; R does not impede this catalytic subsystem overall

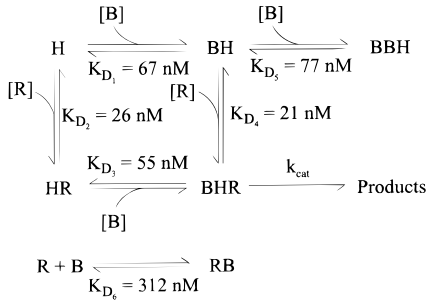

Figure 12. Thermodynamic binding diagram to account for the steady-state kinetics observed for MMOH in the presence of MMOB and MMOR. H = MMOH, B = MMOB, R = MMOR. Data from ref 63.

MMOR and between two MMOBs form that cannot interact with MMOH, thereby removing these components from the equilibria that enhance MMOH reactivity.

b. Cross-Linking. The occurrence of protein complexes can be detected in a straightforward manner through the use of chemical cross-linking reagents. One particularly useful class of such reagents are the carbodiimides, which cross-link protein carboxylate and amine pairs by the elimination of water. These side chains would normally have electrostatic interactions with one another and can form an ion pair across a subunit boundary. The resulting covalent cross-link is "zero length" because no atoms of the carbodiimide are incorporated into the product. The cross-links are detected by changes in the mobility of the component on denaturing PAGE and identified by subsequent sequencing of the N-terminals of the cross-linked peptides. By using this technique, all of the complexes indicated in Figure 12 were identified.[63] MMOB cross-linked only to the α subunit of MMOH and MMOR only to the β subunit, suggestive of specific binding sites. Strong cross-links were detected between the β subunits, as well as the α and β subunits of MMOH, which is indicative of their juxtaposition in the structure. This orientation was later found to be in accord with the X-ray crystal structure.[72,137] In addition, a nonfunctional homodimeric complex of MMOB was detected. It was also demonstrated that facile formation of a cross-link between two groups on the surface of a single MMOB resulted in the loss of ability to stimulate the catalytic reaction, as well as the loss of ability to cross-link with MMOH. This observation is supportive of the proposal that physical complex formation is a requirement for the activation engendered by MMOB.

c. Quantitation by Fluorescence and EPR Titrations. Endogenous tryptophan fluorescence can be used to directly detect and quantitate formation of some component complexes.[63] Complex formation between diferric MMOH and MMOB or MMOR results in fluorescence quenching, allowing the K_d values to be determined by direct titration. Similarly, quenching of the MMOB fluorescence by the essentially nonfluorescent MMOR allowed the formation and stability of this complex to be measured. The dissociation constants measured in this direct way were found to be in good agreement with those used to fit the model presented in Figure 12. Fluorescence titration was also used to detect and quantitate the complex between diferrous MMOH and MMOB, which resulted in an increase in MMOH fluorescence. This complex is at least 3 orders of magnitude weaker than those presented in Figure 12. The ramifications of this decrease in affinity on redox potential and regulation are discussed below.

Spectroscopic techniques have also been used to directly detect component complexes. The first example of this was the observation that the EPR spectrum from the mixed-valence state changed dramatically, in both resonance positions and magnitude of the antiferromagnetic coupling, when the complex between MMOH and component B was formed.[63] Similarly, addition of MMOB to diferrous MMOH resulted in a sharpening of the $g = 16$ EPR signal, which is indicative of complex formation. Although no changes have been noted in the X-ray absorption spectra of the MMOH−MMOB complex[56,78] the MCD[69,138] and ENDOR[139] spectra are perturbed. Recent ligand field CD studies on the MMOH−MMOB complex from *M. trichosporium* have detected conformational changes in the active site after the addition of a substrate or an inhibitor.[138] It should be noted that these conformational changes only occurred in the presence of MMOB, indicating that MMOB may somehow open the active site in order to admit small molecules. However, not all small molecules favorably bind to the irons, because azide and chloride addition caused no spectral perturbations. This indicates that the MMOH active site is less electrophilic that other binuclear iron proteins (R2 and hemerythrin), which have been shown to bind azide,[68,140,141] consistent with the role of the binuclear iron cluster in charge donation in order to activate dioxygen. Complementary MCD data showed that a direct change in the iron ligation was not the cause for the observed spectral changes. More specifically, the binding of MMOB perturbed the ligand field environment of one of the irons, whereas, the binding of substrate seemed to affect the other iron, lending insight into the possible binding mode of MMOB and substrate.

The effects of MMOR on the EPR spectra of MMOH are less dramatic than those of MMOB; however, some perturbations can be detected. For example, there is a detectable change in the coupling constant for the binuclear iron cluster in the mixed-valence state. The mixed-valence state of MMOH has a coupling constant $J = \sim -30$ cm^{-1} ($H = -2JS_1S_2$), but in the presence of MMOB, $J = \sim -5$ cm^{-1},[142] indicating a substantial decrease in the strength of the antiferromagnetic coupling upon complexation. These observations indicate that surface contacts between MMOH and MMOB and/or MMOR cause changes in the environment of the buried active-site binuclear iron cluster and could potentially be involved in regulation of the chemical reactions that occur at this site.

2. Product Distribution in Catalytically Active Subsystems

The discussion of catalysis above indicates that turnover of MMOH can be carried out in at least three systems missing one or more of the components:[27,40,53] system I, NADH, MMOR, MMOH, O_2; system II, diferric MMOH, H_2O_2; and system III, diferrous MMOH, O_2.

The same products result from turnover in these subsystems as observed for the fully reconstituted MMO system. Systems I and II can undergo multiple turnover, whereas system III is a single turnover system. By using these systems, it is possible to evaluate the effect of addition of MMOR and/or MMOB on product formation rate and distribution.

It is clear that the active site of MMO is at the binuclear iron cluster of MMOH. Therefore, it is reasonable to assume initially that the reductase and component B serve only to transfer electrons to MMOH from NADH. However, if this were true, then these components would change only the rate of system I, because only system I uses NADH. Moreover, no effects on the product formation reaction would be expected. However, it has been proven that both MMOB and MMOR affect the rate of the product-forming reaction of each of these subsystems.[53] For example, in system II, no electron transfer is required, but MMOB causes an 80% *decrease* in maximum velocity for most substrates. This is just the opposite from the effect that MMOB has on system I. Also, the product distributions for many substrates that can be oxidized at more than one carbon are different in each system and are dependent upon the presence of MMOR or MMOB. The best-studied example of these effects on product distribution involved the oxidation of isopentane.[53] Although each system yielded all possible isopentanols, the distributions were markedly different. For each system, the addition of MMOB caused the distribution to shift toward hydroxylation of primary carbons. The addition of MMOB to systems I (i.e. the complete reconstituted system) or MMOR and MMOB to system III caused the distribution of isopentanols to become identical. In contrast, addition of the other two components to system II yielded a readily distinguishable distribution. On the basis of the fact that the same types of products are produced by each system, the reactive form of oxygen generated at the binuclear iron cluster in systems I, II, and III is unlikely to be different. Therefore, structural perturbations were proposed to be the cause of the observed product distribution changes. More particularly, the specific active site structure may change the way that a given substrate is presented to the reactive oxygen. A principal difference between the systems is that while both systems I and III require MMOH to pass through the diferrous state, system II does not. Thus, it was proposed that structural changes occur upon reduction. Supportive evidence for this is found in the dramatic changes in binding constant for the complex between MMOB and MMOH upon reduction, which was noted above, as well as by the differences that are observed in the crystal structure of the reduced form of MMOH.[71]

If it is true that the reactive oxygen species is the same for each catalytic subsystem and that the differences in product distribution can be ascribed to structural differences, then it must also be true that the activated MMOH at the point of oxygen insertion has some "memory" of the system that produced it. Spectroscopic evidence for this "hysteresis" derives from the fact that the changes caused in the EPR spectrum of diferrous MMOH are maximized by about 0.3 MMOB per MMOH active site, despite the fact that the fluorescence spectral changes continue at least until a 1:1 stoichiometry is reached.[63] In contrast, the mixed-valence MMOH EPR spectrum continues to change until a 1:1 complex is achieved. Also, for systems I and III, the complete shift in product distribution is observed for MMOB at ~5% of the MMOH active site concentration. On the other hand, a stoichiometric amount of MMOB is required to maximize the distribution shift in system II. Comparison of the effect of MMOB on initial velocity (discussed above) with that on product distribution in system I shows that the former continues at least until a 1 MMOB per active site ratio is achieved, whereas the latter is maximized at greatly substoichiometric levels. This implies that MMOB has at least two roles in catalysis occurring in different relative concentration domains. One explanation for the change in distribution at substoichiometric levels is the occurrence of hysteresis in the relaxation of the component B-induced conformational change of MMOH. This would function to allow the entire population of MMOH to adopt an altered structure with only a small amount of MMOB present. This would only be possible if MMOB can dissociate from MMOH at a high rate relative to the relaxation of the conformational change. Accordingly, rapid dissociation is unlikely from the diferric state of MMOH, which has a high affinity for MMOB, giving rise to the stoichiometric interaction of MMOB and the more oxidized states of MMOH. In contrast, the diferrous state of MMOH has a lower affinity for MMOB, and thus rapid migration of MMOB could be possible.

3. Oxidation–Reduction Potentials of MMOH

The formal redox potential values for MMOH from *M. capsulatus*[61,143] and *M. trichosporium*[87] have been measured, using either the EPR signal from the mixed-valence state [87,143] or the Mössbauer spectra of the three redox states,[87] to quantitate the extent of reduction. The results are summarized in Table 3. The studies gave somewhat different results despite the structural similarity of the enzymes. It is possible that different sets of mediator dyes used in the two studies may account for the differences in measured potentials. The dyes in the *M. trichosporium* study caused no perturbation in the EPR spectrum of the mixed-valence state, whereas this was not the case in the *M. capsulatus* study. The titration of the *M. trichosporium* MMOH showed formal potentials of $E_1^{\circ\prime} = +76$ mV and $E_2^{\circ\prime} = +21$ mV (± 15 mV) ($E_{mid} = \sim +48$ mV). Upon addition of MMOB (1:1 vs MMOH active sites), the MMOH potentials shifted negatively to $E_1^{\circ\prime} = -52$ mV and $E_2^{\circ\prime} = -115$ mV (± 15 mV) ($E_{mid} = \sim -84$ mV). This shift in potential was forecast by the observed change in binding affinity for the MMOH−MMOB complex upon reduction of MMOH. A thermodynamic state diagram predicts a decrease in affinity of 4−5 orders of magnitude. This is somewhat more than the 3−4 orders of magnitude actually observed, but it is within the error of the redox and binding measurements.[87] The redox potential of MMOH from *M. capsulatus* was also observed to decrease when a mixture of MMOB and MMOR was added, but the

Table 3. Summary of the Redox Potential Values of the MMO Component and Substrate Complexes

	M. trichosporium OB3b[g]			*M. capsulatus* (Bath)[h]		
MMO components[a]	$E_1°'$ (mV)[b]	$E_2°'$ (mV)[c]	E_m (mV)[d]	$E_1°'$ (mV)[b]	$E_2°'$ (mV)[c]	E_m (mV)[d]
H	76	21	48	48	−135	−44
HB	−52	−115	−84			
HR	80	114	97			
HBR	76	125	100	*f*	*f*	
H + substrate[e]	72	−33	20	30	−156	−63
HB + substrate[e]	−48	−119	−84			
HBR + substrate[e]	70	128	99	>150	>150	

[a] Stoichiometry of the MMOB and MMOR components are relative to MMOH active sites. H = hydroxylase; B = component B; R = reductase. [b] Represents the formal redox potential value for the first electron transfer. Values given are relative to SHE (standard hydrogen electrode). Error = ±15 mV. [c] Represents the formal redox potential value for the second electron transfer. Values given are relative to SHE. Error = ±15 mV. [d] Represents the overall midpoint potential value. $E_m = (E_1°' + E_2°')/2$. [e] CH_4 was used in the *M. trichosporium* study, whereas, propylene was added to the *M. capsulatus* system. In both studies, saturated solutions of substrate were used. [f] No reduction was observed under these conditions. [g] References 86 and 87. [h] Reference 143.

resulting potential was too low to measure with the system that was being used.[143]

When MMOR was added to the *M. trichosporium* MMOH, or the MMOH−MMOB complex, the midpoint potential was found to be higher that those of MMOH alone.[86,87,144] Measurement of the formal potentials showed that $E_1°'$ and $E_2°'$ were switched in relative magnitude by the addition of MMOR, making two electron transfer favored. The reaction of MMOH with O_2 only occurs at an appreciable rate for the diferrous form. Thus, an important role of MMOR appears to be to change the environment of the cluster such that the correct state to initiate catalysis is produced as electrons are transferred. This is a much more subtle and complex function than simple electron transfer. Because MMOB has little or no effect on potential when MMOR is present, it appears that the effect of MMOB is masked in some way by MMOR. It is clear that MMOR at near stoichiometric concentrations does not block MMOB binding because the characteristic spectroscopic changes caused by MMOB are still observed in the presence of MMOR. These observations also imply that the decrease in affinity between MMOH and MMOB caused by reduction of MMOH is probably not expressed when MMOR is bound. It should also be noted that 0.1 MMOR to MMOH ratio afforded the same shift in redox potentials as the 1:1 MMOR−MMOH case. We proposed that this due to a hysteretic effect on MMOH following dissociation of MMOR. It is interesting to note that this phenomenon may be physiologically relevant, because the MMOR−MMOH ratio in *M. trichosporium* is 1:10.

Substrate addition to MMOH or any of its component complexes has little or no effect on the redox potential in the case of the enzyme from *M. trichosporium*.[86,87,144] In contrast, the potential of the MMOH−MMOB complex of *M. capsulatus* shifts to a very high value upon addition of substrates[143] and may undergo the same exchange of $E_1°'$ and $E_2°'$ observed for the *M. trichosporium* MMOH in the presence of MMOR. Thus far, there is no evidence that the substrate binds in the catalytic cycle before formation of compound Q. Therefore, the significance of the reported effect on redox potential by substrate in the *M. capsulatus* case cannot be determined.

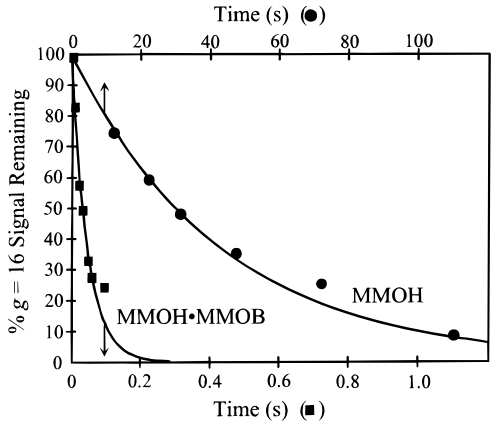

Figure 13. Effect of MMOB on the rate of disappearance of the $g = 16$ EPR signal of diferrous MMOH upon addition of O_2. MMOH (0.5 mM active sites) alone (●) or in the presence of MMOB (0.5 mM) (■) in buffer was rapidly mixed with O_2-saturated buffer (1.4 mM) (1:1) at 4 °C and then frozen at the time points indicated using freeze−quench technique for the preparation of EPR samples. Decay of the $g = 16$ signal of diferrous MMOH was fitted to a single exponential curve (solid line). X-band EPR measurement conditions are as follows: temperature = 8 K; microwave power = 0.4 mW. Data from ref 52.

4. Gating Effects of MMOB on the O_2 Reactivity of MMOH

All of the transient experiments that revealed the intermediates of the MMOH catalytic cycle included MMOB at concentrations stoichiometric with the MMOH active site concentration. This was necessary because diferrous MMOH reacts only very slowly with O_2 in the absence of MMOB. As illustrated in Figure 13, the addition of MMOB causes approximately a 1000-fold increase in the rate of disappearance of diferrous MMOH as monitored by the characteristic $g = 16$ EPR signal of this state.[52] This "gating effect" of MMOB is an important change, because it shifts the reaction with O_2 from rate limiting to not rate limiting for methane turnover.

The impact of the MMOB gating effect on catalysis can be investigated in more detail by observing the effect of the ratio of MMOB to MMOH active sites on the time course of compound Q during a single turnover, as illustrated in Figure 14. It can be seen that the time course is more complex at substoichiometric MMOB to MMOH ratios and can no longer be fit to a two exponential time course characteristic

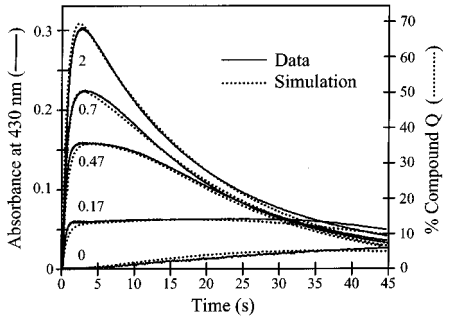

Figure 14. Effect of MMOB on the time course of compound Q after reaction of diferrous MMOH with O_2. MMOH (120 μM active sites) and MMOB (0−240 μM) in buffer were rapidly mixed with O_2-saturated buffer (1:1) at 4 °C. The MMOB−MMOH diiron cluster ratio was as shown in the figure. Time courses of the reactions were monitored at 430 nm, which is maximal for compound Q (solid lines). At a ratio of 1.3:1 MMOB−MMOH sites, the time course was essentially superimposable on the 2:1 curve, so it was omitted for clarity. The dotted lines represent the simulation of the kinetic model shown in Figure 15. Data from ref 52.

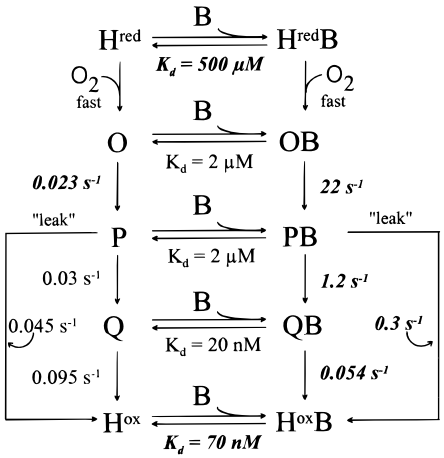

Figure 15. Proposed kinetic model for a single turnover reaction in the absence of substrate. Experimentally determined rate and equilibrium constants are shown in boldface italics. Other constants were chosen to give the best simulation. The abbreviations used in the model: H^{red}, diferrous MMOH; H^{ox}, diferric MMOH; B, MMOB; O, compound O; P, compound P; Q, compound Q; H^rB; OB; PB; QB; and H^oB, MMOB bound form of each species. See Figures 14 and 16 for simulations based on this model.[52]

of a single homogeneous population undergoing two successive, irreversible first-order reactions (formation and decay of compound Q). In particular, a plateau in the time course is evident, especially at low MMOB−MMOH ratios. One hypothetical scheme that accounts well for the data is shown in Figure 15.[52] The scheme was simulated by numerical integration and fitted to the data shown in Figure 14 (dotted lines). Many of the rate constants and equilibrium constants for this model have been directly measured.[51,63,87] A "leak" is incorporated in the model to account for the fact that the product yield from a single turnover is approximately 40% in the absence of MMOB and 80% in its presence. Compounds P and Q are the only known "activated" intermediates that could undergo an alternate reaction that would decrease the product yield. It was observed that similar product yields were obtained even when various substrates were used that react

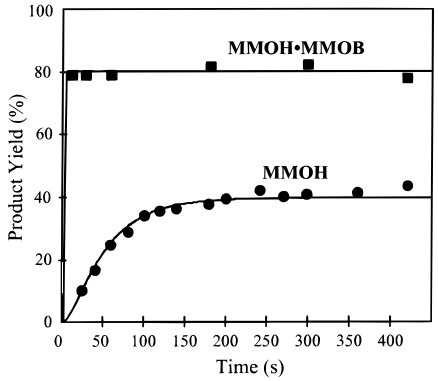

Figure 16. Effect of MMOB on the time course of propylene oxidation during single turnover reactions of diferrous MMOH. Propylene oxide was extracted and analyzed after a single turnover reaction of diferrous MMOH (0.5 mM active sites) without (●) or with a stoichiometric amount of MMOB (■). The solid line indicates the simulated time courses of the product formation based on the kinetic model shown in Figure 15 augmented by a reaction of compound Q with propylene to form product (k = 3500 M^{-1} s^{-1}).[52]

with compound Q at different rates. Since compound Q reacts with high concentrations of substrate so much faster than it autodecays (see Figure 15), it is very unlikely that the leak stems from compound Q. Therefore, the leak is drawn at the level of compound P.[52] The model shown in Figure 15 contains many free constants, however, the significantly different shapes and complexity of the data shown in Figure 14 considerably constrain the range of possible values for the unknown constants. In order to fit the experimental data, the simulation requires: (i) acceleration of both compound P and compound Q formation in the presence of MMOB, (ii) nearly MMOB-independent compound Q decay, and (iii) much higher affinity between MMOB and the MMOH as MMOH becomes diferric. The best fit values of the constants allow some compound Q to quickly form as the diferrous MMOH−MMOB complex is rapidly oxidized. However, the compound Q concentration then plateaus as MMOB is sequestered in the high-affinity diferric MMOH−MMOB complex. The simulation of the model predicts that MMOB is required for both compound Q and compound P to accumulate. This is in accord with the Mössbauer spectrum of ^{57}Fe-enriched diferrous MMOH that was exposed to O_2 saturated buffer and frozen after 35 s at 4 °C, which showed only the presence of diferrous and diferric MMOH in approximately the 1:1 ratio predicted by the model.[145] In contrast, compounds P and Q should accumulate in ≥70% yield during the first few seconds of the reaction in the presence of MMOB, which has been observed in freeze-quenched samples by Mössbauer spectroscopy.[94,95,97]

It is possible to use the model shown in Figure 15 to predict the outcome of substrate turnover and compare it with experimental results. The model is modified such that compound Q reacts with substrate at a rate determined directly by observation of the decay of compound Q in single turnover experiments. The result is illustrated in Figure 16 for propene oxidation. The model correctly predicts that propene is converted to propene oxide much more slowly and in lower yield in the absence of MMOB. However, it is interesting to note that the yield is only a factor of

2 lower in the absence of MMOB despite a greatly extended reaction time during which any of the species could spontaneously react along a different path. Thus, the system remains fairly tightly coupled even in the absence of MMOB. This suggests that the term "coupling protein" suggested for MMOB[123,146] does not reflect its major function, which appears to be better described as the "gating protein".

5. The Effect of MMOR and Ternary Component Complexes on O_2 Reactivity

The addition of MMOR during the reaction of diferrous MMOH with O_2 has no effect on the rate of this reaction. When both MMOB and MMOR are added, the reaction is about 10-fold slower than when only MMOB is added. This change will not be kinetically significant to turnover since this decrease is not great enough to make this process rate limiting in the overall reaction. Preliminary results indicate that MMOR does have an effect on the subsequent reaction, as it may increase the rate of conversion from compound P to compound Q by about 10-fold. These effects of MMOR on the transient kinetics do not alter the rate of multiple turnover, but may have implications on increasing the efficiency of the enzyme. By increasing the rate of the conversion of P to Q, MMOR may stop the small leak, that is modeled in Figure 15, by not allowing compound P to accumulate. Since compound P seems to be a peroxy complex, it is plausible for this species to nonproductively react with an active-site residue or another adventitious substrate. Alternatively, the peroxide may simply dissociate. It is apparent that MMOR plays another role besides electron transfer in MMO catalysis, and this warrants ongoing investigation.[86]

6. Summary of Regulatory Effects of MMOB and MMOR

Both MMOB and MMOR appear to impose several effects during catalysis which are mediated through complex formation and subsequent changes in coupled binding and redox potential energies. The major effect of MMOR appears to be to establish the correct potential values for two electron transfer into MMOH, in order to generate the state that can react with O_2. The major role of MMOB appears to be to allow this diferrous MMOH to react rapidly with O_2 and to facilitate the interconversion of subsequent intermediates leading to compound Q. Because compound Q is the state that reacts with substrate to form product, the combined actions of MMOR and MMOB maximize the overall rate of catalysis for the multiple turnover reconstituted system.

The physical basis for the effects of MMOB on oxygen reactivity are not yet known. It may be related to the substantial decrease in redox potential of the diferrous MMOH when MMOB is bound or it may be due to increased accessibility of the binuclear iron cluster in the MMOH−MMOB complex. Whatever the mechanism, it seems likely that the MMOB-induced conformational change in MMOH detected by EPR, MCD, and other spectroscopies may be responsible. However, two independent EXAFS studies on the MMOH show no significant change in the MMOH binuclear iron site in the presence of MMOB,[56,78] suggesting that the physical change is not large. It may be speculated that the conformational change consists of rather subtle electronic alterations that could not be detected by EXAFS, but do affect the O_2 reactivity. The crystal structures of diferric MMOH show that the binuclear iron cluster is shielded on one side from the outside environment (solvent) only by a one helix layer (two helices total). These two helices border an open "canyon"[71] that could comprise the binding site for the other components. These helices contain four of the amino acid residues that are ligated to the irons (Glu-144, His-147, Glu-243, His-246). Any perturbation in these helices, as might be caused by interactions with MMOB, could alter the active site environment sufficiently to affect the environment of the MMOH binuclear iron cluster. Future studies that detail the structure of the MMOH−MMOB and MMOH−MMOB−MMOR complexes will answer these questions.

III. Other Oxygenases and a Fatty Acid Desaturase That Utilize a Binuclear Iron Cluster

A. Toluene Monooxygenases

Following the discovery of the binuclear iron cluster of MMOH and the elucidation of its function in oxygenase chemistry, several other similar enzymes were recognized and are now being characterized. Among these are three toluene monooxygenases, T2MO, T3MO, and T4MO, that catalyze the formation of *o*-, *m*-, or *p*-cresol, respectively. The gene cluster for T3MO from *Pseudomonas pickettii* PKO1 has been identified,[147] but the enzyme has not been isolated. T4MO was isolated from *Pseudomonas mendocina* KR1 and proposed to be a three-component system;[148,149] however, T4MO has recently been expressed in *E. coli* and purification of the enzyme system demonstrated that T4MO is actually a four component system.[16] The components are (i) a 220 kDa hydroxylase having a subunit composition of $(\alpha\beta\gamma)_2$, with each protomer containing a binuclear iron site; (ii) a 12.5 kDa ferredoxin containing a Rieske-type center; (iii) a 36 kDa NADH oxidoreductase probably containing FAD and a [2Fe-2S] cluster; and (iv) an 11.6 kDa cofactorless effector protein. The hydroxylase component contains two copies of the primary sequence motif $(D/E)X_{(28-37)}DEXRH$, which includes the same Glu-X-X-His motif that provides all of the protein-derived ligands to the diiron clusters of MMO, R2, and stearoyl-ACP Δ^9 desaturase (Δ9D).[17,132,150] In addition to the sequence, Mössbauer and EPR measurements show that the diiron center in the resting (diferric) state probably contains a hydroxo (or otherwise triply substituted) oxygen bridge, as in MMOH. Another similarity to MMO is the presence of the small effector protein that alters the rate of catalysis by the hydroxylase subunit. The catalytic enhancement in the T4MO system is significantly less than that observed in the MMO system, although this may result from the difficulty of separating the hydroxylase from the effector protein. The T4MO system has been demonstrated to oxidize many halocarbon pollutants, such as trichloroethylene, *cis* and *trans*-dibromoethenes, 1,2-dichloroethane, and chloroform.[151] T4MO oxidations

Table 4. Spectroscopic Properties of Toluene Monooxygenase

	TMO_{ox}	TMO_{mv}	TMO_{red}	refs[a]
optical				
λ (nm)	282			15,16
EPR				
g_{max}		1.93	16	15,16
g_{mid}		1.85		
g_{min}		1.74		
Mössbauer				
ΔE_Q (mm s^{-1}), Fe1	0.93		3.21	16
δ (mm s^{-1}), Fe1	1.51		1.31	16
ΔE_Q (mm s^{-1}), Fe2	1.55		2.68	16
δ (mm s^{-1}), Fe2	0.56		1.31	16

[a] Reference 15 refers to T2MO and ref 16 refers to T4MO.

are also inhibited by acetylene, a potent mechanism-based inhibitor of MMO, which further emphasizes the similarities of these two members of the binuclear iron hydroxylase family. The T4MO hydroxylase was also shown to be capable of single turnover following stoichiometric reduction and to exhibit an integer spin EPR signal near $g = 16$ following reduction; both of which are key characteristics of an MMOH-like system. The spectroscopic properties of this and the other TMOs that have been reported are summarized in Table 4. The expression of active enzyme in *E. coli* now allows the use of site-directed mutagenesis, which offers the prospect of examining some of the structural questions that have developed from the MMO studies, but which could not be directly addressed due to the lack of an expression system for MMOH.

Purification studies of the T2MO from *Burkholderia cepacia* G4 have resolved the enzyme into a three-component system.[15] The purified components displayed a remarkable similarity to the corresponding components in the soluble methane monooxygenase enzyme system. The system consisted of (i) a hydroxylase component (211 kDa) with a $(\alpha\beta\gamma)_2$ subunit composition and one binuclear iron center per protomer, (ii) a 40 kDa reductase containing FAD and a [2Fe-2S] that could oxidize NADH to transfer electrons to an acceptor, and (iii) a cofactorless small component (10.4 kDa) that increased toluene oxidation rates by 10-fold in multiple turnover experiments. The hydroxylase component of T2MO was shown to catalyze the H_2O_2-dependent turnover of toluene, presumably through a peroxide shunt mechanism like MMO. EPR studies of T2MO indicated the presence of a mixed-valence state of the iron center with $g_{av} < 2$ when only one reducing equivalent was added, and a diferrous state exhibiting a $g = 16$ EPR signal when two or more equivalents were added. As in the case of diferrous MMOH, the latter resonance disappeared rapidly upon the exposure of the diferrous species to O_2, suggesting that this is the state that initiates catalysis. The genes for T2MO have recently been cloned and sequenced[152,153] to reveal six open reading frames, as were observed for the soluble MMO gene cluster.

Given the similar activities, subunit and component composition, and spectroscopic parameters reported thus far, it is evident that T4MO, T2MO, and MMO are probably very analogous to one another. Along with these enzymes, a number of other bacterial oxygenase systems have recently been compared to soluble MMO and other binuclear iron proteins by sequence alignments of the ligands of the diiron core.[17,132,150] These include phenol hydroxylase (PH) from *Pseudomonas* CF600,[18] xylene monooxygenase from *Pseudomonas putida*,[19] and alkane hydroxylase from *Pseudomonas oleovorans*.[19] A cyanide-resistant "alternative oxidase protein" isolated from the plant mitochondria of many species is also postulated to contain a binuclear iron center[154] on the basis of sequence comparison. An intriguing additional aspect of the iron-binding sequence is that several enzymes, including T4MO, MMOH, PH, and Δ9D, have an arginine preceding the histidine iron ligand. This may indicate a possible contribution to catalysis by a basic residue, as postulated for cytochrome *c* peroxidase.[155]

B. Stearoyl-Acyl Carrier Protein Δ^9 Desaturase

Another type of binuclear iron-containing enzyme that activates oxygen as a part of its catalytic mechanism is Δ9D.[17] Isolated from *Ricinus communis* (castor), this soluble enzyme inserts a 9,10 *cis* double bond into the bound fatty acid of stearoyl-acyl carrier protein (ACP) to convert it to oleoyl-ACP in the presence of O_2, NAD(P)H, NAD(P)H ferredoxin oxidoreductase, and ferredoxin.[33] Despite the requirement for O_2, no oxygen atom is incorporated into the product. Nevertheless, the active site structure and general characteristics of the reaction appear to be similar to those of MMO. Thus, it is possible that this enzyme catalyzes the first half of an MMO-like reaction to generate a radical intermediate of the substrate, but does not complete the OH rebound step to yield an alcohol. Instead, a second electron is apparently abstracted to yield a desaturated bond and a second water.

Δ9D has been purified from a variety of species. The soluble desaturase protein has been shown to be a homodimer with a molecular weight near 70 kDa.[156,157] Past studies have demonstrated that the enzyme contained iron,[158] but more recent optical, Mössbauer, and resonance Raman studies with the castor desaturase have shown that each monomer of the homodimer contains a binuclear iron−oxo core,[17,150] as summarized in Table 5. More specifically, the Mössbauer results indicated that the isolated desaturase contained mostly antiferromagnetically spin-coupled high-spin Fe(III) sites (~80%), which were manifested in two quadrupole doublets, with the minority of the iron (~20%) existing in the high-spin diferrous form.[17] The strong coupling that was observed ($J > 60$ cm^{-1}) is in accord with the existence of an oxo bridge. The isomer shifts of the quadrupole doublets are at the high range of values for diferric clusters, which suggested that the coordination environment of the irons is rich in oxygenous ligands, such as water and carboxylates. Resonance Raman studies revealed symmetric and asymmetric vibrational modes that were typical of oxo-bridged diiron clusters.[150] From the ν_s and ν_{as} and their $^{18}O_2$-dependent frequency shifts, an Fe−O−Fe angle of 123° was calculated, which indicates that the irons are likely to be triply bridged in the diferric state. In contrast to MMO, it is most likely that the binuclear

Table 5. Spectroscopic Properties of Stearoyl-Acyl Carrier Protein Δ^9 Desaturase[a]

	$\Delta 9D_{ox}$	$\Delta 9D_{red}$	refs
optical			
λ (nm)	325 (strong) 355 (strong) 470 (weak) 570 (weak)		17,150
Raman			
ν_s (cm^{-1}), Fe−O−Fe	519		150
ν_{as} (cm^{-1}), Fe−O−Fe	747		
Mössbauer			
ΔE_Q (mm s^{-1}), Fe1		2.75[b] 3.04[c]	17
δ (mm s^{-1}), Fe1		1.24[b] 1.30[c]	17
ΔE_Q (mm s^{-1}), Fe2		3.24[b] 3.36 (4.2)	17
δ (mm s^{-1}), Fe2		1.24[b] 1.30 (4.2)	17
ΔE_Q (mm s^{-1}), species 1 (81%)	1.54[c]		17
δ (mm s^{-1}), species 1 (81%)	0.53[c]		17
ΔE_Q (mm s^{-1}), species 2 (19%)	0.74[c]		17
δ (mm s^{-1}), species 2 (19%)	0.50[c]		17

[a] The data used in this table are on the enzyme isolated from *Ricinus communis* (castor). [b] The data were collected at 180 K. [c] The data were collected at 4 K.

iron center of Δ9D contains an oxo, rather than a hydroxo bridge. This was postulated due to the fact that the intensity and shape of the absorption spectrum was unchanged in the pH range from 6 to 9, whereas a hydroxo species would afford altered spectral frequencies and decreased intensities.[159] More evidence for the oxo bridge comes from the lack of a deuterium isotope shift in resonance Raman experiments. Δ9D has also been shown to form two different azide complexes.[160] Resonance Raman using both $^{14}N_3^-$ and $^{15}N^{14}N_2^-$ has shown that azide will bind to the diiron cluster in either a η^1-terminal fashion or in a μ-1,3-bridging conformation. The type of azide binding is pH dependent, with the end-on species predominating at pH 7.8 and the bridging species maximizing at pH 6.2. The fact that azide can fit into the binuclear iron cluster of Δ9D suggests that the diiron cluster may be more flexible than myohemerythrin, which binds azide only in an end-on fashion. It may be this flexibility of the diiron core that helps determine whether an enzyme can activate O_2 by allowing the irons to bind the O_2 in a bridging manner.

Even though Δ9D does not have the same substrate specificity or catalytic outcome as MMOH and R2, it does seem to have the same active-site residues, which include ligands to the irons (Glu, His), residues involved in a hydrogen bonding network to the iron cluster (Asp, Glu, Arg), and a threonine that may play a part in O_2 binding or proton transport.[150] The fate of O_2 in the reaction of Δ9D has been compared with that in R2 through resonance Raman studies.[161] In spite of these striking similarities of these two enzymes, a single turnover of the diferrous Δ9D with $^{18}O_2$ does not result in incorporation of ^{18}O into the binuclear iron cluster bridge as occurs in R2. Therefore, stearoyl-ACP desaturases may use a different oxygen activation pathway than R2. The reaction of O_2 with Δ9D is significantly affected by the presence of ACP, as the addition of ACP to Δ9D will decrease the time of reaction with O_2 from several hours to minutes. The cause of this enhancement of O_2 reactivity is not known, since there is currently no spectroscopic evidence for an alteration in the diiron site structure in the oxidized enzyme upon binding to ACP.[150] This result can be compared to the increased oxygen reactivity observed in MMOH in the presence of MMOB,[52] which is also unexplained.

IV. Ribonucleotide Reductase

A. Introduction

The reduction of ribonucleotides by the enzyme, ribonucleotide reductase (RR), is essential for the production of the deoxyribonucleotides utilized in DNA biosynthesis. The overall function of RR involves the reduction of the hydroxyl group on the 2′-carbon of the ribose moiety of nucleoside diphosphates and triphosphates (NDPs and NTPs), thus converting a ribonucleotide into a deoxyribonucleotide. Three unique classes of this enzyme have been characterized, differing in composition and cofactor requirements; however, all of them make use of metals and free radical chemistry to initiate catalysis.[162,163] Only the so called "class I" ribonucleotide reductases, which utilize a binuclear iron cluster to initially establish the free radical used in the reaction, will be discussed here. The reader is referred to several excellent reviews that deal with the ribonucleotide reductase reaction and structure in a more complete and general fashion.[10,11,20−23,164,165]

Class I RRs consist of a homodimer of two protein subunits R1 and R2 in an $\alpha_2\beta_2$ structure. Subunit R1 contains the substrate binding site and other sites for allosteric regulation. At this substrate binding site, R1 has redox-active cysteine residues that are involved in the reduction of the NDP.[10,166−173] Each R2 subunit contains one binuclear iron cluster that undergoes oxygen activation to produce a stable radical at Tyr-122. The tyrosyl radical has been described as a "pilot light"[174] in that once it is generated, the radical is stored for use in many subsequent turnovers at the remote site on R1. Presumably, the radical returns to Tyr-122 after each cycle, and the binuclear iron cluster is not used until the pilot light burns out for some reason. The radical has been identified as an oxidized deprotonated form of tyrosine, and it is stable for days at room temperature due to the tightly packed, hydrophobic environment that surrounds the Tyr-122 in the protein.[175−177] The tyrosyl radical and binuclear iron center are known to be embedded deep within the protein, far away from the active site of R1 (∼35 Å), so long-range electron transfer is thought to occur to form a cysteinyl radical on Cys-439 at the R1 substrate binding site.[11,178,179] Site-directed mutagenesis studies have indicated that Tyr-356 and perhaps Glu-350 may be the residues closest to R1 in this electron-transfer chain.[10,180] It has also been indirectly demonstrated that electron transfer may only be initiated when a nucleotide is bound at the active site of R1.[173]

B. Structure of the Binuclear Iron Cluster

The R2 subunit can be isolated from the R1 subunit by purification from the native organism or it can be

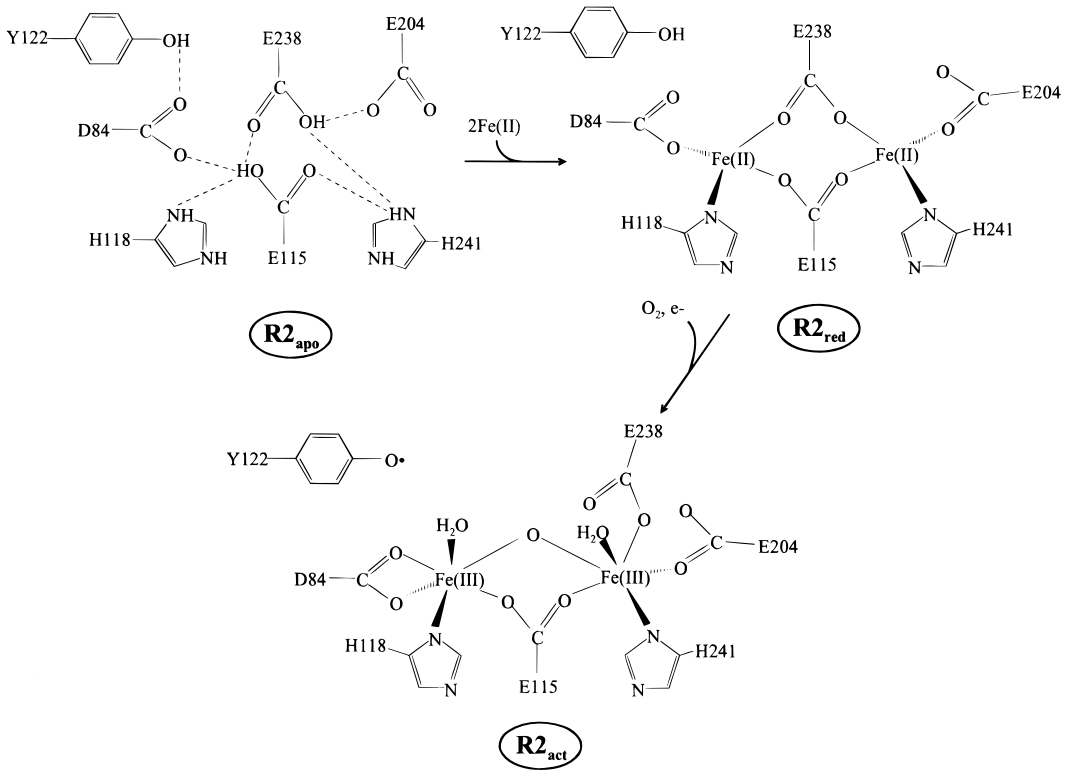

Figure 17. Structural representation of different redox states of the binuclear iron site of protein R2. (Adapted with permission from ref 20.)

overexpressed independently from the R1 protein in a recombinant strain.[181−184] In its active state, the binuclear iron cluster is in the diferric form and the tyrosine radical is present ($R2_{act}$). Several other states can be prepared in near stoichiometric yields including the apoprotein ($R2_{apo}$), protein with a diferric binuclear iron cluster but no tyrosine radical ($R2_{met}$), and the protein with a diferrous cluster and no radical ($R2_{red}$). $R2_{apo}$ can be isolated from overproducing bacteria grown in iron-depleted medium,[185] or after chelating the irons under mild denaturing conditions.[175] Anaerobic addition of Fe(II) to $R2_{apo}$[186] or reduction of $R2_{act}$ with hydroxylamine or hydrazine[187] will produce the reduced form, $R2_{red}$. Subsequent addition of O_2 and one electron to $R2_{red}$ will yield $R2_{act}$. It is also possible for some forms of R2 to undergo a one-electron reduction of the diferric state or one-electron oxidation of the diferrous state to generate a mixed valent form ($R2_{semimet}$).[187−191]

The structure of the R2 protein from *E. coli* in the $R2_{met}$, $R2_{red}$, and $R2_{apo}$ forms have been determined by X-ray crystallography.[77,178,192,193] The structure of the R1 protein has also recently been reported,[168,194] but will not be reviewed here. The overall structure of the R2 homodimer takes on the shape of a heart in which the two binuclear iron clusters are 25 Å apart. The structure consists of more than 70% α helix with the main helices forming an eight-stranded barrel. Five of the helices are oriented approximately antiparallel to each other, with four of them providing ligands to the binuclear iron cluster. A similar arrangement of helices was found for MMOH,[71] and, just as in the MMOH case, the Fe−O−Fe axis in R2 lies essentially parallel relative to the long axis of the helices. In contrast, the structure of hemerythrin (Hr) shows that the Fe−O−Fe axis of its binuclear iron cluster is approximately perpendicular to the long axis of a different four-stranded helix bundle.[57−59,195,196] The active site of R2 includes the same conserved Glu-X-X-His motif that is seen in MMOH. The structure of the binuclear iron cluster of R2 and its ligands in the different forms are depicted in Figure 17. The coordination geometry at the diiron core of $R2_{met}$ resembles that of both hemerythrin and MMOH, in that it contains an oxo-carboxylato bridged binuclear iron center. However, in contrast to Hr which provides five His residues to the binuclear iron cluster, R2 provides only two His-based nitrogen ligands; one to each iron. As in the case of MMOH, oxygen from carboxylates and solvent comprise the remainder of the coordination sphere of the iron cluster in R2. Another striking similarity between the binuclear iron clusters of R2 and MMOH is the change in ligand environment with the redox states of the irons. One such change in R2, which occurs upon reduction, is the loss of the μ-oxo bridge concomitant with a shift in the position of Glu-238, that causes it to convert from monodentate binding of Fe2 to a bridging position between the irons. A similar "carboxylate shift" was noted above for Glu-243 in MMOH,[65,70] but in that case only one of the two carboxylate oxygens was involved in bridging the irons. In addition, Asp-84 of R2 also undergoes a shift from a bidentate to monodentate ligation of Fe1 with reduction of the irons. As a result, Asp-84 moves closer to the Tyr-122 position upon reduction of the cluster which may facilitate electron transfer between these moieties. The catalytically functional Tyr-122 is about 5.3 Å away from Fe1, and it resides in a group of hydrophobic residues, which may function to stabilize the Tyr-122 radical. Since the production of the Tyr-122 radical is the first step in

Table 6. Spectroscopic Properties for the Various Forms of Ribonucleotide Reductase R2

	$R2_{red}$	$R2_{act}$	$R2_{met}$	$R2_{semimet}$	refs	**U**	**X**	refs
optical								
λ, nm		325 (9400)	325 (9400)		249	565	360	216,217
(ϵ, M^{-1} cm^{-1})		370 (7200)	370 (7200)					
		412 (4100)	500 (800)					
		500 (800)	600 (300)					
		600 (300)						
exchange coupling								
J, cm^{-1} [a]	−0.5	∼−90 to −108	∼−90 to −108	−10	141,199,202,207,212			
EPR								
g_{max}, g_{mid}, g_{min}	∼17	2		1.936, 1.82 1.92,1.73,1.60	190,204		2.007, 1.999, 1.994[b]	222
Raman								
ν_s(Fe−O−Fe), cm^{-1}		496	496		176,198,250,251			
ν_{as}(Fe−O−Fe), cm^{-1}		756	756		176,198,251			
Mössbauer								
δ (mm s^{-1}), Fe1	1.26	0.53	0.53		175,204		0.56	174,211
ΔE_Q (mm s^{-1}), Fe1	3.13	1.66	1.66		175,204		−0.9	174,211
δ (mm s^{-1}), Fe2		0.44	0.44		175		0.26	174,211
ΔE_Q (mm s^{-1}), Fe2		2.45	2.45		175		−0.6	174,211
ENDOR								
Fe1, A_1, A_2, A_3 (MHz)							−74.2, −72.2, −73.2	174,222
Fe2, A_1, A_2, A_3 (MHz)							+27.5, +36.8, +36.8	
$^{17}O_a$, A_1, A_2, A_3 (MHz)							+31, +25, +25	

[a] These values are reported using the convention $H = -2JS_1S_2$. [b] Resolution of EPR values were done at Q band; at X band, only a $g = 2.00$ could be observed.

the overall reaction of RR, it would be very important to stabilize this radical once it is generated, as it could potentially be lost to solvent or other hydrophilic (redox active) residues that are nearby. Indeed, a recent study demonstrates that a major function of residues in the hydrophobic pocket, such as Phe-208, Phe-212, and Ile-234, is to shield the radical from potential electron donors that are not involved in the normal electron transfer pathway (see F208Y, section D, part 4b).[197] The environment of the binuclear iron cluster is tightly packed and the cluster is 10 Å from the closest surface. This lack of a possible binding pocket for substrates may be one of the major reasons that R2 lacks the monooxygenase activity of MMO despite the very similar binuclear iron cluster structure.

C. Spectroscopic Studies of the Binuclear Iron Cluster and Tyrosyl Radical

Some of the spectroscopic properties of R2 in various states are summarized in Table 6. The $R2_{act}$ exhibits an optical spectrum with maxima at 325, 370, and 412 nm, with weaker absorbance maxima at 500 and 600 nm. The 325 and 370 nm absorption bands are derived from ligand to metal charge transfer transitions in the diferric state; the most important of which arises from the μ-oxo bridge. The tyrosyl radical is the source of the narrow, characteristic optical band at 412 nm. Resonance Raman studies have shown bands at 493 and 756 cm^{-1}, which arise from the symmetric and asymmetric stretching modes of the Fe−O−Fe core.[176,198] The $R2_{act}$ state exhibits an EPR signal only from the stable radical because the two irons of the cluster are antiferromagnetically coupled to yield a diamagnetic state. Numerous recent EPR and ENDOR studies have been conducted on the tyrosyl radical[177,191,199−203] and have yielded information about magnetic coupling with paramagnetic states of the binuclear iron cluster, the extent of hydrogen bonding to nearby amino acids, and the spin density distribution of the Tyr-122 radical. Mössbauer spectroscopy of $R2_{act}$ shows that both irons are high-spin ferric and that they are in slightly different electronic environments.[204]

The mixed-valence state of R2 ($R2_{semimet}$) has been generated from $R2_{met}$ by radiolytic reduction (γ- or X-irradiation) at 77 K.[188,190] The species has an $S = {}^1/_2$ spin state ($g_\perp = 1.936$ and $g_\parallel = 1.82$). When the temperature was raised briefly to 165 K, then lowered to <35 K, an $S = {}^9/_2$ state was observed with resonances at $g = 5.4$, 6.7, and 14.8. Measurements of the coupling constant J for the $S = {}^1/_2$ state showed that the antiferromagnetic interaction is relatively weak (about -10 cm^{-1}), suggesting that the bridge is protonated in this state. Mild chemical reduction of $R2_{met}$ from mouse and herpes simplex virus was shown to produce a relaxed mixed-valence state which is stable at room temperature.[189]

Mössbauer,[204,205] CD/MCD,[141] magnetic susceptibility,[206−208] and EPR[140,204,207] studies of $R2_{red}$ have been conducted in recent years. The EPR spectra are similar to those observed for diferrous MMOH in that they exhibit the characteristic $g \approx 17$ signal. In the case of $R2_{red}$, however, the two Fe(II) ions appear to be weakly antiferromagnetically coupled ($J = -0.5$ cm^{-1}). MCD experiments showed that diferrous R2 was best fit with an $M_s = \pm 2$ ground state, with the D values of the irons having opposite signs.[141] These CD/MCD studies on $R2_{red}$ have indicated that the two irons probably have different coordination numbers.[141] In the absence of other ligands, the two irons appear to be 4 and 5 coordinate, respectively, while in the azide complex, the five-coordinate iron gains an additional ligand. Although the crystal structure of this state does not provide evidence for a difference in coordination number for the irons in $R2_{red}$, the presence of three ligand field transitions in the 5000−10000 cm^{-1} spectral region clearly indicates that the coordination numbers are different. The Mössbauer

spectrum also shows that the irons are in slightly different environments but does not directly reveal the coordination number. It is possible that the binuclear iron center is ferromagnetically coupled in the case of MMOH because one of the bridging carboxylates is in a μ-1,1 binding mode, whereas both bridging carboxylates in the case of $R2_{red}$ bind in the μ-1,3 mode (bidentate carboxylato). The CD/MCD studies indicate that it is also possible to bind one azide to each iron of the cluster in $R2_{red}$. Similarly, it was shown that an NO molecule is likely to bind to each of the irons in $R2_{red}$ to yield two $S = {}^3/_2$ iron centers that antiferromagnetically couple to give a diamagnetic system.[209] It is interesting that in a subsequent reaction, N_2O is formed to yield $R2_{met}$. Together these spectroscopic studies suggest that $R2_{red}$ has at least one available coordination site on each iron, which is consistent with the hypothesis that O_2 binding and activation involves both irons of the cluster.

D. R2 Activation and Intermediates Involved in this Process

*1. Detection of Intermediates **U** and **X***

There have been many recent studies on the formation of the diferric center and tyrosyl radical.[204,205,210−218] The R2 activation reaction can be formally written as

$$R2_{apo}\,(Tyr_{122}\text{-}OH) + 2Fe^{II} + e^- + O_2 + H^+ \rightarrow R2_{act}\,(Tyr_{122}\text{-}O^{\bullet}) + H_2O$$

The second atom of oxygen from O_2 is also reduced to the level of water, but resonance Raman experiments have shown that it is incorporated into the binuclear iron cluster as the bridging oxygen.[161] Four electrons are required to reduce O_2 to two waters; three of which derive from oxidation of the 2Fe(II) and the formation of the oxidized tyrosyl radical. It is known that *in vitro*, the fourth reducing equivalent can be donated from a chemical reductant such as ascorbate, an additional Fe(II) ion, or even the reduced binuclear iron site in the neighboring protomer.[215,216,219] The ability to activate the R2 protein *in vitro* by chemical methods has allowed some elegant experiments that focused on the intermediates in the R2 activation reaction. As they were originally formulated, these experiments involved rapidly mixing $R2_{apo}$ with Fe(II) and O_2. During the ensuing formation of $R2_{act}$, two transient species, termed **U** and **X**, were formed prior to the tyrosyl radical[205,210,211,216−218] (see Figure 18). It is of great importance to elucidate the chemical nature of intermediates **U** and **X**, because they appear to be the species involved in the oxygen activation and net hydrogen atom abstraction from Tyr-122.

*2. Nature of Intermediates **U** and **X***

Some of the properties of intermediates **U** and **X** are summarized in Table 6. At 5 °C, in the presence of excess Fe(II), **U** formed at 5−10 s^{-1} and decayed to **X** very rapidly ($k > 20\ s^{-1}$). **X** then converted to $R2_{act}$ at a rate constant of about 1 s^{-1}. When Fe(II)

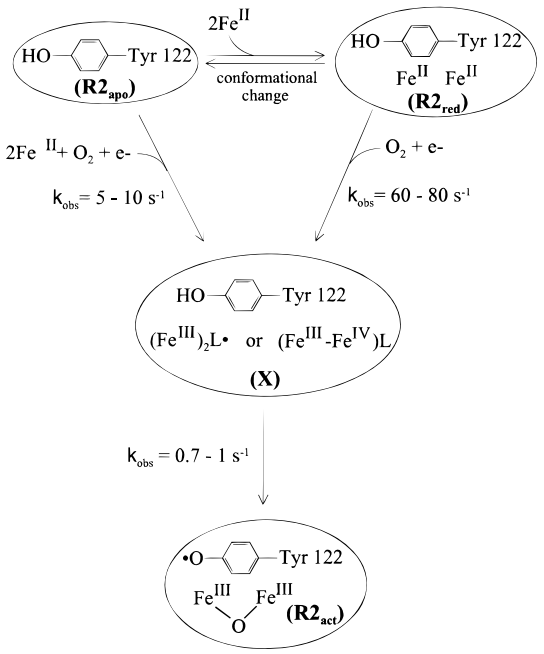

Figure 18. Schematic of the formation of the active diferric cluster/tyrosyl radical from the reaction of O_2 with the Fe(II)-preloaded form of R2. (Adapted with permission from ref 225.)

was limiting, **U** accumulated and was shown to have an absorption maximum near 560 nm. This is quite different than the 325 and 370 nm absorbance features characteristic of the diferric binuclear iron cluster in $R2_{act}$. **U** also lacked the 412 nm absorbance that derives from the Tyr-122 radical, in accord with the proposal that **U** precedes both formation of resting μ-oxo bridged diferric cluster and the tyrosine radical. Initially, it was suggested that **U** is a μ-peroxy adduct of the oxo-bridged binuclear iron cluster due to similarities with the optical spectrum of the peroxy-model complex shown in Figure 3b.[216] However, other spectroscopic features of **U** are not consistent with this assignment.[210] In particular, Mössbauer measurements of samples taken during the time course of the reconstitution failed to show any evidence for the characteristic spectral features of complexes like that shown in Figure 3b, even when the concentration of the 560 nm species was maximal. The possibility that the 560 nm absorbance arises from a transient protonated tryptophan radical was suggested on the basis of optical similarities[218] and the presence of a broad EPR resonance at $g = 2$ at an early phase of the reconstitution process.

The second intermediate, **X**, has been more thoroughly characterized because the rates of its formation and decay allow it to accumulate in higher yield. This species has an absorbance maximum at 360 nm, but still lacks the absorbance band of the tyrosyl radical. Freeze−quench EPR experiments have shown that it has an isotropic signal at $g = 2.00$ which is quite distinct from that of tyrosyl radical both in terms of spectral line shape and time dependence of its formation.[211,217] The signal was found to display hyperfine broadening with ^{57}Fe incorporation into the cluster or when the formation reaction was carried out with $^{17}O_2$ or in $H_2{}^{17}O$ indicating that the spin is coupled to the cluster iron(s) and oxygen(s).

Table 7. Model Compounds of Binuclear Iron-Oxo Clusters

no.	compound	solvent	λ_{max}, nm (ϵ, M^{-1} cm^{-1})	ν, Fe−O (^{18}O)	ν, O−O (^{18}O)	binding mode	ref
			***μ*-Oxo and *μ*-Hydroxo Species**				
1	$[Fe_2(\mu\text{-}O)(\mu\text{-}OH)(6TLA)_2](ClO_4)_3$	CH_3OH/H_2O	396 (4150) 550 (670)			μ-OH, μ-O	110
2	$[Fe_2(\mu\text{-}O)_2(6TLA)_2](ClO_4)_2$	CH_3CN	375 (2000) 470 (560)			bis μ-O	111
3	$[Fe_2(\mu\text{-}O)_2(5\text{-}Me\text{-}TPA)_2](ClO_4)_3$	CH_3CN	366 (7900) 616 (5200)	676,656 (634)		bis μ-O	109
4a	$[Fe_2O(2,2\text{-}bipy)_4(H_2O)_2](ClO_4)_4$	CH_3CN	360 (10700)				241
4b	$[Fe_2O(4,4'\text{-}Me_2\text{-}2,2'\text{-}bipy)_4(CFCO_2)_2](ClO_4)_4$	CH_3CN	360 (1100)			μ-O	
5	$[Fe_2O(O_2CH)_4(BIPhMe)_2]\cdot H_2O$	$CHCl_3/CH_3OH$ (20:1)		520 (502)		μ-O	75
6a	$[Fe(HB(3,5\text{-}iPr_2pz)_3)]_2(OH)(OBz)$	MeCN				μ-OH	235
6b	$[Fe(HB(3,5\text{-}iPr_2pz)_3)]_2(OH)(OBz) + O_2$	pentane	~700				
6c	$[Fe(HB(3,5\text{-}iPr_2pz)_3)]_2(OH)_2$	pentane				bis μ-OH	
6d	$[Fe(HB(3,5\text{-}iPr_2pz)_3)]_2(OH)_2 + O_2$	pentane					
7a	$[Fe_2(OH)(O_2CCH_3)_2(HBpz_3)_2](ClO_4)$	CH_2Cl_2	375 (4750)			μ-OH	159
7b	$[Fe_2(OH)[O_2P(C_6H_5)_2]_2(HBpz_3)_2](BF_4)$	CH_3CN	346 (3860)			μ-OH	159
7c	$[Fe_2(OH)[O_2P(OC_6H_5)_2]_2(HBpz_3)_2](BF_4)$	CH_2Cl_2	372 (4300)			μ-OH	159
8	$[Fe_2(HPTB)(OH)(NO_3)_2](NO_3)_2$	CH_3OH	340 (7300)			μ-OH	252
9	$[Fe_2O(H_2O)_2(tmima)_2](ClO_4)_4$	CH_3CN	315, 480			μ-O	243
10	$[FeL_2]_2(\mu\text{-}O)(\mu\text{-}OH)(ClO_4)_3\cdot 2H_2O$[b]	CH_3CN	374 (5085) 562 (601)			μ-OH, μ-O?	257
11	$[Fe_2(\mu\text{-}O)(6\text{-}Me\text{-}TPA)_2(OH)(H_2O)](ClO_4)_3/H_2O_2$	CH_3CN	355 (8000)				112
12	$[Fe_2O(XDK)(BIDPhE)_2(NO_3)_2$	CH_2Cl_2	644 (430)				264
13	$[Fe_2O(O_2CCH_3)_2(TPA)_2](BPh_4)_2$	CH_3CN	320 (10000) 360 (8000)				260
14	$[Fe_2O(DPAH)_2]_2$	CH_3CN					258
15	$[Fe_2O(TPA)_2](ClO_4)_2 + H_2O_2$	CH_3CN	614 (3500)	416 (408)			108
			***μ*-Peroxo Species**				
16	$[Fe_2(Ph\text{-}bimp)(C_6H_5COO)(O_2)](BF_4)_2\cdot 2CH_3CN\cdot C_2H_5OC_2H_5\cdot H_2O$	CH_3CN	500−800 (1700)			*cis* μ-1,2	103
17	$[Fe_2O_2(N\text{-}Et\text{-}HPTB)(OPPh_3)_2](BF_4)_3$	CH_3CN		476 (460)	900 (850)	*cis* μ-1,2	102
18	$[Fe_2(\mu\text{-}O_2)(\mu\text{-}O_2CCH_2Ph)_2\{HB(pz')_3\}_2]$	toluene	694 (2650)	415 (404)	888 (842)	*trans* μ-1,2	104
19	$[Fe_2(N\text{-}Et\text{-}HPTB)OBz](BF_4)_2 + O_2$	CH_2Cl_2	588 (1500)	476 (460)	900 (850)		101,124
20	$[Fe_2(HPTP)OBz](BF_4)_2 + O_2$	CH_3CN/DMSO (8:2)	572 (2060)	481,453 (444)	893,877 (834)		101,124
21	$[Fe_2(HPTB)(OH)(NO_3)_2](NO_3)_2 + H_2O_2$	CH_3OH	604 (1600)	476 (457)	895 (854)		252
22	$[FeO(Ph_3PO)_4]_2\cdot(ClO_4)_4 2H_2O + H_2O_2$	CH_3CN	576 (3540)	445	882 (848)		253
23	$[Fe(HB(3,5\text{-}iPr_2pz)_3)]_2(O)(OBz)$	toluene	679 (3454)	418 (409)	876 (827)		254
24	$(FeL_1)_2O_2$[a]	water	540 (187)				255
25	$[Fe_2(5\text{-}Me\text{-}HXTA)(O_2)(OAc)]^{2-}$	CH_3OH, DMSO	480 (2370)		884		256
			Other Species (*μ*-Carboxylato, *μ*-Phenoxo)				
26	$[Fe_2(\mu\text{-}OBz)(XDK)(ImH)_2(OBz)(MeOH)]$	CH_3OH/CH_2Cl_2				tris μ-carboxyl	240
27	$[Fe_2(H_2Hbab)_2(N\text{-}MeIm)_2]$	DMF	270−280 312 (30000)			bis μ-phenoxo	238
28	$[Fe_2(salmp)_2]^{2-}(Et_4N)_2$	CH_3CN	800 (1010)			bis μ-phenoxo	259
29	$[Fe_2(O_2CCH_3)_2(TPA)_2](BPh_4)_2$	CH_3CN	388 (2600)			bis μ-carboxyl	260
30	$[Fe_2(\mu\text{-}H_2O)(\mu\text{-}OAc)_2(OAc)_3(py)_2](Et_4N)$	CH_2Cl_2				bis μ-carboxyl μ-H_2O	265

[a] L1 = 3,6,10,13,19-pentaazabicyclo[13.3.1]nonadeca-1(19),15,17-triene. [b] L2 = *N*,*N* ′-dimethyl-*N*,*N* ′-bis(2-pyridylmethyl)ethane-1,2-diamine.

The formation of both **X** and **U** were affected by the absolute concentration of Fe(II), and they were observed to form slower when the Tyr-122 was replaced by a phenylalanine (Y122F), thereby preventing formation of the final Tyr-122 radical. Essentially stoichiometic formation of **X** was possible using Y122F. Freeze−quench Mössbauer and EPR studies of samples prepared in this way indicated that **X** is a high-spin diferric center magnetically coupled to an unidentified radical that was distinct from the eventual tyrosyl radical.[217] This could give cluster **X** the required $S = {}^1/_2$ spin state and the g value at 2.00, despite the apparent presence of antiferromagnetically coupled ferric ions. The formal oxidation state of **X** would be [Fe^{III}-Fe^{IV}]; one electron more oxidized than the resting diferric cluster and one electron more reduced than compound Q of the MMOH cycle.[205,211,220] However, in contrast to compound Q, no evidence for Fe(IV) was obtained for either **U** or **X**. This was somewhat unexpected because earlier experiments had shown that the reconstitution process could be run using H_2O_2 or single atom oxygen donors in place of O_2, suggesting that a high-valent ferryl or perferryl species was generated.[161,213,214] If species **X** were a high-valent iron−oxo species, it might be able to perform the (direct or indirect) hydrogen atom abstraction that is needed to generate the Tyr-122 radical. Both the formal redox state of **X** and its observed EPR spectrum are mimicked well by the 6-Me-TPA-based model complex (**11**) listed in Table 7.[112] However, the isomer shift of Mössbauer spectrum for **X** ($\delta = 0.56$ and 0.36 mm s^{-1}) is significantly different than the isomer shift values observed for both irons of the model complex ($\delta = 0.48$ and $\delta = 0.08$ mm s^{-1}). This is consistent with the proposal that one of the irons

of the model has Fe(IV) character, whereas those of **X** are predominantly Fe(III). Recent experiments employing rapid freeze−quench techniques in conjunction with Q-band ENDOR spectroscopy using ^{57}Fe have shown that, although one of the irons of the **X** cluster (Fe1) is clearly Fe(III) with a nearly isotropic hyperfine tensor, the other iron (Fe2) exhibits considerable anisotropy, indicating that it possesses substantial high-spin Fe(IV) character.[174] The X-band EPR spectrum of the $g = 2.00$ signal of cluster **X** was isotropic; however, at Q band, it was shown that this $S = {}^1/_2$ spin system exhibited considerable anisotropy. Since three, distinct g values could now be associated with **X**, ENDOR could be performed to calculate more reliable hyperfine coupling constants for the irons. Using these A values allowed for the reanalysis of the Mössbauer data for cluster **X**. This resulted in a significantly smaller isomer shift for Fe2 (0.26 mm s^{-1}), which is much more consistent with an Fe(IV) oxidation state.[174] Therefore, cluster **X** is presently described as a spin-coupled Fe^{III}-Fe^{IV} center without a ligand radical, but with significant spin delocalization onto the oxygen ligand(s). ^{17}O-ENDOR studies have allowed the further characterization of intermediate **X** by demonstrating that there are three exogenous O atoms, two of which derive from O_2 and the third from water.[221,222] ^{1}H ENDOR studies demonstrate the presence of strongly coupled, exchangeable proton(s) associated with one or more of the sites, indicating that cluster **X** probably has at least one hydroxo bridge.[222] In another ^{1}H ENDOR study on the R2-Y122F/Y356F mutant, it was concluded that a large hyperfine coupling in the 18−23 MHz range probably ruled out **X** containing a terminally bound water, and suggested the presence of a bridging hydroxide or a strongly bound terminal hydroxide.[223] Recent EXAFS characterization of **X** from the wild-type enzyme has been performed and shown to contain a very short Fe−Fe distance of 2.5 Å.[224]

a. A Model for Intermediate X. With the discovery of high-valent intermediates in enzymatic systems, it was important to synthesize and characterize chelate model compounds that possessed high-valent properties. The first model that was found to have high-valent iron was ([Fe_2O_2(5-Me-TPA)$_2$]) (Table 7, structure **3**). This complex was thought to be a valence delocalized $Fe^{III}Fe^{IV}$ cluster with double exchange coupling between low spin Fe(IV) and Fe(III) centers.[109] The model is characterized by a green color, a single Mössbauer feature for both irons, and an $S = {}^3/_2$ spin state. A variation of this model, which was described in the above section, has also been reported[221] in which the methyl groups present on each of the pyridyl ligand arms of the tripodal ligand are placed in the 6 position instead of the 5 position ([Fe_2O_2(6-Me-TPA)$_2$]) (**11**). In contrast to the green complex **3**, this model has $S = {}^1/_2$ ground state that produces a narrow, isotropic EPR signal centered at $g = 2.00$. Analysis of the Mössbauer spectra revealed that cluster **11** contains trapped-valence Fe(IV) and Fe(III) sites. The isomer shift, $\delta = 0.48$ mm s^{-1} of the Fe(III) site was found to be identical to those of the two high-spin ferric sites of the complex from which **11** is derived by reaction with peroxide. The Fe(IV) site has a much smaller isomer shift, namely $\delta = 0.08$ mm s^{-1}. Since the $S_1 = {}^5/_2$ spin of the Fe(III) site is exchange coupled to the spin S_2 of the Fe(IV) site to produce the observed $S = {}^1/_2$ cluster spin, it follows that $S_2 = 2$, i.e. the Fe(IV) site is high spin. In the interpretation of the data of intermediate X, the observation of an isotropic $S = {}^1/_2$ EPR signal at $g = 2.00$ was taken as evidence against the presence of an $Fe^{IV}Fe^{III}$ state, and it lent support for a model consisting of a diferric cluster coupled to an (unspecified) radical. Complex **11**, however, has demonstrated that an antiferromagnetically coupled $Fe^{IV}Fe^{III}$ pair can indeed produce an $S = {}^1/_2$ ground state that yields an isotropic EPR signal at $g = 2.00$. The recent insight into the electronic nature of intermediate **X** from Q-band ENDOR spectroscopy[174] suggests that the features of this model are generally in accord with those of **X**. However, the isomer shift for the iron with Fe(IV) character in **X** is significantly higher, supporting the proposal that the electron density is distributed significantly onto the bridging oxygen moiety.

3. Conformational Change

When Fe(II) was added stoichiometrically or in excess, the rate of formation of **X** was found to be independent of the concentration of Fe(II), O_2, and $R2_{apo}$, and thus it was proposed that the $R2_{apo}$ must undergo some kind of conformational change upon binding to the Fe(II) and/or O_2 before the formation of **X** is possible.[205] Moreover, the structural studies of R2[192] showed that the binuclear iron site is buried >10 Å from the outside surface such that a conformational change may be required to allow iron to enter. In order to explore this possibility, $R2_{apo}$ was allowed to be preincubated with excess Fe(II) to allow any slow conformational change that occurs upon Fe(II) binding to reach equilibrium (see Figure 18).[225] Then O_2 was rapidly added and the formation of **X** and $R2_{act}$ were monitored. The formation of **X** was still observed, but it occurred at ∼60−80 s^{-1}, which is 1 order of magnitude faster than the formation of **X** during experiments that did not use the Fe(II)-preloaded $R2_{apo}$. The decay of intermediate **X** was concomitant with the formation of the tyrosyl radical (see Figure 19), which is indicative of the presence of $R2_{act}$. These kinetics demonstrate that the conversion of $R2_{apo}$ to the $R2_{red}$ complex is a slow process, consistent with conformational reorganization as an essential step in Fe(II) binding to $R2_{apo}$. Once this conformational change has occurred, the reaction of O_2 with the R2-bound iron is rapid, indicating that O_2 diffuses rapidly through the protein as expected.

4. Mutations

a. Y122F. The Y122F mutation has been of use in numerous experiments including the kinetic studies of intermediates **U** and **X** described above. Other transient kinetic experiments focused on the fact that the lack of Tyr-122 changes the course of the reconstitution reaction that leads to the formation of the activated diferric cluster. Under these conditions, it was observed that other residues could supply an electron and give rise to a free radical. Stopped-flow absorption spectroscopy and freeze−quench EPR

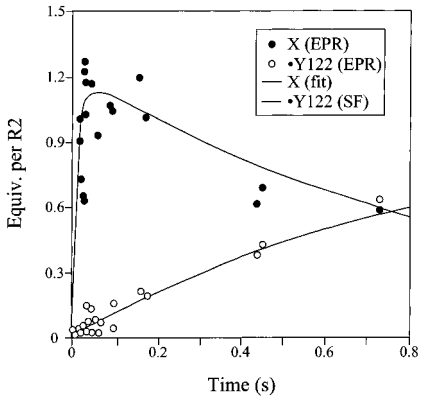

Figure 19. Kinetics of the formation of **X** and •Y122 in the reaction of Fe^{II}-R2 with O_2. The quantities of **X** and •Y122 are from the rapid freeze quench EPR time course of the reaction. The trace for •Y122 is from monitoring the A_{410} by the optical stopped-flow method. The trace for **X** is obtained by nonlinear least-squares fitting of the measured quantities of **X** and •Y122 as functions of time to the experimental data corresponding to a k_1 of 60 s^{-1} and a k_2 of 1 s^{-1}. (Adapted with permission from ref 225.)

detected six intermediate radical species, of which at least two, and probably three, were found to be tryptophan radicals based on line-shape characteristics and deuterium-labeling effects.[226,227]

Redox potentials have also been measured for the native R2 and the Y122F mutant.[228] It was found that the midpoint potential of the native protein, $R2_{met}$, (E_m = −115 mV at pH 7.6, 4 °C) shifted to −178 mV in the mutant, showing that Tyr-122 does affect the environment of the cluster. Interestingly, it was also shown that the large subunit R1 shifts the potentials of both the wild-type R2 and the Y122F mutant negatively by over 100 mV, demonstrating that the binding of R1 and R2 is coupled to the redox state of the cluster. R1 would preferentially bind to the R2 containing the oxidized (active) state of the cluster, thereby maximizing the active concentration of enzyme. This aspect of the regulation of the system is apparently not affected by Tyr-122.

b. F208Y. Another mutant of R2 that has provided insight into oxygen activation is the F208Y mutant.[76,185,229] Phe-208 plays a role in formation of the hydrophobic pocket that houses and stabilizes the Tyr-122 radical. Following isolation, the F208Y mutant was found to be purple in color (λ_{max} = 460, 720 nm). The resonance Raman spectrum and the crystal structure of the mutant showed that the new Tyr-208 had been converted to 3,4-dihydroxyphenylalanine (DOPA), which had then bound to the iron to yield the purple color.[185,229] Apo F208Y, prepared by growth of the recombinant strain on low iron, also became purple after addition of O_2 and Fe(II) to the mutant enzyme. These results show that the mutant has tyrosine hydroxylase activity, suggesting that an activated form of O_2 may be generated in the active site that could abstract an electron from Tyr-208 and then rebound to form DOPA. However, further studies with $^{18}O_2$ and $H_2{}^{18}O$ showed that the source of the oxygen in the DOPA-208 was actually water rather than molecular oxygen.[161] As a result, the authors proposed that an activated form of the binuclear iron cluster can abstract an electron from Tyr-208, but that the rebound occurs from a solvent binding site on one of the irons.

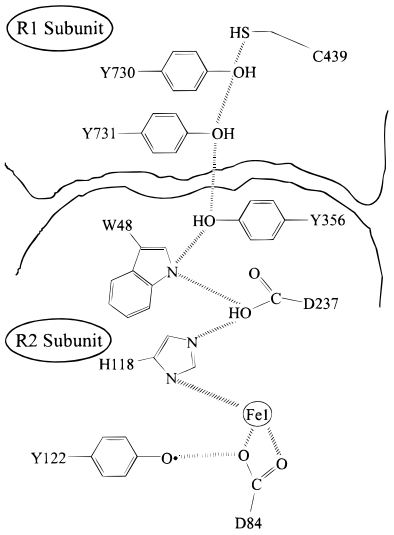

Figure 20. The proposed radical pathway from the binuclear iron site of R2 to the active site of R1. (Adapted with permission from ref 20.)

c. Mutations of the Cluster Ligands and Residues in the Electron-Transfer Path to R1. Examination of the crystal structure in the context of conserved residues has allowed speculation on the path that the electron stored on Tyr-122 takes as it moves to the active site on R1 during catalysis. As illustrated in Figure 20, it is proposed that on R1, the catalytically essential C439, as well as Y730, and Y731 are part of the pathway. On R2, residues Y356, W48, D237, H118, D84, and Y122 form the pathway. Past studies using site-directed mutagenesis have strongly supported the importance of all of these residues except the binuclear iron cluster ligands H118 and D84.[169,170,178−180,230,231] Recently, H118 and D84 have each been mutated to alanine.[233] It was observed that although the mutant enzymes could each form the binuclear iron cluster and the tyrosine radical, they were inactive overall, in accord with their proposed role of transferring the radical to R1. In the same study, each of the other iron ligands of the cluster were changed in individual mutants to alanine or histidine, and then characterized by optical, EPR, resonance Raman, and activity measurements. In contrast to recombinant wild-type R2, none of the mutant R2 proteins could efficiently bind iron during growth of the recombinant strain, therefore they were all isolated in the apo form. Each mutant was able to bind iron after reconstitution; however, they all lost the bound iron ions over time upon storage. Only D84A and E115A bound substantially less iron than the wild-type R2. The spectroscopic features and other properties of the binuclear iron clusters in these mutants showed substantial variation. For example, the E238A and H241A mutants stabilized substantial amounts of the mixed-valence state. Most of the mutants could not form or stabilize the Tyr-122 radical and were consequently inactive. Of the three mutants that could form the radical (D84A, H118A, and E204A), two formed only transiently stable radicals (H118A and E204A), and only one of these (E204A) was able to transfer the electron to R1.

In order to mimic the active site of MMO, as well as investigate the importance of the bidentate ligand D84, the D84E mutant was constructed and analyzed by UV−vis, EPR, and Mössbauer spectroscopies, as well as by redox potential studies.[232] As in the other D84 mutant (D84A),[233] this mutant R2 bound substantially less iron, as only 1.7 irons were found in the R2 dimer, compared to the 3.5 Fe/R2 dimer ratio of the wild-type enzyme. The characteristic optical band of the tyrosyl radical at 410 nm was absent. The spectroscopic studies suggested that the new glutamic acid may bind to Fe1 in a monodentate fashion in the oxidized form, as opposed to the bidentate binding found in the oxidized wild-type R2. This mutation also resulted in significant electronic changes in the binuclear iron center that allowed for the stabilization of the mixed valent state, as in the case of MMOH in the absence of MMOR. Altogether, these results agree with the proposal that D84 is an important residue in the electron pathway between Tyr-122 and the diiron core. These observations also suggest that the carboxylate shift that D84 undergoes simultaneously with the redox state may also be an extremely important process in the catalytic function of the R2 subunit.

A recent mutagenesis study on another residue in the proposed electron transfer pathway of R2 has raised some interesting questions about the mechanism of tyrosyl radical formation.[234] It is known that in the activation of the R2 diiron center, an "extra" electron must be injected into the diiron core prior to or during the formation of **X**, with **X** then oxidizing Tyr-122 by one electron to form the tyrosyl radical and the diferric cluster.[210,211,217] The nature of process by which this extra electron is gained may dictate the outcome of its O_2-activating reaction. It was previously proposed that the tryptophan at position 48 near the surface of R2 may shuttle the extra electron to the reacting diiron cluster by undergoing a transient oxidation to its radical form.[210] To address this hypothesis, an R2-W48F mutant has been recently constructed and shown to bind iron and activate O_2 *in vitro*.[234] However, as predicted by the earlier hypothesis, the O_2 activation process was altered. First, under limiting Fe(II) conditions, the optical band at 560 nm was not present, suggesting that characteristic band in the visible spectrum of intermediate **U** may indeed have come from a tryptophan radical cation. In addition to that observation, preliminary evidence also suggests that the proposed extra electron injection does not occur in the mutant. A new EPR-active intermediate, termed **X′**, was formed initially followed by the *concomitant* formation of the tyrosyl radical and **X**. This result is very different than the earlier studies of the wild-type R2, where the decay of X was shown to be concomitant with the formation of the tyrosyl radical[225] (see Figure 19). In this mutant, the tyrosyl radical is not stable, as it is further oxidized by or undergoes radical recombination with the second oxidizing equivalent (**X**) that is still remaining in the active site. An altered, diamagnetic $Fe^{III}Fe^{III}$ species is the result of the proposed interaction between **X** and the tyrosyl radical. This set of experiments supports the hypothesis that Trp-48 may play a pivotal role in the formation of the tyrosyl radical by donating an electron to the diiron core to form the catalytically active species, **X**. One interesting aspect of these results is that there is a possibility of a compound Q-like precursor to **X** (one electron more oxidized than **X**) that is transiently produced in the R2 activation process, but decays too rapidly to be observed. The construction of the double mutant R2-W48F/Y122F may allow for the observation, and even the trapping, of this putative $Fe^{IV}Fe^{IV}$ intermediate in the activation of R2.

V. Oxygen Activation by Model Complexes

The range of chelate model complexes for the binuclear iron centers of enzymes shown in Table 7 have, for the most part, been synthesized during the last five years. The initial studies of these complexes have been largely directed toward characterizing the structure and spectroscopic features for comparison with those of the enzymes. Some evaluation of the ability of these compounds to catalyze oxidation chemistry has been completed, but much more can be expected in the near future. In general, several of the chelate complexes can catalyze oxidation of hydrocarbons; however, none will oxidize the most stable hydrocarbons such as methane. For example, many of the diiron complexes can catalyze the oxidation of substrates such as cyclohexane or PPh_3, when combined with H_2O_2, TBHP, or O_2.[101,108,235,236] In many of these cases, a substantial amount of ketone product is also formed in addition to the hydroxylated product. Complex **3** has been shown to oxidize phenol to its radical form,[237] which is analogous to the tyrosyl radical formation by R2. Also, it can catalyze the oxidation of cumene to cumyl alcohol,[237] demonstrating that it can also hydroxylate an aliphatic C−H bond, much like the reaction of MMO with substrate. However, no reaction of **3** with a short-chain alkane has been observed. It should be remembered that **3** has one less oxidizing equivalent than compound Q of the MMOH cycle, suggesting that if it could be further oxidized by one electron, it may be an effective oxidation catalyst for short-chain alkanes.

It seems likely that more potent oxidizing catalysts will require development of models with properties more in line with those of the binuclear iron clusters found in the enzymes. Most of the chelators used in model systems described in Table 7 employ nitrogen and phenolic oxygen ligands to the iron due to the known chemistry and availability of such ligands. Also, most of the first models were symmetrical dinuclear Fe(III) complexes with octahedral coordination at each iron. It is now clear that the predominant ligation of the binuclear clusters in the enzymes is non-phenolic oxygen and that it is the Fe(II) state of the enzymes that reacts with O_2. Also, the environment of the cluster is somewhat asymmetric and at least one of the irons is five-coordinate. Finally, changes in the cluster structure with oxidation state, such as carboxylate shifts and coordination number, are likely to occur and may be important to catalysis.

There are now considerable efforts to synthesize ligands with predominantly oxygen ligation (**26** and

27)[238−240] and stable binuclear Fe(II) environments (**19** and **26**).[101,240] Asymmetry and five-coordinate irons are difficult to build into oxo-bridged iron clusters; however, elements of both are being incorporated in models by creating a site for small, readily dissociable molecules in the iron coordination. These allow association of dioxygen, H_2O_2, or, potentially, substrates at the appropriate point in catalysis. It is possible that different solvents, water, or solution ions bind to each iron in the cluster, in some cases making the sites distinguishable.[109] The importance of a dissociable ligand was investigated in a set of experiments in which μ-oxo−diiron(III) complexes were synthesized with the formula, $Fe_2O(bipy)_4X_2(ClO_4)_4$ (**4**).[241] Interestingly, it was discovered that the more labile the X ligand was, the more effective the complex was in catalysis. The most efficient catalyst had H_2O as the X ligand in analogy with the enzyme active site clusters.

The roles played by the specific amino acids present in the cluster ligation of enzymes and proteins are emerging. For example, it has been shown using a family of complexes based on **17** that replacing the neutral phosphine oxides with the more electron donating anionic benzoate dramatically increases the rate of oxygen activation. Moreover, the rate of reaction with O_2 could be modulated by the introduction of new substituents on the bridging benzoate. This phenomenon is analogous to the "push" mechanism described for the O−O cleavage in heme−peroxy acid complexes.[242] Clearly, the electron density contributed by the ligands can modulate the reactivity of the O_2 adduct in this model system and is likely to be important in the enzymes. Accordingly, it has been shown that the MMOH cluster undergoes a carboxylate shift in the formation of the reduced diiron core, which also shows that O_2 binding and reactivity might be changed by ligand environment.[70]

It is also possible that the water ligand bound to the active site cluster of MMOH and R2 plays a specific role in catalysis. In studies of model complex **9**, it was suggested that an aqua ligand played a possible role in alkane functionalization.[243,244] These studies illustrate that the activity of the diiron core can be finely tuned by the modification of the ligand environment.

VI. Overview

Thanks to the combined efforts of enzymologists, crystallographers, spectroscopists, molecular biologists, and chemists we now have a great deal of structural, kinetic, and mechanistic information available for comparison of binuclear iron clusters that activate and fail to activate O_2. Unfortunately, a consensus view has not emerged for either the mechanism of O_2 activation or the difference between oxygen activating and nonactivating systems. However, some common characteristics which help to distinguish O_2-activating systems are now known. (1) The oxygen-activating systems appear to have iron ligand spheres composed of a single histidyl nitrogen and several carboxylate oxygens plus the oxo or hydroxo bridge(s). In contrast, the oxygen carrier Hr has predominantly nitrogen ligation and the enzyme purple acid phosphatase (PAP), which does not catalyze oxygen activation chemistry, has a phenolic oxygen ligand on one of the irons. (2) The oxygen-activating enzymes appear to have comparatively flexible ligand coordinations that can undergo rearrangements upon reduction. These include loss of a bridging oxygen and shift of the carboxylate ligands to any of several new binding modes. (3) The oxygen-activating enzymes appear to have open or otherwise accessible coordination sites for exogenous ligands on each iron. Moreover, the sites appear to be organized such that a single exogenous ligand such as O_2 could occupy both sites simultaneously and the sites do not represent greatly different chemical environments from the prospective of the iron ligation. In contrast, Hr only has one site that is readily occupied by exogenous ligands and PAP has two quite different iron environments due to the tyrosine ligation of one site. (4) The oxygen-activating monooxygenase enzymes appear to have an open pocket large enough for exogenous molecules near the binuclear iron site, whereas R2 and Hr have limited accessibility for larger substrates. This is likely to determine what type of reactions can be carried out. (5) The O_2-activating monooxygenases appear to have protonated bridging oxygens and may have two oxygen bridges instead of one. (6) The O_2-activating monooxygenases appear to have a threonine residue in the active site that can serve to provide protons either directly or via a hydrogen bound solvent.

Upon consideration of these common and contrasting aspects of the active sites of binuclear iron cluster-containing proteins, it seems reasonable to speculate that O_2 activation by these sites is facilitated by a site that can be stabilized through all of the possible redox states between $Fe^{II}Fe^{II}$ and $Fe^{IV}Fe^{IV}$. Sites like that found in PAP cannot readily stabilize the $Fe^{II}Fe^{II}$ state due to the phenolate ligand and, as a consequence, do not catalyze two electron oxygen reduction chemistry necessary to initiate O−O bond cleavage. The predominantly nitrogen-rich site of Hr cannot catalyze O−O bond cleavage from the peroxy state or yield the $Fe^{IV}Fe^{IV}$ state, presumably because there is insufficient charge donation to cleave the O−O bond. A carboxylate-rich environment appears to allow for both the formation of a peroxy adduct and the facilitation of O−O bond cleavage to yield an oxo−$Fe^{VI}Fe^{IV}$ state that is sufficiently electrophilic to directly or indirectly attack unactivated C−H bonds.

The presence of two adjacent sites for exogenous ligands on the two irons of the MMOH and R2 clusters and the symmetry of the Mössbauer spectrum of MMOH compound P suggest that O_2 activation may involve some sort of bridging complex. This stands in contrast to the monodentate peroxy complex of Hr (oxy-Hr) in which the distal oxygen of the peroxide is protonated and hydrogen bonded to the bridging oxygen. If the peroxide intermediate of MMOH is bridging between two irons with similar ligand environments, then it seems likely that the initial bond breakage is homolytic. This would not require proton donation, but if protons are available from the bridging oxygen, a bound solvent, or a group in the active site, one of the bound oxygen atoms of dioxygen might be protonated and dissociate as

water. This would leave the oxo−$Fe^{IV}Fe^{IV}$ state, which is the equivalent of the proposed P450-π-cation radical reactive species. This would also serve to pull the reaction toward completion by allowing a comparatively facile homolytic O−O bond cleavage to yield the more reactive heterolytic cleavage product.

VII. Abbreviations

ACP	acyl carrier protein
B	methane monooxygenase component B
BIDPhE	1,1-bis(1-methyl-2-imidazolyl)-1-(3,5-di-*tert*-butyl-4-hydroxyphenyl)ethane
BIPhMe	bis(1-methyl-2-imidazolyl)phenylmethoxymethane
bimp	2,6-bis[[bis[(1-methylimidazol-2-yl)methyl]amino]methyl]-4-methylphenolate
bipy	2,2′-bipyridine
CD	circular dichroism
CD_4	deuterated methane
Δ9D	stearoyl-acyl carrier protein Δ^9 desaturase
$\Delta9D_{ox}$	oxidized form of stearoyl-acyl carrier protein Δ^9 desaturase
$\Delta9D_{red}$	reduced form of stearoyl-acyl carrier protein Δ^9 desaturase
DMF	dimethylformamide
DMSO	dimethyl sulfoxide
DOPA	dihydroxyphenylalanine
DPAH	dipicolinic acid
$E_1°'$	formal potential value for first electron transfer
$E_2°'$	formal potential value for second electron transfer
E_m, E_{mid}	midpoint potential value for overall electron transfer
ENDOR	electron nuclear double resonance
EPR	electron paramagnetic resonance
Et	ethyl
EXAFS	extended X-ray absorption fine structure
FAD	flavin adenine dinucleotide
$[Fe_2S_2]$	two iron−two sulfur cluster
H	methane monooxygenase hydroxylase component
$HB(iPr_2pz)_3$	hydrotris(3,5-diisopropyl-1-pyrazolyl)borate
$HBpz_3$	hydrotris(1-pyrazolyl)borate
H_{mv}	mixed valence form of methane monooxygenase hydroxylase component
H_{ox}	oxidized form of methane monooxygenase hydroxylase component
H_2Hbab	1,2-bis(2-hydroxybenzamido)benzene
HPTB	*N*,*N*,*N*′,*N*′-tetrakis(2-benzimidazolylmethyl)-2-hydroxy-1,3-diaminopropane
Hr	hemerythrin
H_{red}	reduced form of methane monooxygenase hydroxylase component
HXTA	*N*,*N*′-(2-hydroxy-1,3-xylylene)bis(*N*-(carboxymethyl)glycine)
ImH	imidazole
K_D	dissociation constant
KIE	kinetic isotope effect
MCD	magnetic circular dichroism
Me	methyl
MMO	methane monooxygenase
MMOB	methane monooxygenase component B
MMOH	methane monooxygenase hydroxylase component
$MMOH_{ox}$	diferric form of methane monooxygenase hydroxylase component
$MMOH_{red}$	diferrous form of methane monooxygenase hydroxylase component
MMOR	methane monooxygenase reductase component
NAD^+	nicotinamide adenine dinucleotide
NADH	reduced nicotinamide adenine dinucleotide
NDP	nucleoside diphosphate
NTP	nucleoside triphosphate
OAc	acetate anion
OBz	benzoate anion
P	methane monooxygenase compound P
P450	cytochrome P450
PAGE	polyacrylamide gel electrophoresis
Ph	phenyl
PH	phenol hydroxylase
Ph-bimp	2,6-bis[[bis[(1-methyl-4,5-diphenylimidazol-2-yl)methyl]amino]methyl]-4-methylphenolate
pMMO	particulate methane monooxygenase
PPh_3	triphenylphosphine
py	pyridine
pz	pyrazolyl
Q	methane monooxygenase compound Q
R	methane monooxygenase reductase component
R1	ribonucleotide reductase subunit R1
R2	ribonucleotide reductase subunit R2
$R2_{act}$	active form (diferric/tyrosyl radical) of ribonucleotide reductase subunit R2
$R2_{apo}$	apo form of ribonucleotide reductase subunit R2
$R2_{met}$	met form (diferric) of ribonucleotide reductase subunit R2
$R2_{red}$	reduced form of ribonucleotide reductase subunit R2
$R2_{semimet}$	semimet form of ribonucleotide reductase subunit R2
RH	hydrocarbon
ROH	hydroxylated hydrocarbon
RR	ribonucleotide reductase
salmp	bis(salicylidenamino)-2-methylphenolate
T2MO	toluene 2-monooxygenase
T3MO	toluene 3-monooxygenase
T4MO	toluene 4-monooxygenase
TBHP	*tert*-butyl hydroperoxide
TLA	tris(2-pyridylmethyl)amine
tmima	tris((1-methylimidazol-2-yl)methyl)amine
TMO_{mv}	mixed-valent form of toluene monooxygenase
TMO_{ox}	oxidized form of toluene monooxygenase
TMO_{red}	reduced form of toluene monooxygenase
TPA	tris(2-pyridylmethyl)amine
U	ribonucleotide reductase intermediate **U**
X	ribonucleotide reductase intermediate **X**
XDK	*m*-xylenediamine bis(Kemp's triacid)imide

VIII. Acknowledgments

We thank all of our colleagues who have provided us with reprints of their recent work and/or preprints of their unpublished work: K. K. Andersson, A. A. DiSpirito, Y. Dong, H. G. Floss, A. Gräslund, B. M. Hoffman, B.-H. Huynh., D. M. Kurtz, S. J. Lippard, E. Münck, M. Newcomb, I. Okura, L. Que, Jr., J. Sanders-Loehr, A. E. Shilov, A. A. Shteinman, B.-M. Sjöberg, E. I. Solomon, M. Stankovich, J. Stubbe, H. Uchiyama, and L. P. Wackett. We would also like to especially thank Jeremy Nesheim, Sang-Kyu Lee, and Yi Jin for helpful discussions and revisions of the initial draft.

References

(1) Que, L., Jr.; Ho, R. Y. N. *Chem. Rev.* **1996**, *96*, 2607−2624 (this issue).
(2) Lipscomb, J. D.; Orville, A. M. *Mechanistic Aspects of Dihydroxybenzoate Dioxygenases*; Sigel, H., Sigel, I., Eds.; Marcel Dekker: New York, 1992; Vol. 28, pp 243−298.

(3) Shu, L.; Chiou, Y.-M.; Orville, A. M.; Miller, M. A.; Lipscomb, J. D.; Que, L., Jr. *Biochemistry* **1995**, *34*, 6649−6659.
(4) Ortiz de Montellano, P. R. *Cytochrome P-450*; Ortiz de Montellano, P. R., Ed.; Plenum Press: New York, 1985; pp 217−271.
(5) McMurry, T. J.; Groves, J. T. *Metalloporphyrin Models for Cytochrome P-450*; Ortiz de Montellano, P. R., Ed.; Plenum Press: New York, 1986; pp 1−28.
(6) Groves, J. T.; McClusky, G. A.; White, R. E.; Coon, M. J. *Biochem. Biophys. Res. Commun.* **1978**, *81*, 154−160.
(7) Feig, A. L.; Lippard, S. J. *Chem. Rev.* **1994**, *94*, 759−805.
(8) Reichard, P. *Basic Life Sci.* **1985**, *31*, 33−45.
(9) Reichard, P. *J. Biol. Chem.* **1993**, *268*, 8383−6.
(10) Sjöberg, B. M. *Structure* **1994**, *2*, 793−6.
(11) Stubbe, J. *J. Biol. Chem.* **1990**, *265*, 5329−5333.
(12) Anthony, C. *The Biochemistry of Methylotrophs*; Academic Press: London, 1982.
(13) Dalton, H. *Adv. Appl. Microbiol.* **1980**, *26*, 71−87.
(14) Lipscomb, J. D. *Annu. Rev. Microbiol.* **1994**, *48*, 371−99.
(15) Newman, L. M.; Wackett, L. P. *Biochemistry* **1995**, *34*, 14066−14076.
(16) Pikus, J. D.; Studts, J. M.; Achim, C.; Kauffmann, K. E.; Münck, E.; Steffan, R. J.; McClay, K.; Fox, B. G. *Biochemistry* **1996**, *35*, 9106−9119.
(17) Fox, B. G.; Shanklin, J.; Somerville, C.; Münck, E. *Proc. Natl. Acad. Sci. USA* **1993**, *90*, 2486−90.
(18) Nordlund, I.; Powlowski, J.; Shingler, V. *J. Bacteriol.* **1990**, *172*, 6826−6833.
(19) Shanklin, J.; Whittle, E.; Fox, B. G. *Biochemistry* **1994**, *33*, 12787−12794.
(20) Sjöberg, B.-M. *Structure of Ribonucleotide Reductase from Escherichia coli*; Eckstein, F., Lilley, D. M. J., Eds.; Springer-Verlag: Berlin, 1995; Vol. 9, pp 192−221.
(21) Andersson, K. K.; Gräslund, A. *Diiron-Oxygen Proteins*; Academic Press, Inc.: New York, 1995; Vol. 43, pp 359−408.
(22) Nordlund, P.; Ecklund, H. *Curr. Opin. Struct. Biol.* **1995**, *5*, 758−766.
(23) Fontecave, M.; Nordlund, P.; Eklund, H.; Reichard, P. *Adv. Enzymol. Relat. Areas Mol. Biol.* **1992**, *65*, 147−83.
(24) Liu, K. E.; Lippard, S. J. *Adv. Inorg. Chem.* **1995**, *42*, 263−289.
(25) Que, L., Jr.; Dong, Y. *Acc. Chem. Res.* **1996**, *29*, 190−196.
(26) Kurtz, D. M. *Chem. Rev.* **1990**, *90*, 585−606.
(27) Andersson, K. K.; Froland, W. A.; Lee, S.-K.; Lipscomb, J. D. *New J. Chem.* **1991**, *15*, 411−415.
(28) Colby, J.; Stirling, D. I.; Dalton, H. *Biochem. J.* **1977**, *165*, 395−402.
(29) Fox, B. G.; Borneman, J. G.; Wackett, L. P.; Lipscomb, J. D. *Biochemistry* **1990**, *29*, 6419−27.
(30) Green, J.; Dalton, H. *J. Biol. Chem.* **1989**, *264*, 17698−703.
(31) Higgins, I. J.; Best, D. J.; Hammond, R. C. *Nature* **1980**, *286*, 561−564.
(32) Rataj, M. J.; Kauth, J. E.; Donnelly, M. I. *J. Biol. Chem.* **1991**, *266*, 18684−18690.
(33) Nagai, J.; Bloch, K. *J. Biol. Chem.* **1968**, *243*, 4626−4633.
(34) Zahn, J. A.; DiSpirito, A. A. *J. Bacteriol.* **1996**, *178* (4), 1018−1029.
(35) Wilkinson, B.; Zhu, M.; Priestley, N. D.; Nguyen, H.-H. T.; Morimoto, H.; Williams, P. G.; Chan, S. I.; Floss, H. G. *J. Am. Chem. Soc.* **1996**, *118* (4), 921−922.
(36) Chan, S. I.; Nguyen, H.-H. T.; Shiemke, A. K.; Lidstrom, M. E. *Biochemical and Biophysical Studies Toward Characterization of the Membrane-Associated Methane Monooxygenase*; Murrell, J. C., Kelly, D. P., Eds.; Intercept Ltd.: Andover UK, 1993; pp 93−107.
(37) Smith, D. D.; Dalton, H. *Eur. J. Biochem.* **1989**, *182*, 667−671.
(38) Nguyen, H. H.; Shiemke, A. K.; Jacobs, S. J.; Hales, B. J.; Lidstrom, M. E.; Chan, S. I. *J. Biol. Chem.* **1994**, *269*, 14995−15005.
(39) Semrau, J. D.; Zolandz, D.; Lidstrom, M. E.; Chan, S. I. *J. Inorg. Biochem.* **1995**, *58*, 235−244.
(40) Fox, B. G.; Froland, W. A.; Dege, J. E.; Lipscomb, J. D. *J. Biol. Chem.* **1989**, *264*, 10023−33.
(41) Fox, B. G.; Froland, W. A.; Jollie, D. R.; Lipscomb, J. D. *Methods Enzymol.* **1990**, *188*, 191−202.
(42) Nakajima, T.; Uchiyama, H.; Yagi, O.; Nakahara, T. *Biosci. Biotech. Biochem.* **1992**, *56*, 736−740.
(43) Patel, R. N.; Savas, J. C. *J. Bacteriol.* **1987**, *169*, 2313−7.
(44) Pilkington, S. J.; Dalton, H. *Methods Enzymol.* **1990**, *188*, 181−190.
(45) Woodland, M. P.; Dalton, H. *J. Biol. Chem.* **1984**, *259*, 53−59.
(46) Fox, B. G.; Surerus, K. K.; Münck, E.; Lipscomb, J. D. *J. Biol. Chem.* **1988**, *263*, 10553−6.
(47) Ericson, A.; Hedman, B.; Green, J.; Bentsen, J. G.; Beer, R. H.; Lippard, S. J.; Dalton, H.; Hodgson, K. O. *J. Am. Chem. Soc.* **1988**, *110*, 2330−2332.
(48) DeRose, V. J.; Liu, K. E.; Kurtz, D. M., Jr.; Hoffman, B. M.; Lippard, S. J. *J. Am. Chem. Soc.* **1993**, *115*, 6440−6441.
(49) Fox, B. G.; Hendrich, M. P.; Surerus, K. K.; Andersson, K. K.; Froland, W. A.; Lipscomb, J. D. *J. Am. Chem. Soc.* **1993**, *115*, 3688−3701.
(50) Thomann, H.; Bernardo, M.; McCormick, J. M.; Pulver, S.; Andersson, K. K.; Lipscomb, J. D.; Solomon, E. I. *J. Am. Chem. Soc.* **1993**, *115*, 8881−8882.
(51) Lee, S. K.; Nesheim, J. C.; Lipscomb, J. D. *J. Biol. Chem.* **1993**, *268*, 21569−77.
(52) Liu, Y.; Nesheim, J. C.; Lee, S. K.; Lipscomb, J. D. *J. Biol. Chem.* **1995**, *270*, 24662−24665.
(53) Froland, W. A.; Andersson, K. K.; Lee, S. K.; Liu, Y.; Lipscomb, J. D. *J. Biol. Chem.* **1992**, *267*, 17588−97.
(54) DeWitt, J. G.; Bentsen, J. G.; Rosenzweig, A. C.; Hedman, B.; Green, J.; Pilkington, S.; Papaefthymiou, G. C.; Dalton, H.; Hodgson, K. O.; Lippard, S. J. *J. Am. Chem. Soc.* **1991**, *113*, 9219−9233.
(55) Prince, R. C.; George, G. N.; Savas, J. C.; Cramer, S. P.; Patel, R. N. *Biochim. Biophys. Acta* **1988**, *952*, 220−9.
(56) DeWitt, J. G.; Rosenzweig, A. C.; Salifoglou, A.; Hedman, B.; Lippard, S. J.; Hodgson, K. O. *Inorg. Chem.* **1995**, *34*, 2505−2515.
(57) Holmes, M. A.; Le Trong, I.; Turley, S.; Sieker, L. C.; Stenkamp, R. E. *J. Mol. Biol.* **1991**, *218*, 583−593.
(58) Stenkamp, R. E.; Sieker, L. C.; Jensen, L. H.; McCallum, J. D.; Sanders-Loehr, J. *Proc. Natl. Acad. Sci. USA* **1985**, *82*, 713−716.
(59) Stenkamp, R. E. *Chem. Rev.* **1994**, *94*, 715−726.
(60) Andersson, K. K.; Elgren, T. E.; Que, L., Jr.; Lipscomb, J. D. *J. Am. Chem. Soc.* **1992**, *114*, 8711−8713.
(61) Woodland, M. P.; Patil, D. S.; Cammack, R.; Dalton, H. *Biochim. Biophys. Acta* **1986**, *873*, 237−242.
(62) Hendrich, M. P.; Fox, B. G.; Andersson, K. K.; Debrunner, P. G.; Lipscomb, J. D. *J. Biol. Chem.* **1992**, *267*, 261−9.
(63) Fox, B. G.; Liu, Y.; Dege, J. E.; Lipscomb, J. D. *J. Biol. Chem.* **1991**, *266*, 540−50.
(64) DeRose, V. J.; Liu, K. E.; Lippard, S. J.; Hoffman, B. M. *J. Am. Chem. Soc.* **1996**, *118*, 121−134.
(65) Rosenzweig, A. C.; Frederick, C. A.; Lippard, S. J. *Proceedings of the 8th International Symposium on Microbial Growth on C_1 Compounds*; Lidstrom, M. E., Tabita, F. R., Eds., Kluwer: Boston, 1995; pp 141−149.
(66) Hendrich, M. P.; Münck, E.; Fox, B. G.; Lipscomb, J. D. *J. Am. Chem. Soc.* **1990**, *112*, 5861−5865.
(67) Hendrich, M. P.; Debrunner, P. G. *Biophys. J.* **1989**, *56*, 489−506.
(68) Reem, R. C.; Solomon, E. I. *J. Am. Chem. Soc.* **1987**, *109*, 1216−1226.
(69) Pulver, S.; Froland, W. A.; Fox, B. G.; Lipscomb, J. D.; Solomon, E. I. *J. Am. Chem. Soc.* **1993**, *115*, 12409−12422.
(70) Rosenzweig, A. C.; Nordlund, P.; Takahara, P. M.; Frederick, C. A.; Lippard, S. J. *Chemistry & Biology* **1995**, *2*, 409−418.
(71) Rosenzweig, A. C.; Frederick, C. A.; Lippard, S. J.; Nordlund, P. *Nature* **1993**, *366*, 537−43.
(72) Elango, N.; Radhakrishman, R.; Froland, W. A.; Wallar, B. J.; Earhart, C. A.; Lipscomb, J. D.; Ohlendorf, D. H. *Protein Sci.* **1996**, submitted for publication.
(73) Cohen, C.; Parry, D. A. D. *Proteins: Struct., Funct, Genet.* **1990**, *7*, 1−15.
(74) DeGrado, W. F. *Adv. Protein Chem.* **1988**, *39*, 51−124.
(75) Tolman, W. B.; Liu, S.; Bentsen, J. G.; Lippard, S. J. *J. Am. Chem. Soc.* **1991**, *113*, 152−164.
(76) Åberg, A. Thesis, Stockholm University, 1993.
(77) Nordlund, P.; Åberg, A.; Uhlin, U.; Eklund, H. *Biochem. Soc. Trans.* **1993**, *21*, 735−8.
(78) Shu, L.; Liu, Y.; Lipscomb, J. D.; Que, L., Jr. *J. Biol. Inorg. Chem.* **1996**, *1*, 297−304.
(79) Lund, J.; Dalton, H. *Eur. J. Biochem.* **1985**, *147*, 291−6.
(80) Prince, R. C.; Patel, R. N. *FEBS Lett.* **1986**, *203*, 127−130.
(81) Gibson, D. T.; Subramanian, V. *Microbial Degradation of Aromatic Hydrocarbons*; Gibson, D. T., Ed.; Marcel Dekker: New York, 1984; Vol. 13, pp 181−252.
(82) Correll, C. C.; Batie, C. J.; Ballou, D. P.; Ludwig, M. L. *Science* **1992**, *258*, 1604−1610.
(83) Green, J.; Dalton, H. *Biochem. J.* **1989**, *259*, 167−172.
(84) Lund, J.; Woodland, M. P.; Dalton, H. *Eur. J. Biochem.* **1985**, *147*, 297−305.
(85) Green, J.; Dalton, H. *J. Biol. Chem.* **1985**, *260*, 15795−801.
(86) Liu, Y.; Nesheim, J.; Kauffman, K.; Paulsen, K. E.; Stankovich, M. T.; Münck, E.; Lipscomb, J. D. Manuscript in preparation, 1996.
(87) Paulsen, K. E.; Liu, Y.; Fox, B. G.; Lipscomb, J. D.; Münck, E.; Stankovich, M. T. *Biochemistry* **1994**, *33*, 713−22.
(88) Stainthorpe, A. C.; Murrell, J. C.; Salmond, G. P.; Dalton, H.; Lees, V. *Arch. Microbiol.* **1989**, *152*, 154−9.
(89) Stainthorpe, A. C.; Lees, V.; Salmond, G. P.; Dalton, H.; Murrell, J. C. *Gene* **1990**, *91*, 27−34.
(90) Cardy, D. L.; Laidler, V.; Salmond, G. P.; Murrell, J. C. *Arch. Microbiol.* **1991**, *156*, 477−83.
(91) Cardy, D. L.; Laidler, V.; Salmond, G. P.; Murrell, J. C. *Mol. Microbiol.* **1991**, *5*, 335−42.
(92) West, C. A.; Salmond, G. P.; Dalton, H.; Murrell, J. C. *J. Gen. Microbiol.* **1992**, *138*, 1301−7.

(93) Jahng, D.; Wood, T. K. *Appl. Environ. Microbiol.* **1994**, *60*, 2473−82.
(94) Liu, K. E.; Valentine, A. M.; Wang, D. L.; Huynh, B. H.; Edmondson, D. E.; Salifoglou, A.; Lippard, S. J. *J. Am. Chem. Soc.* **1995**, *117*, 10174−10185.
(95) Liu, K. E.; Wang, D.; Huynh, B. H.; Edmondson, D. E.; Salifoglou, A.; Lippard, S. J. *J. Am. Chem. Soc.* **1995**, *116*, 7465−7466.
(96) Liu, K. E.; Valentine, A. M.; Qiu, D.; Edmondson, D. E.; Appelman, E. H.; Spiro, T. G.; Lippard, S. J. *J. Am. Chem. Soc.* **1995**, *117*, 4997−4998.
(97) Lee, S.-K.; Fox, B. G.; Froland, W. A.; Lipscomb, J. D.; Münck, E. *J. Am. Chem. Soc.* **1993**, *115*, 6450−6451.
(98) Priestley, N. D.; Floss, H. G.; Froland, W. A.; Lipscomb, J. D.; Williams, P. G.; Morimoto, H. *J. Am. Chem. Soc.* **1992**, *114*, 7561−7562.
(99) Nesheim, J. C.; Lipscomb, J. D. *Biochemistry* **1996**, *35*, 10240−10247.
(100) Deighton, N.; Podmore, I. D.; Symons, M. C. R.; Wilkins, P. C.; Dalton, H. *J. Chem. Soc., Chem. Commum.* **1991**, 1086−1088.
(101) Dong, Y.; Menage, S.; Brennan, B. A.; Elgren, T. E.; Jang, H. G.; Pearce, L. L.; Que, L., Jr. *J. Am. Chem. Soc.* **1993**, *115*, 1851−1859.
(102) Dong, Y.; Yan, S.; Young, J., V. G.; Que, L., Jr. *Angew. Chem., Int. Ed. Engl.* **1996**, *35* (6), 618−620.
(103) Ookubo, T.; Sugimoto, H.; Nagayama, T.; Masuda, H.; Sato, T.; Tanaka, K.; Maeda, Y.; Okawa, H.; Hayashi, Y.; Uehara, A.; Suzuki, M. *J. Am. Chem. Soc.* **1996**, *118*, 701−702.
(104) Kim, K.; Lippard, S. J. *J. Am. Chem. Soc.* **1996**, *118*, 4914−4915.
(105) McCandlish, E.; Miksztal, A. R.; Nappa, M.; Sprenger, A. G.; Valentine, J. S.; Stong, J. D.; Spiro, T. G. *J. Am. Chem. Soc.* **1980**, *102*, 4268−4271.
(106) Burstyn, J. N.; Roe, J. A.; Miksztal, A. R.; Shaevitz, B. A.; Lang, G.; Valentine, J. S. *J. Am. Chem. Soc.* **1988**, *110*, 1382−1388.
(107) Ahmad, S.; McCallum, J. D.; Shiemke, A. K.; Appelman, E. H.; Loehr, T. M.; Sanders-Loehr, J. *J. Inorg. Chem.* **1988**, *27*, 2230−2233.
(108) Leising, R. A.; Brennan, B. A.; Fox, B. G.; Münck, E.; Que, L., Jr. *J. Am. Chem. Soc.* **1991**, *113*, 3988−3990.
(109) Dong, Y.; Fujii, H.; Hendrich, M. P.; Leising, R. A.; Pan, G.; Randall, C. R.; Wilkinson, E. C.; Zang, Y.; Que, L., Jr.; Fox, B. G.; Kauffmann, K.; Münck, E. *J. Am. Chem. Soc.* **1995**, *117*, 2778−2792.
(110) Zang, Y.; Pan, G.; Fox, B. G.; Münck, E.; Que, L., Jr. *J. Am. Chem. Soc.* **1994**, *116*, 3653−3654.
(111) Zang, Y.; Dong, Y.; Kauffmann, K.; Münck, E.; Que, L., Jr. *J. Am. Chem. Soc.* **1995**, *117*, 1169−1170.
(112) Dong, Y.; Kauffmann, K.; Münck, E.; Que, L., Jr. *J. Am. Chem. Soc.* **1995**, *117*, 11377−11378.
(113) Jiang, Y.; Wilkins, P. C.; Dalton, H. *Biochim. Biophys. Acta* **1993**, *1163*, 105−12.
(114) Bowry, V. W.; Lusztyk, J.; Ingold, K. U. *J. Am. Chem. Soc.* **1989**, *111*, 1927−1928.
(115) Bowry, V. W.; Ingold, K. U. *J. Am. Chem. Soc.* **1991**, *113*, 5699−5707.
(116) Stearns, R. A.; Ortiz de Montellano, P. R. *J. Am. Chem. Soc.* **1985**, *107*, 4081−4082.
(117) Ortiz de Montellano, P. R. *Trends Pharmacol. Sci.* **1989**, *10*, 354−359.
(118) Miller, V. P.; Fruetel, J. A.; Ortiz de Montellano, P. R. *Arch. Biochem. Biophys.* **1992**, *298*, 697−702.
(119) Atkinson, J. K.; Hollenberg, P. F.; Ingold, K. U.; Johnson, C. C.; Le Tadic, M.-H.; Newcomb, M.; Putt, D. A. *Biochemistry* **1994**, *33*, 10630−10637.
(120) Novoa, J. J.; Constans, P.; Whrang, M.-H. *Angew. Chem., Int. Ed. Engl.* **1993**, *32*, 588.
(121) Ortiz de Montellano, P. R.; Stearns, R. A. *J. Am. Chem. Soc.* **1987**, *109*, 3415−3420.
(122) Ruzicka, F.; Huang, D. S.; Donnelly, M. I.; Frey, P. A. *Biochemistry* **1990**, *29*, 1696−700.
(123) Liu, K. E.; Johnson, C. C.; Newcomb, M.; Lippard, S. J. *J. Am. Chem. Soc.* **1993**, *115*, 939−947.
(124) Choi, S.-Y.; Eaton, P. E.; Hollenberg, P. F.; Liu, K. E.; Lippard, S. J.; Newcomb, M.; Putt, D. A.; Upadhyaya, S. P.; Xiong, Y. *J. Am. Chem. Soc.* **1996**, *118*, 6547−6555.
(125) Shapiro, S.; Piper, J. U.; Caspi, E. *J. Am. Chem. Soc.* **1982**, *104*, 2301.
(126) Liu, K. E.; Lippard, S. J.; Floss, H. G.; Williams, P. G. Unpublished results, 1995.
(127) Wilkins, P. C.; Dalton, H.; Samuel, C. J.; Green, J. *Eur. J. Biochem.* **1994**, *226*, 555−560.
(128) Nesheim, J. C.; Lipscomb, J. D. *J. Inorg. Biochem.* **1995**, *59*, 369.
(129) Schaller, C. P.; Bonnano, J. B.; Wolczanski, P. T. *J. Am. Chem. Soc.* **1994**, *116*, 4133−4134.
(130) Shestakov, A. F.; Shilov, A. E. *J. Mol. Catal.* **1996**, submitted for publication.
(131) Shteinman, A. A. *Russ. Chem. Bull.* **1995**, *44*, 975−984.
(132) Nordlund, P.; Dalton, H.; Eklund, H. *FEBS Lett.* **1992**, *307*, 257−62.
(133) Newcomb, M.; Tadic-Biadatti, M.-H. L.; Chestney, D. L.; Roberts, E. S.; Hollenberg, P. F. *J. Am. Chem. Soc.* **1995**, *117*, 12085−12091.
(134) Barton, D. H. R.; Beviere, S. D.; Chavasiri, W.; Csuhai, E.; Doller, D.; Liu, W.-G. *J. Am. Chem. Soc.* **1992**, *114*, 2147−2156.
(135) Barton, D. H. R.; Doller, D. *Acc. Chem. Res.* **1992**, *25*, 504−512.
(136) Barton, D. H. R.; Taylor, D. K. *Russ. Chem. Bull.* **1995**, *44*, 575−583.
(137) Korzekwa, K.; Trager, W.; Gouterman, M.; Spangler, D.; Loew, G. H. *J. Am. Chem. Soc.* **1985**, *107*, 4273−4279.
(138) Pulver, S. C.; Froland, W. A.; Lipscomb, J. D.; Solomon, E. I. Manuscript in preparation, 1996.
(139) Hendrich, M. P.; Lipscomb, J. D. Unpublished results.
(140) Elgren, T. E.; Hendrich, M. P.; Que, L., Jr. *J. Am. Chem. Soc.* **1993**, *115*, 9291.
(141) Pulver, S. C.; Tong, W. H.; Bollinger, J. M.; Stubbe, J.; Solomon, E. I. *J. Am. Chem. Soc.* **1995**, *117*, 12664−12678.
(142) Liu, Y. Ph.D. Thesis, 1995.
(143) Liu, K. E.; Lippard, S. J. *J. Biol. Chem.* **1991**, *266*, 12836−9.
(144) Liu, Y.; Nesheim, J. C.; Paulsen, K. E.; Wallar, B. J.; Stankovich, M. T.; Lipscomb, J. D. *J. Inorg. Biochem.* **1995**, *59*, 368.
(145) Liu, Y.; Kauffmann, K.; Nesheim, J. C.; Münck, E.; Lipscomb, J. D. Unpublished results.
(146) Hazzard, J. T.; Poulos, T. L.; Tollin, G. *Biochemistry* **1987**, *26*, 2836−48.
(147) Byrne, A. M.; Kukor, J. J.; Olsen, R. H. *Gene* **1995**, *154*, 65−70.
(148) Whited, G. M.; Gibson, D. T. *J. Bacteriol.* **1991**, *173*, 3017−3020.
(149) Whited, G. M.; Gibson, D. T. *J. Bacteriol.* **1991**, *173*, 3010−3016.
(150) Fox, B. G.; Shanklin, J.; Ai, J.; Loehr, T. M.; Sanders-Loehr, J. *Biochemistry* **1994**, *33*, 12776−12786.
(151) McClay, K.; Fox, B. G.; Steffan, R. J. *Appl. Environ. Microbiol.* **1996**, in press.
(152) Francesconi, S. C.; Blake, A. C.; Shields, M. S. *Annu. Meet. Am. Soc. Nicrobiol. Abstr.* **1995**, *K198*, 570.
(153) Johnson, G. R.; Olsen, R. H. *Appl. Environ. Microbiol.* **1995**, *61*, 3336−3346.
(154) Siedow, J. N.; Umbach, A. L.; Moore, A. L. *FEBS Lett.* **1995**, *362*, 10−14.
(155) Poulos, T. L.; Kraut, J. *J. Biol. Chem.* **1980**, *255*, 8199−8205.
(156) Shanklin, J.; Somerville, C. *Proc. Natl. Acad. Sci. USA* **1991**, *88*, 2510−2514.
(157) McKeon, T. A.; Stumpf, P. K. *J. Biol. Chem.* **1982**, *257*, 12141−12147.
(158) Strittmatter, P.; Spatz, L.; Corcoran, D.; Rogers, M. J.; Setlow, B.; Redline, R. *Proc. Natl. Acad. Sci. USA* **1974**, *71*, 4565−4569.
(159) Turowski, P. N.; Armstrong, W. H.; Liu, S.; Brown, S. N.; Lippard, S. J. *Inorg. Chem.* **1994**, *33*, 636−645.
(160) Ai, J.; Broadwater, J. G.; Fox, B. G.; Sanders-Loehr, J. Conference on Oxygen Intermediates in Nonheme Metallobiochemistry 1996, Minneapolis, MN.
(161) Ling, J.; Sahlin, M.; Sjöberg, B. M.; Loehr, T. M.; Sanders-Loehr, J. *J. Biol. Chem.* **1994**, *269*, 5595−601.
(162) Reichard, P. *Science* **1993**, *260*, 1773−1777.
(163) Atkinson, J. K.; Ingold, K. U. *Biochemistry* **1993**, *32*, 9209−9214.
(164) Stubbe, J. *Adv. Enzymol. Relat. Areas Mol. Biol.* **1990**, *63*, 349−419.
(165) Gräslund, A.; Sahlin, M. *Annu. Rev. Biophys. Biomol. Struct.* **1996**, *25*, 259−286.
(166) Mao, S. S.; Holler, T. P.; Yu, G. X.; Bollinger, J., Jr.; Booker, S.; Johnston, M. I.; Stubbe, J. *Biochemistry* **1992**, *31*, 9733−43.
(167) Lin, A. N.; Ashley, G. W.; Stubbe, J. *Biochemistry* **1987**, *26*, 6905−6909.
(168) Uhlin, U.; Eklund, H. *Nature* **1994**, *370*, 533−539.
(169) Åberg, A.; Hahne, S.; Karlsson, M.; Larsson, A.; Ormö, M.; Åhgren, A.; Sjöberg, B.-M. *J. Biol. Chem.* **1989**, *264*, 12249−52.
(170) Mao, S. S.; Yu, G. X.; Chalfoun, D.; Stubbe, J. *Biochemistry* **1992**, *31*, 9752−9.
(171) Kurtz, D. M., Jr.; Shriver, D. F.; Klotz, I. M. *Coord. Chem. Rev.* **1977**, *24*, 145−178.
(172) Thelander, L. *J. Biol. Chem.* **1974**, *249*, 4858.
(173) Karlsson, M.; Sahlin, M.; Sjöberg, B. M. *J. Biol. Chem.* **1992**, *267*, 12622−6.
(174) Sturgeon, B. E.; Burdi, D.; Chen, S.; Huynh, B.-H.; Edmondson, D. E.; Stubbe, J.; Hoffman, B. M. *J. Am. Chem. Soc.* **1996**, *118*, 7551−7557.
(175) Atkin, C. L.; Thelander, L.; Reichard, P.; Lang, G. *J. Biol. Chem.* **1973**, *248*, 7464−7472.
(176) Backes, G.; Sahlin, M.; Sjöberg, B. M.; Loehr, T. M.; Sanders-Loehr, J. *Biochemistry* **1989**, *28*, 1923−1929.
(177) Bender, C.; Sahlin, M.; Babcock, G. T.; Chandrashekov, T. L.; Sabowe, S. P.; Stubbe, J.; Lindstrom, B.; Petersson, L.; Ehrenberg, A.; Sjöberg, B.-M. *J. Am. Chem. Soc.* **1989**, *111*, 8076−8083.
(178) Nordlund, P.; Sjöberg, B. M.; Eklund, H. *Nature* **1990**, *345*, 593−598.
(179) Rova, U.; Goodtzova, K.; Ingemarson, R.; Behravan, G.; Gräslund, A.; Thelander, L. *Biochemistry* **1995**, *34*, 4267−4275.
(180) Climent, I.; Sjöberg, B. M.; Huang, C. Y. *Biochemistry* **1992**, *31*, 4801−4807.

(181) Sjöberg, B. M.; Hahne, S.; Karlsson, M.; Jornvall, H.; Goransson, M.; Uhlin, B. E. *J. Biol. Chem.* **1986**, *261*, 5658−5662.
(182) Sjöberg, B. M.; Karlsson, M.; Jornvall, H. *J. Biol. Chem.* **1987**, *262*, 9736−9743.
(183) Salowe, S. P.; Stubbe, J. *J. Bacteriol.* **1986**, *165*, 363−366.
(184) Thelander, L.; Sjöberg, B.-M.; Eriksson, S. *Methods Enzymol.* **1978**, *51*, 227−237.
(185) Åberg, A.; Ormö, M.; Nordlund, P.; Sjöberg, B.-M. *Biochemistry* **1993**, *32*, 9845−9850.
(186) Sahlin, M.; Gräslund, A.; Petersson, L.; Ehrenberg, A.; Sjöberg, B. M. *Biochemistry* **1989**, *28*, 2618−2625.
(187) Gerez, C.; Fontecave, M. *Biochemistry* **1992**, *31*, 780−786.
(188) Hendrich, M. P.; Elgren, T. E.; Que, L., Jr. *Biochem. Biophys. Res. Commun.* **1991**, *176*, 705−710.
(189) Atta, M.; Andersson, K. K.; Ingemarson, R.; Thelander, L.; Gräslund, A. *J. Am. Chem. Soc.* **1994**, *116*, 6429−6430.
(190) Davydov, R.; Kuprin, S.; Gräslund, A.; Ehrenberg, A. *J. Am. Chem. Soc.* **1994**, *116*, 11120−11128.
(191) Davydov, R.; Sahlin, M.; Kuprin, S.; Gräslund, A.; Ehrenberg, A. *Biochemistry* **1996**, *35*, 5571−5576.
(192) Nordlund, P.; Eklund, H. *J. Mol. Biol.* **1993**, *232*, 123−164.
(193) Åberg, A.; Nordlund, P.; Eklund, H. *Nature* **1993**, *361*, 276−278.
(194) Uhlin, U.; Uhlin, T.; Eklund, H. *FEBS Lett.* **1993**, *336*, 148−152.
(195) Holmes, M. A.; Stenkamp, R. E. *J. Mol. Biol.* **1991**, *220*, 723−737.
(196) Stenkamp, R. E.; Sieker, L. C.; Jensen, L. H. *J. Am. Chem. Soc.* **1984**, *106*, 618−622.
(197) Ormö, M.; Regnstrom, K.; Wang, Z.; Que, L., Jr.; Sahlin, M.; Sjöberg, B. M. *J. Biol. Chem.* **1995**, *270*, 6570−6576.
(198) Sanders-Loehr, J.; Wheeler, W. D.; Shiemke, A. K.; Averill, B. A.; Loehr, T. M. *J. Am. Chem. Soc.* **1989**, *111*, 8084−8093.
(199) Galli, C.; Atta, M.; Andersson, K. K.; Gräslund, A.; Brudvig, G. W. *J. Am. Chem. Soc.* **1995**, *117*, 740−746.
(200) Un, S.; Atta, M.; Fontecave, M.; Rutherford, A. W. *J. Am. Chem. Soc.* **1995**, *117*, 10713−10719.
(201) Allard, P.; Barra, A. L.; Andersson, K. K.; Schmidt, P. P.; Atta, M.; Gräslund, A. *J. Am. Chem. Soc.* **1996**, *118*, 895−896.
(202) Hirsh, D. J.; Beck, W. F.; Lynch, J. B.; Que, L., Jr.; Brudvig, G. W. *J. Am. Chem. Soc.* **1992**, *114*, 7475−7481.
(203) Hoganson, C. W.; Sahlin, M.; Sjöberg, B.-M.; Babcock, G. T. *J. Am. Chem. Soc.* **1996**, *118*, 4672−4679.
(204) Lynch, J. B.; Juarez-Garcia, C.; Münck, E.; Que, L., Jr. *J. Biol. Chem.* **1989**, *264*, 8091−8096.
(205) Bollinger, J. M., Jr.; Tong, W. H.; Ravi, N.; Huynh, B. H.; Edmondson, D. E.; Stubbe, J. *J. Am. Chem. Soc.* **1994**, *116*, 8015−8023.
(206) Atta, M.; Debaecker, N.; Andersson, K. K.; Latour, J.-M.; Thelander, L.; Gräslund, A. *J. Biol. Inorg. Chem.* **1996**, *1*, 210−220.
(207) Atta, M.; Scheer, C.; Fries, P. H.; Fontecave, M.; Latour, J.-M. *Angew. Chem., Int. Ed. Engl.* **1992**, *31*, 1513−1515.
(208) Atta, M.; Scheer, C.; Fries, P. H.; Fontecave, M.; Latour, J.-M. *Angew. Chem., Int. Ed. Engl.* **1992**, *31*, 1513−1515.
(209) Haskin, C. J.; Ravi, N.; Lynch, J. B.; Münck, E.; Que, L., Jr. *Biochemistry* **1995**, *34*, 11090−11098.
(210) Bollinger, J. M., Jr.; Tong, W. H.; Ravi, N.; Huynh, B. H.; Edmondson, D. E.; Stubbe, J. *J. Am. Chem. Soc.* **1994**, *116*, 8024−8032.
(211) Ravi, N.; Bollinger, J. M.; Huynh, B. H.; Edmondson, D. E.; Stubbe, J. *J. Am. Chem. Soc.* **1994**, *116*, 8007−8014.
(212) Petersson, L.; Gräslund, A.; Ehrenberg, A.; Sjöberg, B.-M.; Reichard, P. *J. Biol. Chem.* **1980**, *255*, 6706−6712.
(213) Sahlin, M.; Sjöberg, B. M.; Backes, G.; Loehr, T.; Sanders-Loehr, J. *Biochem. Biophys. Res. Commun.* **1990**, *167*, 813−818.
(214) Fontecave, M.; Gerez, C.; Atta, M.; Jeunet, A. *Biochem. Biophys. Res. Commun.* **1990**, *168*, 659−664.
(215) Ochiai, E.; Mann, G. J.; Gräslund, A.; Thelander, L. *J. Biol. Chem.* **1990**, *265*, 15758−15761.
(216) Bollinger, J., Jr.; Edmondson, D. E.; Huynh, B. H.; Filley, J.; Norton, J. R.; Stubbe, J. *Science* **1991**, *253*, 292−298.
(217) Bollinger, J. M., Jr.; Stubbe, J.; Huynh, B. H.; Edmondson, D. E. *J. Am. Chem. Soc.* **1991**, *113*, 6289−6291.
(218) Bollinger, J. M., Jr.; Ravi, N.; Tong, W. H.; Edmondson, D. E.; Huynh, B. H.; Stubbe, J. *J. Inorg. Biochem.* **1993**, *51*, 6.
(219) Elgren, T. E.; Lynch, J. B.; Juarez-Garcia, C.; Münck, E.; Sjöberg, B. M.; Que, L., Jr. *J. Biol. Chem.* **1991**, *266*, 19265−19268.
(220) Ravi, N.; Bominaar, E. L. *Inorg. Chem.* **1995**, *34*, 1040−1043.
(221) Burdi, D.; Sturgeon, B. E.; Tong, W. H.; Edmondson, D. E.; Chen S; Huynh, B.-H.; Stubbe, J.; Hoffman, B. M. Conference on Oxygen Intermediates in Nonheme Metallobiochemistry Abstracts 1996, 4A, Minneapolis, MN.
(222) Burdi, D.; Sturgeon, B. E.; Tong, W. H.; Stubbe, J.; Hoffman, B. M. *J. Am. Chem. Soc.* **1996**, *118*, 281−282.
(223) Veselov, A.; Scholes, C. P. *Inorg. Chem.* **1996**, *35*, 3702−3705.
(224) Riggs-Gelasco, P. J.; Shu, L.; Chen, S.; Burdi, D.; Huynh, B.-H.; Que, L., Jr.; Stubbe, J. Conference on Oxygen Intermediates in Nonheme Metallobiochemistry Abstract 1996, 16B, Minneapolis, MN.
(225) Tong, W. H.; Chen, S.; Lloyd, S. G.; Edmondson, D. E.; Huynh, B.-H.; Stubbe, J. *J. Am. Chem. Soc.* **1996**, *118*, 2107−2108.
(226) Sahlin, M.; Lassmann, G.; Potsch, S.; Slaby, A.; Sjöberg, B.-M.; Gräslund, A. *J. Biol. Chem.* **1994**, *269*, 11699−11702.
(227) Sahlin, M.; Lassmann, G.; Potsch, S.; Sjöberg, B.-M.; Gräslund, A. *J. Biol. Chem.* **1995**, *270*, 12361−12372.
(228) Silva, K. E.; Elgren, T. E.; Que, L., Jr.; Stankovich, M. T. *Biochemistry* **1995**, *34*, 14093−14103.
(229) Ormö, M.; deMare, F.; Regnstrom, K.; Åberg, A.; Sahlin, M.; Ling, J.; Loehr, T. M.; Sanders-Loehr, J.; Sjöberg, B.-M. *J. Biol. Chem.* **1992**, *267*, 8711−8714.
(230) Beratan, D. N.; Onuchic, J. N.; Winkler, J. R.; Gray, H. B. *Science* **1992**, *258*, 1740−1741.
(231) Franzen, S.; Goldstein, R. F.; Boxer, S. G. *J. Phys. Chem.* **1993**, *97*, 3040−3053.
(232) Haskin, C. J.; Silva, K. E.; Ravi, N.; Münck, E.; Wang, Z.; Sjöberg, B.-M.; Stankovich, M. T.; Que, L., Jr. Conference on Oxygen Intermediates in Nonheme Metallobiochemistry Abstract 1996, 9D, Minneapolis, MN.
(233) Persson, B. O.; Karlsson, M.; Climent, I.; Ling, J.; Sanders Loehr, J.; Sahlin, M.; Sjöberg, B.-M. *J. Biol. Inorg. Chem.* **1996**, *1*, 247−256.
(234) Bollinger, M. J., Jr.; Ley, B. A.; Chen, S.; Huynh, B.-H.; Edmondson, D. E. Conference on Oxygen Intermediates in Nonheme Metallobiochemistry Abstract 1996, 3B, Minneapolis, MN.
(235) Kitajima, N.; Tamura, N.; Tanaka, M.; Moro-oka, Y. *Inorg. Chem.* **1992**, *31*, 3342−3343.
(236) Fish, R. H.; Konings, M. S.; Oberhausen, K. J.; Fong, R. H.; Yu, W. M.; Christou, G.; Vincent, J. B.; Coggin, D. K.; Buchanan, R. M. *Inorg. Chem.* **1991**, *30*, 3002−3006.
(237) Kim, C.; Dong, Y.; Que, L., Jr. Unpublished results, 1996.
(238) Stassinopolous, A.; Schulte, G.; Papaefthymiou, G. C.; Caradonna, J. P. *J. Am. Chem. Soc.* **1991**, *113*, 8686−8697.
(239) Stassinopoulos, A.; Caradonna, J. P. *J. Am. Chem. Soc.* **1990**, *112*, 7071−7073.
(240) Herold, S.; Pence, L. E.; Lippard, S. J. *J. Am. Chem. Soc.* **1995**, *117*, 6134−6135.
(241) Menage, S.; Vincent, J. M.; Lambeaux, C.; Chottard, G.; Grand, A.; Fontecave, M. *Inorg. Chem.* **1993**, *32*, 4766−4773.
(242) Yamaguchi, K.; Watanabe, Y.; Morishima, I. *J. Am. Chem. Soc.* **1993**, *115*, 4058−4065.
(243) Buchanan, R. M.; Chen, S.; Richardson, J. F.; Bressan, M.; Forti, L.; Morvillo, A.; Fish, R. H. *Inorg. Chem.* **1994**, *33*, 3208−3209.
(244) Rabion, A.; Chen, S.; Wang, J.; Buchanan, R. M.; Seris, J.-L.; Fish, R. H. *J. Am. Chem. Soc.* **1995**, *117*, 12356−12357.
(245) Rosenzweig, A. C.; Feng, X.; Lippard, S. J. In *Applications of Enzyme Biotechnology*; Kelly, J. W., Baldwin, T. O., Eds.; Plenum Press: New York, 1991; pp 69−85.
(246) Kauffmann, K.; Liu, Y.; Nesheim, J. C.; Lipscomb, J. D.; Münck, E. Unpublished results.
(247) Liu, Y.; Lipscomb, J. Unpublished results.
(248) Balch, A. L. *Inorg. Chim. Acta* **1992**, *198*−*200*, 297−307.
(249) Sanders-Loehr, J. *Binuclear Iron Proteins*; Loehr, T. M., Ed.; VCH: New York, 1989; pp 375−466.
(250) Sjöberg, B.-M.; Loehr, T. M.; Sanders-Loehr, J. *Biochemistry* **1982**, *21*, 96−102.
(251) Sjöberg, B.-M.; Sanders-Loehr, J.; Loehr, T. M. *Biochemistry* **1987**, *26*, 4242−4247.
(252) Brennan, B. A.; Chen, Q.; Juarez-Garcia, C.; True, A. E.; O'Connor, C. J.; Que, L., Jr. *Inorg. Chem.* **1991**, *30*, 1937−1943.
(253) Sawyer, D. T.; McDowell, M. S.; Spencer, L.; Tsang, P. K. S. *Inorg. Chem.* **1989**, *28*, 1166−1170.
(254) Kitajima, N.; Fukui, H.; Moro-oka, Y.; Mizutani, Y.; Kitagawa, T. *J. Am. Chem. Soc.* **1990**, *112*, 6402−6403.
(255) Kimura, E.; Kodama, M.; Machida, R.; Ishizu, K. *Inorg. Chem.* **1982**, *21*, 595−602.
(256) Murch, B. P.; Bradley, F. C.; Que, L., Jr. *J. Am. Chem. Soc.* **1986**, *108*, 5027−5028.
(257) Hazell, R.; Jensen, K. B.; McKenzie, C. J.; Toftlund, H. *J. Chem. Soc., Dalton Trans.* **1995**, 707−717.
(258) Sheu, C.; Sawyer, D. T. *J. Am. Chem. Soc.* **1990**, *112*, 8212−8214.
(259) Hendrich, M. P.; Day, E. P.; Wang, C.-P.; Synder, B. S.; Holm, R. H.; Münck, E. *Inorg. Chem.* **1994**, *33*, 2848−2856.
(260) Menage, S.; Zang, Y.; Hendrich, M. P.; Que, L., Jr. *J. Am. Chem. Soc.* **1992**, *114*, 7786−7792.
(261) Shestakov, A. F.; Shilov, A. E. *Z. Obshch. Khim.* **1995**, *65*, 622−633.
(262) Barton, D. H. R.; Doller, D. *Relevance of Gif Chemistry to Enzyme Mechanisms*; Kelly, J. W., Baldwin, T. O., Eds.; Plenum Press: New York, 1991; pp 87−98.
(263) Tian, G.; Berry, J. A.; Klinman, J. P. *Biochemistry* **1994**, *33*, 226−234.
(264) Goldberg, D. P.; Koulougliotis, D.; Brudvig, G. W.; Lippard, S. J. *J. Am. Chem. Soc.* **1995**, *117*, 3134−3144.
(265) Coucouvanis, D.; Reynolds, R. A., III; Dunham, W. R. *J. Am. Chem. Soc.* **1995**, *117*, 7570−7571.

CR9500489